Technical Report

SEPTEMBER, 1960

Bomb Penetration Tests, Fort Churchill, Canada

U. S. ARMY
SNOW ICE AND PERMAFROST
RESEARCH ESTABLISHMENT
Corps of Engineers

Technical Report 71

SEPTEMBER, 1960

Bomb Penetration Tests, Fort Churchill, Canada

by Clifton W. Livingston

U. S. ARMY SNOW ICE AND PERMAFROST
RESEARCH ESTABLISHMENT
Corps of Engineers
Wilmette, Illinois

PREFACE

This is the final report on work accomplished under Contract DA-11-190-ENG-22 with Barodynamics, Inc., under SIPRE Project 22.4-7, Penetration of projectile into frozen ground. The purpose of this work was to observe projectile penetration and to determine the feasibility of using bombs released from aircraft for producing entrenchments for troops in frozen ground.

The scope of the Fort Churchill bomb penetration tests was planned by W. K. Boyd, Chief, Frozen Ground Applied Research Branch.

Arrangements for joint participation in the project of the Royal Canadian Airforce and U. S. Army Corps of Engineers were made through the Office, Chief of Engineers. The field work and analysis of data were undertaken by Barodynamics, Inc. The field work at Fort Church, Manitoba, Canada, was supervised by Clifton W. Livingston, aided by Boyd M. Harnden and F. J. Mossman. It would have been impossible to overcome the many problems of operating under arctic conditions without the assistance of Major John H. Weaver, Commanding Officer, Field Test Team Arctic, and Flight Lieutenant Robert Coulter, Royal Canadian Airforce.

The data were analyzed and the report was written by Clifton W. Livingston, with the assistance of Frank J. Lynch, Boyd M. Harnden, and Helen J. Livingston. During the analysis, Dr. Glen Murphy reviewed the data and contributed to the analysis. The draft report was edited by E. G. Fisher.

The report has been reviewed and approved for publication by the Office, Chief of Engineers.

W. L. NUNGESSER
Colonel, Corps of Engineers
Director

Manuscript received 15 April 1959

Department of the Army Project 8-66-02-400

CONTENTS

ILLUSTRATIONS

ILLUSTRATIONS (cont'd)

TABLES

SUMMARY

Inert mortar shells and inert general-purpose, semi-armor-piercing, and armor-piercing bombs were dropped on frozen ground (glacial till) near Fort Churchill, Manitoba, Canada during the winter 1956-57 to observe projectile penetration and determine the feasibility of forming trenches and foxholes in frozen ground by means of bombs released from aircraft. Projectiles ranging from 81-mm mortar shells to 1600 AP bombs were released from altitudes of 2000 to 24,500 ft. Analysis of the test data was directed towards determining fundamentals of penetration of projectiles into materials of the earth's crust.

Previously, experiments had been conducted to observe the effects of explosions in deeply frozen glacial till and to observe penetration of projectiles into concrete slabs, rocks, soils, and armor. As a result of experiments in United States and England, several empirical penetration formulas were available. It had been observed in granite that a stress range existed in which penetration was greater than could be explained by a brittle-state failure.

Although the evidence suggests that the laws for penetration by pure brittle-state failure differ from the laws for penetration by plastic deformation, it seems possible to correlate the behavior of a wide range of materials subjected to impact of projectiles by means of a postulated model law for impact

$$y = \tau m \sqrt[3]{I} \qquad (2)$$ Postulated model law for impact

where

- y is the vertical distance (ft) from the ground surface to the nose of the projectile at the end of its underground trajectory
- τ is a transition ratio (dimensionless) which indicates the relative proportions of brittle fracture and plastic deformation
- m the plastic deformation index expresses the tendency of material to deform plastically
- I is the energy of impact (ft-lb).

As the energy of impact of a bomb that strikes a massive target is increased, the bomb passes through the ricochet range into the cratering range, where penetration is accomplished primarily by brittle-state failure. If the energy of impact is increased further, a point is reached at which penetration is accomplished by plastic deformation. This point has been chosen as the standard of reference of the postulated model law for impact. It designates the energy level at which the transition ratio τ is 1.00 and at which the behavior of various materials can be compared.

As the energy level increases beyond that at $\tau = 1.00$, penetration is accomplished by plastic deformation, and empirically derived penetration formulas now in use do not appear to be applicable.

An analogy was drawn between plastic deformation and fluid flow, and the equation

$$L = \frac{W}{C_3 \delta D^2} \ln \frac{C_1}{C_1 + C_3 \rho V D^2} \qquad (8)$$

was derived using laws for the motion of a body through a fluid. The equation expresses the path length of a bomb penetrating a solid in terms of the weight and diameter of the bomb, the striking velocity of the bomb, the density and unit weight of the material penetrated, and two coefficients C_1 and C_3, which are related to the material and its resistance to penetration by the bomb. The coefficients C_1 and C_3 (which equal a constant times the drag coefficient) vary in a complex manner. The equation has been reduced to the equivalent form

$$L = \frac{W}{\delta D^2}\left(\frac{\Delta y}{\Delta x} V+b\right). \tag{9}$$

Values of $\Delta y/\Delta x$ and b depend upon both the material penetrated and the bomb. Values within the range of the tests have been determined for the shells, general-purpose bombs, semi-armor-piercing bombs, and armor-piercing bombs that were dropped on peat-covered frozen Churchill till.

Using the plastic deformation equation and the postulated model law for impact, the following equations were derived:

$$\tau = \frac{W\theta}{\delta D^3 m \sqrt[3]{I}}\left(\frac{\Delta y}{\Delta x} V+b\right) \tag{10}$$

$$m = \frac{W\theta}{\delta D^2 \tau \sqrt[3]{I}}\left(\frac{\Delta y}{\Delta x} V+b\right) \tag{11}$$

$$\frac{Q}{C_3} = \frac{\delta D^2 \tau m \sqrt[3]{I}}{W\theta}. \tag{12}$$

Equation 10 makes it possible to predict the type of fracturing, the degree of fragmentation, and the shape of the underground trajectory or to classify the impact of a body upon a solid into one of three ranges of behavior--the ricochet range, the cratering range, or the tunneling range. Equation 11 makes it possible to determine the variation of penetration in a given material due to bomb type, nose shape, and body shape; and equation 12 may prove helpful in evaluating the coefficients C_1 and C_3 and in extrapolating the data to materials other than frozen ground.

None of the presently available general-purpose, semi-armor-piercing, or armor-piercing bombs meet the requirements of a bomb for making trenches and foxholes in frozen ground. However, using the above penetration equations and the "concept of optimum weight", which states that the weight of the bursting charge should equal the weight at Livingston's lower limit of the shock range, a series of bombs designated the FH series (for foxhole) were designed.

It is predicted that the proposed FH bombs will have a greater ballistic coefficient and a lesser bombing error and that they will penetrate to greater depths than conventional bombs of the same diameter.

BOMB PENETRATION TESTS, FORT CHURCHILL, CANADA

by

C. W. Livingston

INTRODUCTION

Objectives

Previous military experience has shown that conventional entrenching tools are useless for making trenches and foxholes in frozen ground. The inability of troops to entrench themselves properly has resulted in high casualties both from cold weather and from enemy fire. The use of explosives for excavations in shallowly frozen ground and in deeply frozen ground was investigated in 1954 and 1955. (Livingston, 1956; 1959). Field tests at Houghton, Michigan, and at Fort Churchill, Manitoba, Canada, demonstrated the feasibility of using explosives for entrenching troops and excavating for structures. However, the equipment required for drilling holes in which to place the explosives charge is vulnerable to enemy fire under front-line battle conditions.

Results of tests of the penetration of bombs into rocks (Livingston and Smith, 1951) suggested that the hole might be drilled by means of a projectile released from aircraft. Logistical considerations favor the use of a projectile designed to explode after penetrating to the proper depth.

The objectives of the Fort Churchill bomb penetration tests are:

1) To determine the feasibility of using projectiles released from aircraft to make trenches and foxholes in deeply frozen ground.

2) To investigate penetration characteristics of the muskeg-covered, frozen glacial till which occurs throughout vast areas of the sub-arctic and arctic.

3) To obtain data fundamental to the penetration of projectiles into materials and to the elastic or plastic behavior of the materials.

4) To obtain data essential to the design of projectiles intended for entrenching troops rapidly in frozen ground under battle conditions.

Site selection

It was known from previous SIPRE field work near Fort Churchill, Manitoba (lat. N 58° 45'), that the ground was frozen to a depth much greater than that required for the proposed tests. It was known also that the mantle of glacial debris overlying the bedrock reached a thickness as great as 90 ft. Preliminary reconnaissance work at the close of the Fort Churchill blast tests indicated that a suitable site could be found in the vicinity of Fort Churchill.

The site was chosen in accordance with the following requirements:

1) The site to be not less than 4000 ft diam, as flat as possible, and free of large stones and boulders. The frozen ground to be as homogeneous as possible to a depth of approximately 40 ft.

2) The minimum distance from any habitation to be 2 miles. The minimum distance from a town or city to be 5 miles.

3) The location to be such as to minimize interference with other cold weather test programs at Fort Churchill and to avoid interference with the operation of aircraft approaching the Fort Churchill airport.

The site selected (Fig. 1) lies between a timber-covered glacial esker (locally known as "Cornell Ridge") and McQueen's Lake. The bombing range is a square, 3000 m on a side. The limits of the range coincide with grid limits as established on Canada Department of Defence Army Survey Establishment Sheet, 54 K/12 West Half. The area within the grid lines is a marsh land 75 ft above sea level and has a flat and level surface (Fig. 2). A layer of peat ranging from 6 to 15 in. thick covers the underlying glacial till (Fig. 3).

Pebbles observed within the clay matrix of the unstratified Fort Churchill glacial till range from basic ferro-magnesian rocks to acid granitic rocks. Not only igneous rocks, but also sedimentary and metamorphic rocks are present. To accumulate such a wide range of rock types, it is evident that the advancing ice

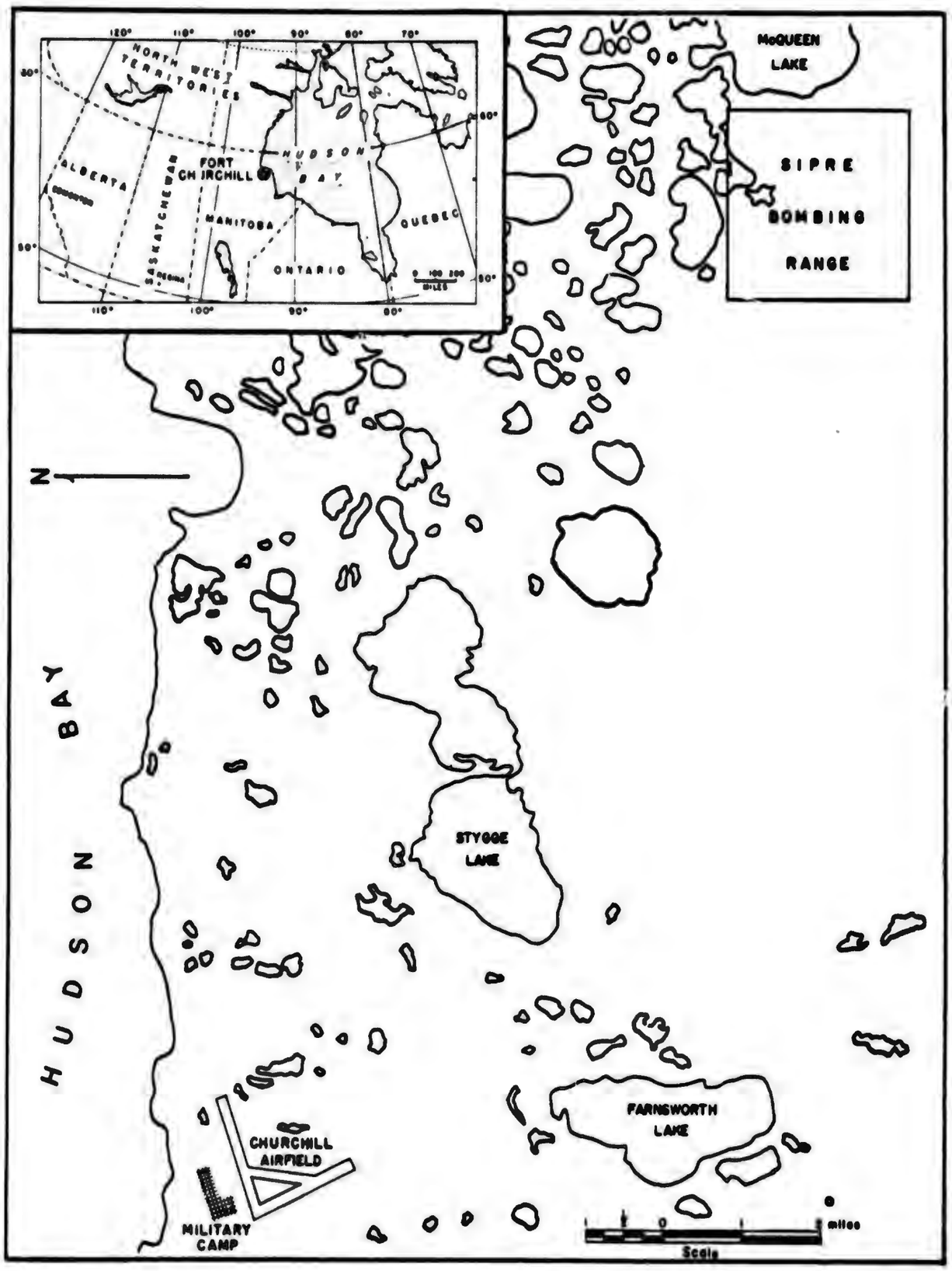

Figure 1. Site location map.

Figure 2. Muskeg surface at Fort Churchill bombing range after snow removal to permit travel of dragline.

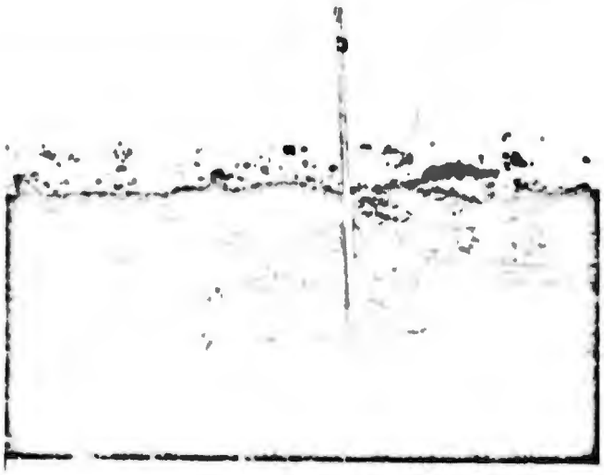

Figure 3. Layer of peat above frozen glacial till, Fort Churchill bombing range.

sheet traversed several geologic provinces. In traveling such a great distance, the aggregate was thoroughly mixed. As the glacier retreated, the upper part of the till was reworked by stream action, and in places by beach action. The coarse reworked material is stratified and lies on top of undisturbed material that is unstratified. The process of reworking accumulated the coarse component, which represents perhaps less than 1% of the unstratified till, in a linear pattern that resembles an esker. The finer components are dispersed laterally.

One such esker-like area lies immediately to the west of the Fort Churchill bombing range. The flat surface of the bombing range, its relation to the esker-like area, and the predominance of clay-size material observed in most of the bomb craters suggests that the original mantle of glacial till may have been reworked. However, the nature of the erosion surface that lies immediately below the layer of peat (Fig. 3), the absence of statification in the till, and the random dispersal of the pebbles and boulders within the matrix show that it has not. It is probable, therefore, that the esker-like area has been formed by beach action.

In summer, the Fort Churchill bombing range becomes a marsh land. Water accumulates in the depressions and at times forms a sheet that covers much of the surface. Vegetable matter of the marsh land has decayed in places to form a layer of peat that covers the site and ranges from 6 to 15 in. in thickness.

The "active layer" is from 1 to 5 ft thick at the Fort Churchill bombing range, depending upon the insulation of the peat cover. The glacial till below is perennially frozen. The temperature of the ground varies with the depth below surface and with the ambient temperature. Ground temperatures were not measured during the bombing tests, but they were measured at 2 ft intervals from 1 to 7 ft below the surface during March, April, and May of the previous year (Livingston and Murphy, 1959, Fig. 5). It is assumed that the ground temperatures do not differ enough from one winter to the next to greatly modify the rock factor R.

Although ground temperature does not vary directly with the ambient temperature, it may be inferred from the trend of wind chill and trend of ambient temperature (Fig. 4) that the ground temperature within the active layer was substantially below freezing during the period of the test drops 21 February to 21 March. In March of the previous year the ground temperature at a depth of 7 ft below the surface was 10F.

Because of the variation in size and the random distribution of pebbles and boulders within the glacial till it is impossible to obtain a soil sample that is truly representative. However, the three characteristic types of glacial till near South Camp, Fort Churchill, for which gradation curves are presented in Figure 5 and

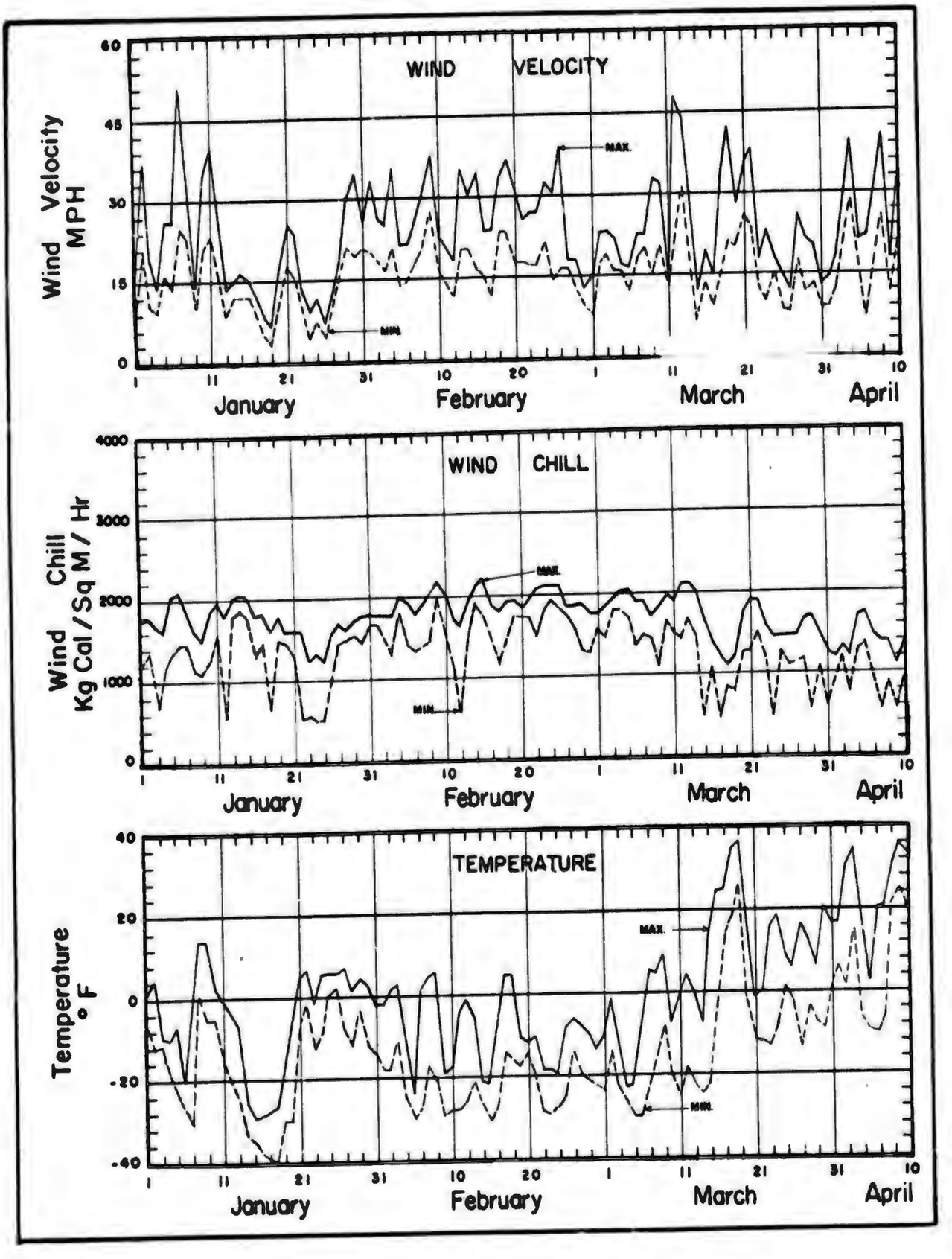

Figure 4. Weather data.

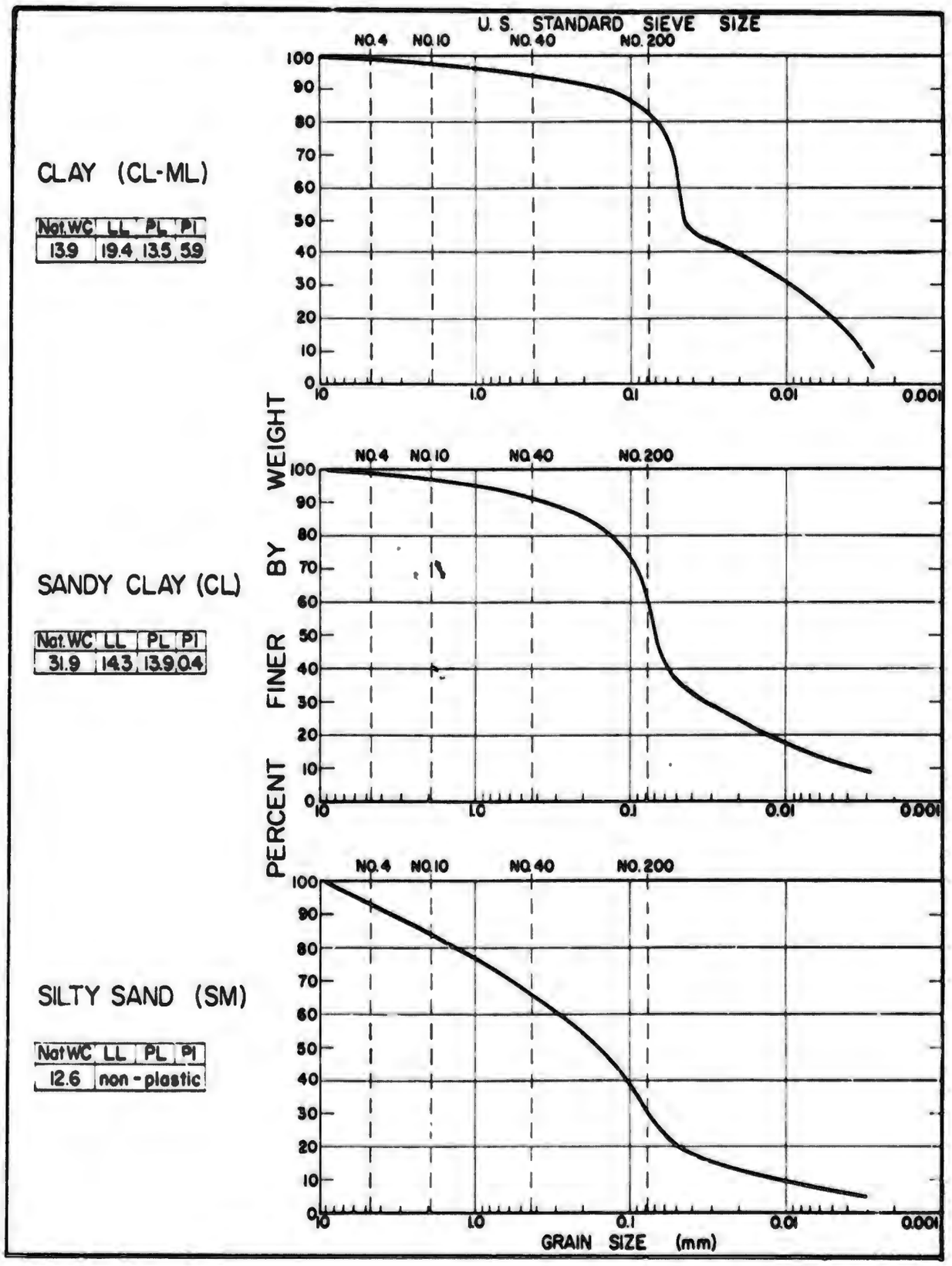

Figure 5. Gradation curves, Fort Churchill till.

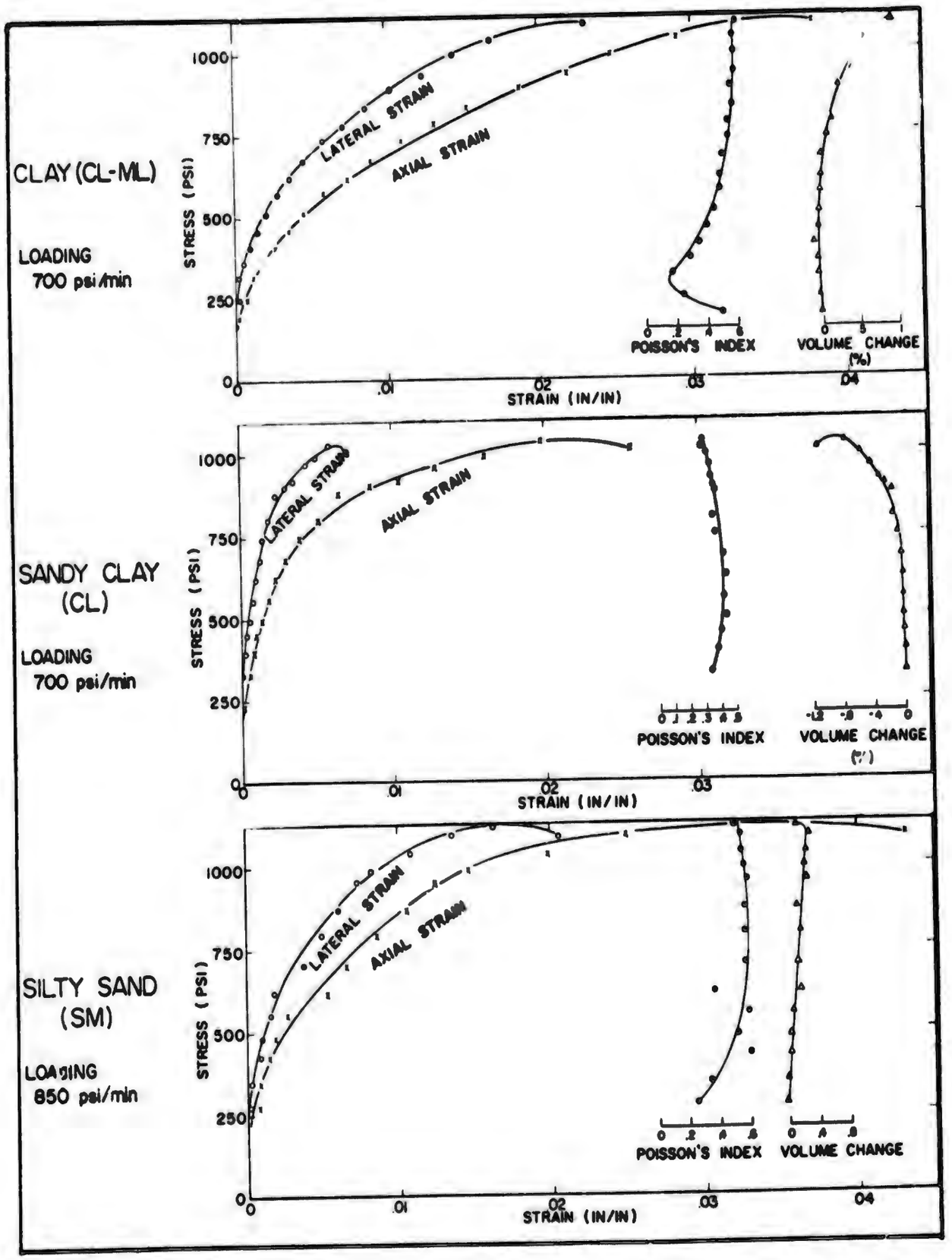

Figure 6. Compression test data, Fort Churchill till.

compression test data in Figure 6, are considered representative of the variation in physical properties of the unstratified glacial till in the general vicinity of Fort Churchill. The sample classified in standard Corps of Engineers terminology as clay (CL-ML) is characteristic of most of the bombing range. Soil samples from various bomb craters at the test site are being analyzed at SIPRE laboratories. The results will be presented at a later date.

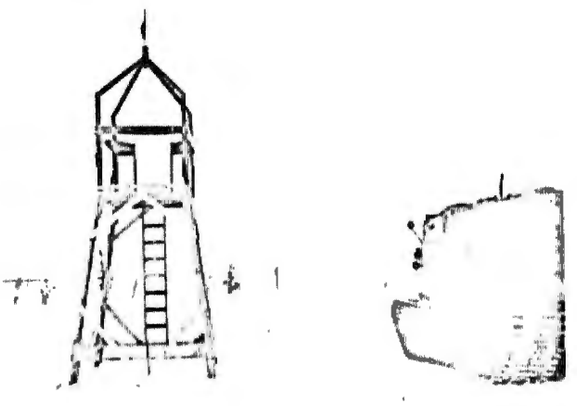

Figure 7. Observation tower.

Surveying and target layout

Because of the flat topography and the limits of accuracy with which the altitude of aircraft is known with respect to the ground, it was concluded that the target elevation could be taken directly from Canada Department of Defence topographic maps. Aerial photographs and an aerial mosaic of the area furnished additional detail. It was concluded that a local survey system properly tied to the aerial mosaic would adequately serve the requirements of the test program.

Points on the ground that were easily accessible and could be identified readily on the aerial mosaic were marked with flag poles and red cloth. These points were spotted on the aerial mosaic. Tentative target locations chosen from the aerial photographs and the aerial mosaic were established, and an inspection was made on the ground to observe the nature of the vegetation, the regularity of the ground surface, the thickness of the snow, and the visibility of the target from various directions.

A line of flight bearing N 20° W was chosen as the approach line to the target. When the plane is flying in this direction, the bombardier has his back to the sun most of the time during the months of January and February at the latitude of Fort Churchill, and the plane is heading into the direction of the prevailing wind. The direction of flight avoids interference with other aircraft approaching Fort Churchill, and in the event of a "hung bomb", the path of the aircraft avoids all installations and inhabited areas.

Three ground observation towers were fixed 4000 ft south, northeast and northwest from the center of the target (Fig. 7). The distance was based upon limits of accuracy for visual bombing with several of the same types of bombs in previous tests, with a suitable safety factor. The observation stations were placed so that radial lines from the center of the target to the towers intersected at angles of 120° (Fig. 8). A triangulation base line was measured between "You-All" and "Puget Sound", and a triangulation net was expanded from the base line to include "Wall Street", the target, and identifiable points on the aerial mosaic. A coordinate grid system with grid lines 200 ft apart and extending 2000 ft on each side of the center of the target was laid out and marked on the ground.

After preliminary experiments, a method of target marking using chemical dyes, mixed with water and antifreeze and sprayed on the surface of the snow was abandoned. Although the sprayed area could be seen from the air at a substantial distance, it was difficult to keep the spray nozzle from freezing, it was difficult to confine the fine spray to the target when the wind was blowing, and the colored surface soon was obliterated by drifting snow.

The method that was chosen for target marking incorporated experience gained by the Royal Canadian Airforce* in search and rescue operations. It had been observed that a regular geometric pattern in the snow and the light and shadow color contrast produced by rays of the sun striking the snow at a low angle were more

* Personal communication, Flight Lieutenant Wier, Operations Officer, Fort Churchill, Manitoba, Canada.

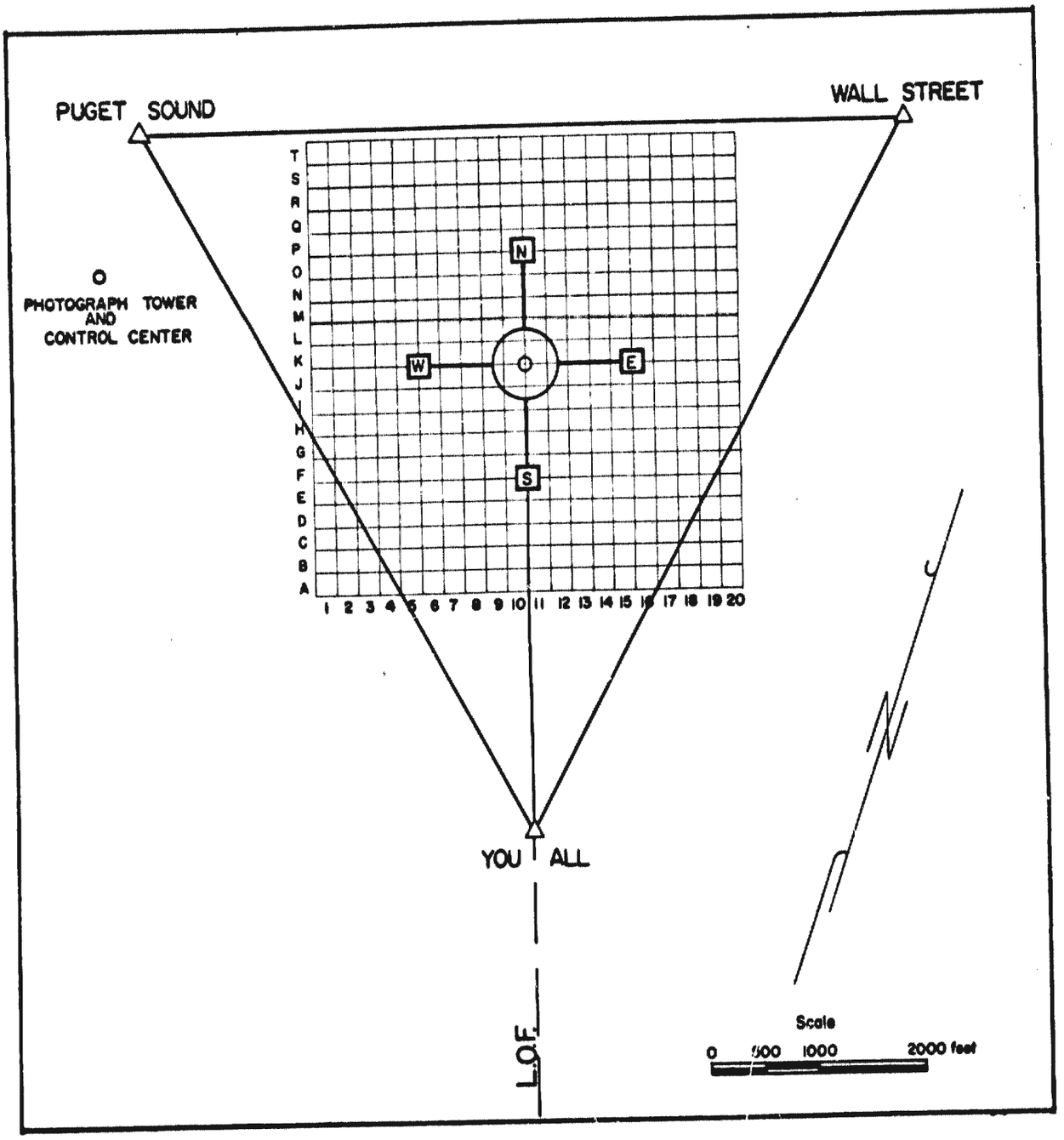

Figure 8. Target layout.

effective than the use of bright colors. It had also been observed that certain types of fluorescent cloth worn as a hood over the shoulders of ground troops aided a pilot in observing troop positions on the ground. Ordinary red cloth was tested at Fort Churchill, but proved to be of little value because when viewed from a mile or so it appears black and blends with the trees. Fluorescent pink cloth, on the other hand, appears much the same at a distance as it does when viewed close at hand.

A huge equilateral triangle (see Fig. 8) was plowed in the snow with bulldozers. The sides of the triangle were projected with a transit as straight lines between the three observation stations. The line of flight was plowed out as a solid path in a northerly direction between "You-All" and the target and as a dashed line to the south of "You-All". The snow was removed from four marker areas, each 200 ft square, to expose the brown surface of the muskeg. The centers of the marker areas were

1000 ft from the center of the target, and arranged so that the north and south markers were on the line of flight and the east and west markers were at right angles to it. Two circles, each the width of a bulldozer blade, were plowed-out around the center of the target, one 100 ft in diameter, the other 600 ft in diameter. Lanes then were plowed between the marker areas and the outer circle to form a huge cross. To complete the bulls-eye, a fluorescent pink target cloth, 20 ft in diameter, was pinned down over the exact target center before each day's bombing. The target was visible for more than 25 miles.

Bombs tested

The following types of projectiles were tested:

Type		Number
81 MM -T28E7	Shell	12
105 MM -T53E2	Shell	10
100 GP -ANM30A1	Bomb	4
250 GP -ANM57A1	Bomb	12
200 GP -ANM64	Bomb	6
500 SAP -ANM58A1	Bomb	12
1000 SAP -ANM59A1	Bomb	12
1000 AP -ANMMK33	Bomb	6
1600 AP -ANMK1	Bomb	6
	Total	80

Photographs of each type of bomb and fin assembly, and a cross section of each are presented in the Appendix, Fig. A-1 to A-9. Certain characteristics and dimensions of the bombs are summarized in Table I.

The inert bombs and mortar shells were assembled at the U. S. Engineer maintenance shop at South Camp. A mixture of sand and sawdust, of such proportions as to have the same density as TNT, was used for filler. The bombs and fins were delivered separately to the hangar at Fort Churchill in the sequence in which the bombs were to be dropped. The fins were attached just prior to hoisting the bombs into the bombing racks of the aircraft. Mortar shells were dropped by hand through the flare tube rather than being released from the bombing racks.

Table I. Bomb characteristics and nominal dimensions.

Type	Avg wt (lb)	Diam (in.)	Sectional pressure $4W/\pi d^2$	Section density W/d^3	Caliber radius head	Slenderness ratio
81 mm	11.0	3.18	1.38	0.342	2.83	3.89
105 mm	26.6	4.11	2.00	0.383	2.83	5.32
100 GP	103.0	8.00	2.05	0.201	1.26	3.56
250 GP	239.0	10.75	2.63	0.192	0.81	3.29
500 GP	468.5	14.00	3.04	0.171	1.26	3.24
500 SAP	527.0	11.75	4.86	0.325	1.50	3.86
1000 SAP	991.2	15.09	5.54	0.288	1.50	3.70
1000 AP	1015.3	12.00	8.98	0.588	2.00	4.83
1600 AP	1523.0	14.00	9.89	0.555	2.00	4.80

PROCEDURE

Bombing procedure

After making sure that the target was ready for bombing, that the area was clear, that ground communications were in operating condition, that all safety precautions had been complied with, and after the bombing program for the day had been reviewed, members of the ground observation crews were transported by oversnow vehicle to their respective stations. The ground crew consisted of:

1) ground control officer
2) range safety officer
3) air-to-ground communications officer
4) ground communications coordinator
5) plotting table operator
6) motion picture operator and assistant
7) vehicle operators for each of two road blocks
8) transit operator and observer at each tower
9) rover vehicle two-man crew.

The captain of the aircraft was advised by telephone that the ground crew was ready, and he in turn notified the ground control officer of the time of take-off from the Fort Churchill airport. Air-to-ground radio communications were established while the bomber was climbing to bombing altitude. After radio request from the aircraft and approval from the ground control officer, clearance was given for a dummy run or for a live run over the target. Conversations between the ground control officer, the air-to-ground communications officer, and the bombing crew on a live run were relayed to the various ground observation stations by field telephone. Work of the motion picture camera operator and the transit operators was synchronized by the signal "bombs gone" which was given by the bombardier at the instant of release. Separate bombing runs were made for each bomb drop.

Approximate bearings from each of the observation stations to the point of impact were plotted on the plotting board, and the approximate coordinates of impact then were given by radio to the rover vehicle crew. The rover crew placed a flag in the center of the crater and radioed information to the ground control officer concerning the results of impact upon the bomb or upon the frozen ground. Final bearings then were taken to the flag from the observation stations, the results plotted, and the range and drift error reported to the crew of the aircraft. After marking the crater with a sign containing the bomb number, the rover vehicle crew returned to its base at the ground control center. The crew of the aircraft then was advised that the target was clear for the next run.

Because of the many different activities performed by the ground crew and the difficulty of moving heavy equipment into and out of the target area during the progress of the tests, it was found necessary to leave most of the bombs in the ground until all of the bombs had been dropped. Craters were observed promptly after each day's bombing in search for information that might affect the conduct of the tests.

Plan of tests

Although previous tests (Livingston and Smith, 1951) show that considerable variation in penetration of a given type of bomb from a given altitude occurs, it was more advantageous to drop bombs from several altitudes than to drop several bombs of a given type from the same altitude. Accordingly, the plan followed in the tests was to cover as wide a range of impact energy as possible with each type of bomb. Drops with each type of bomb covered a range of altitudes of release from an altitude at which ricochet occurs to an altitude approaching that at which the terminal velocity of the projectile is reached, or to the maximum operational altitude of a B-25 Mitchell aircraft. Mortar shells and general-purpose, semi-armor-piercing, and armor-piercing bombs were dropped. Thus, it was possible to observe the effect of varying the bomb diameter from 3.18 inches to 15.09 inches and of varying the bomb weight from 10 pounds to 1600 pounds. It was possible also to compare penetration and path shapes of the different shapes of bombs in a given medium.

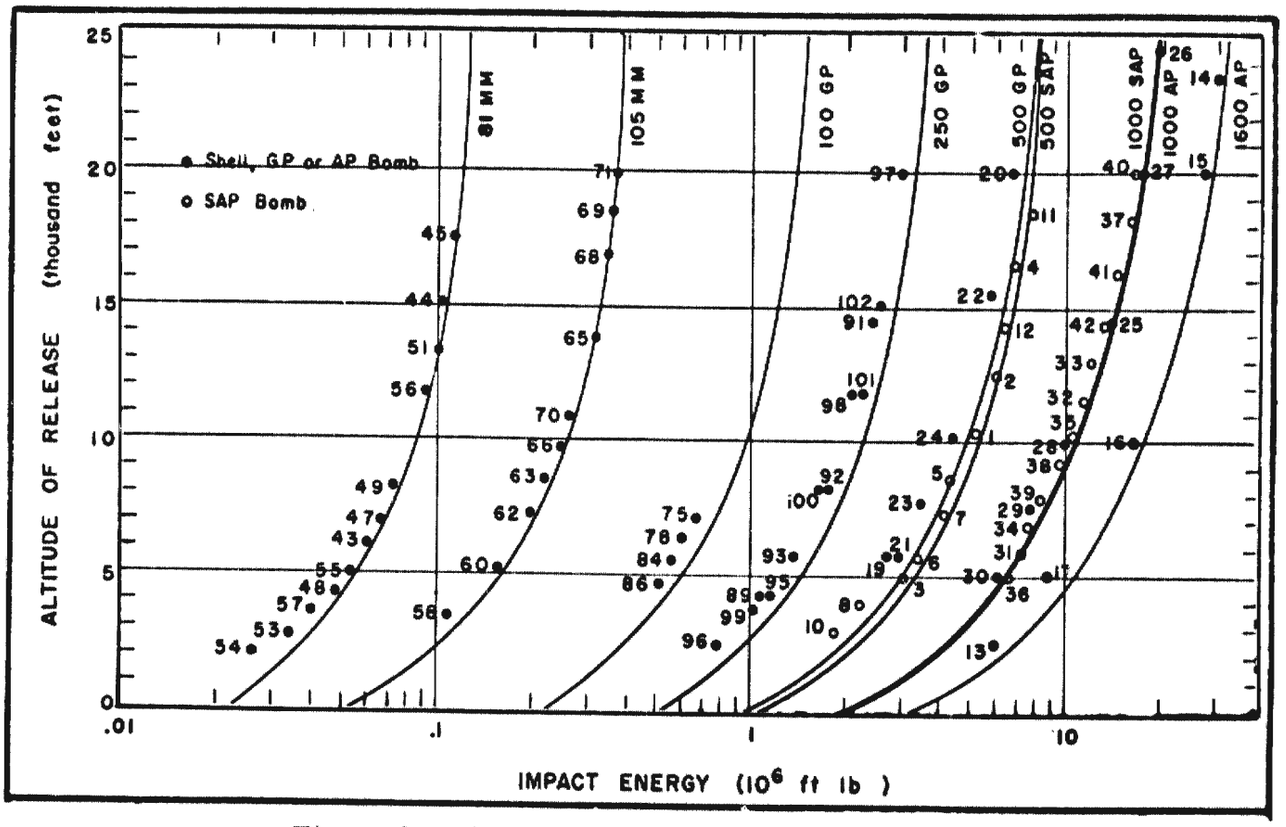

Figure 9. Altitude of release vs impact energy.

Figure 9 shows the relations between impact energy and altitude of release for a target 100 ft above sea level and for each of the types of projectiles used in the tests. The curves are based upon release of bombs from aircraft in horizontal flight at a ground speed of 250 mph. As the ground speed of the aircraft at the instant of release usually was less than 250 mph, the points are to the left of the curves.

Figure 10. Damage to casing of 100 GP bomb released 4750 ft above the target.

Casing damage

Although general-purpose bombs are designed for airburst rather than for penetration, three of the small sizes of general-purpose bombs were included in the tests, as semi-armor-piercing bombs smaller than 500 lb were not available. The effect of impact upon the casing of 2000 GP bombs striking a rock surface was known from the New Mexico tests (Livingston and Smith, 1951, p. 105-110), and it was assumed that damage to the casing would vary inversely as the diameter, other factors remaining constant. The small general-purpose bombs proved to be stronger than the 2000 GP bomb, but the smallest of the three small general-purpose bombs unexpectedly proved to be the weakest. As shown in Figure 10, the casing of the 100 GP bomb is dented near the rear of the bomb body. Three other bombs of the same type were dropped from slightly higher altitudes and the same type of denting occurred. Some were damaged at the nose, others at

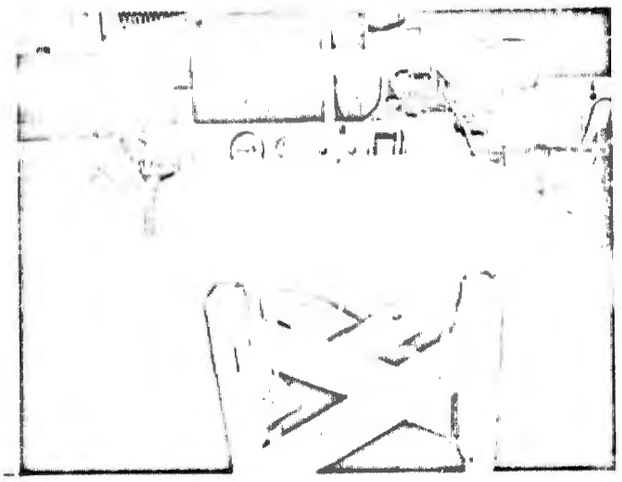

Figure 11. A sharp nose was substituted for the nose plug on several of the general-purpose bombs.

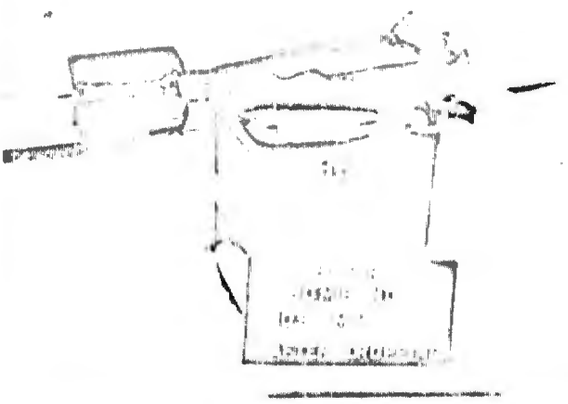

Figure 12. Rupture of casing of 105-mm shell after striking a granite boulder in frozen glacial till.

the tail, but the amount of denting did not differ greatly. The tests of the 100 GP bombs were not extended to altitudes above 7200 ft because it was obvious that the casing was about to rupture.

A flat nose plug such as was supplied is undesirable. It was discovered that the force of impact was sufficient to strip the threads, bend the shoulder, and push the nose plug inside the casing of the 500 GP bomb. Except for the nose plug, the casings of the 250 GP bombs were not damaged. A sharp nose (Fig. 11) was substituted for the nose plug on half of the 250 GP bombs dropped. The sharp nose plug did not fail, but neither did it increase the depth of penetration.

The aluminum nose that is standard for the two types of mortar shells was replaced before the tests with steel noses. After being used on the mortar shells, several of the steel noses were salvaged to replace nose plugs on the 500 GP bombs.

Casings of the semi-armor-piercing and armor-piercing bombs dropped were not damaged. Only one of the mortar shells was damaged. In this instance, a 105-mm mortar shell released from 6250 ft above the target penetrated through the layer of frozen peat, struck a granite boulder in the glacial till, and ruptured (Fig. 12). Inasmuch as none of the other mortar shells struck boulders and none ruptured, even though some were released from much higher altitudes, it is concluded that casing damage depends not only upon the design of the projectile but also upon both the energy of impact and the nature of the target material. Boulders embedded in the frozen glacial till offer greater resistance to penetration of small projectiles than does the matrix of the till.

Although metals are known to be brittle at low temperatures and although temperatures as low as -45F were recorded at bombing altitude, there is little reason to assume that the casing of bombs designed for penetrating a specific target in a warmer climate should be redesigned for bombing the same type of target in the arctic.

Accuracy of bombs

Figure 13 shows points of impact of the bombs relative to the target, including the 81-mm and 105-mm shells. The shells were dropped by hand from the flare chute upon a verbal signal from the bombardier. Thus no attempt is made to compare their accuracy with that of the bombs.

Eliminating the 81-mm and 105-mm shells, 95% of the bombs fell within a circle of 1500-ft radius, 68% fell within a circle of 760-ft radius, 17% fell within a circle of 300-ft radius. The maximum error was 3248 ft, the minimum error 58 ft, the mean error 816 ft, and the median error 588 ft. The percentages are based upon a total of 58 bombs.

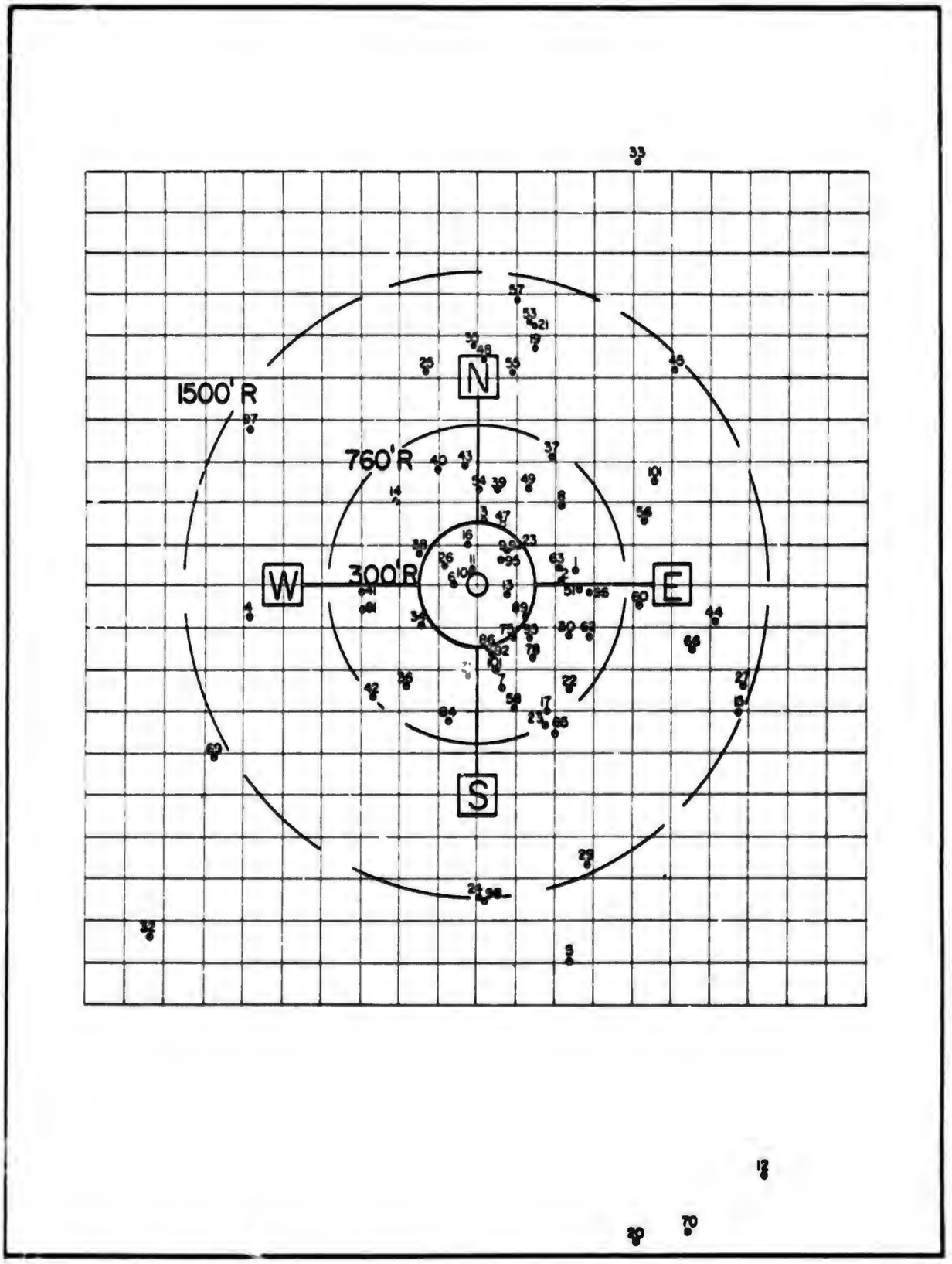

Figure 13. Spotting map.

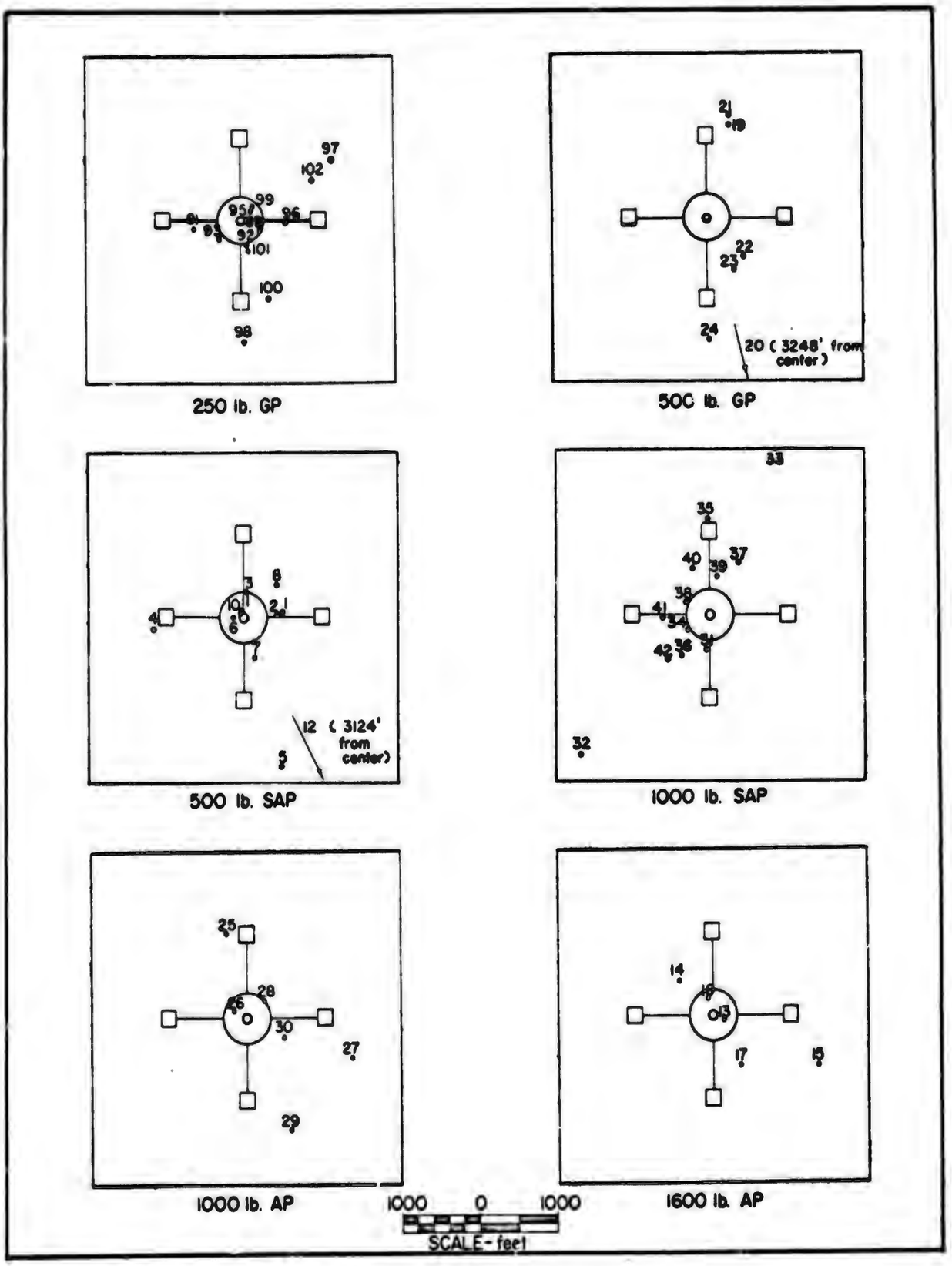

Figure 14. Impact patterns, GP, SAP, and AP bombs.

Figure 14 shows impact patterns by bomb type, eliminating the 100 GP bombs (only 4 were dropped). The number of bombs of each type is too small to draw final conclusions but the trend of the comparative accuracy is indicated (Table II).

Table II. Relative bombing accuracy.

Bomb type	Relative error* (ft)
1000 AP	318
1600 AP	339
250 GP	348
500 SAP	388
1000 SAP	416
100 GP	420
500 GP	762

* Adjusted to 5780-ft altitude of release.

The relative error increased in the same order as the ballistic coefficient† decreases. As the order of decreasing ballistic coeeficient is consistent for all seven types of bombs, the data suggest that bombing accuracy, among other considerations, is dependent upon the ballistic coefficient.

Crater mapping and excavation

The first step in recovering a bomb was to clear the snow from the area surrounding the crater with a bulldozer. Loose "rock" then was removed, using a pick and shovel (Fig. 15) or a clamshell (Fig. 16), depending upon the quantity to be removed. If the bomb had not "tunneled" to the extent where blasting was necessary, it was completely uncovered, but left in position. If the bomb had tunneled (Fig. 17), the crater was cleaned, and as much materal as possible was removed to reveal the path of the bomb.

Considerable difficulty was experienced in the early stages of excavation of bombs that were deeply buried. The first procedure tried was to drill with a jackhammer of a wagon drill mounted on an adjustable boom, then load the drill holes with explosives and blast to form a shaft of such size as to permit mucking with the clamshell. In spite of the considerable experience obtained at South Camp the previous year, and the fact that special types of bits had been developed for drilling in frozen ground, the glacial till below the bombing range proved to be nearly impossible to drill with a rock drill to depths greater than 4 ft. The rate of penetration was so slow that repeated impact of the bit caused the frozen ground to melt and plug the drill steel. It is assumed that the difficulty was due to the greater percentage of either clay size or colloidal particles. Difficulty increased with the depth of hole because of inability to remove the cuttings before melting. So much trouble was experienced with stuck steel that it seldom was attempted to drill a hole deeper than 2 ft. The shallow depth of ground made clamshell mucking impractical because only a few buckets of soil were broken when the round was fired.

The method was abandoned because of the slow rate of progress. It was found that the tunnel made by the bomb could be cleaned out using a post-hole digger and a homemade "spoon". An explosive charge of weight calculated from the depth of the charge using the data of the Fort Churchill blast tests (Livingston and Murphy, 1959), was placed directly in the tunnel as deep as possible. The effect of the blast is similar to that of a crater blast in a borehole, except that the form of the resulting crater is modified somewhat by the form of the crater produced by impact of the bomb. Material loosened by the blast was excavated with a clamshell, and the process repeated until the tail of the bomb was exposed. The rest of the excavation was completed using a few well-placed drill holes (Fig. 18).

† See Terminology, app B.

Figure 15. Removal of loose "rock" from craters with a pick and shovel.

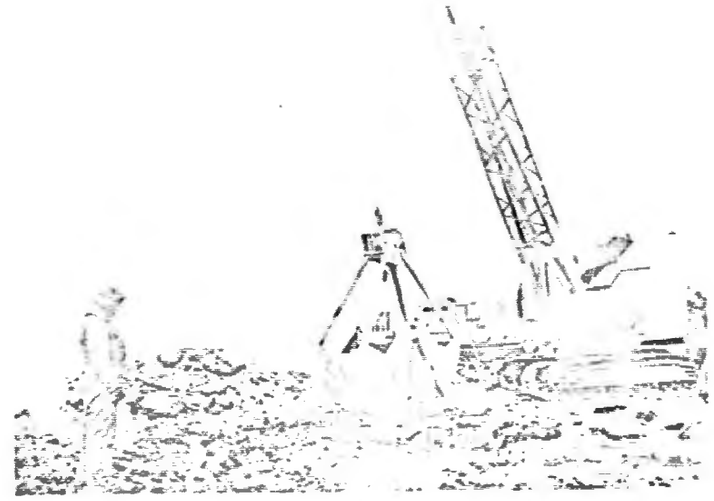

Figure 16. Mucking with a clamshell.

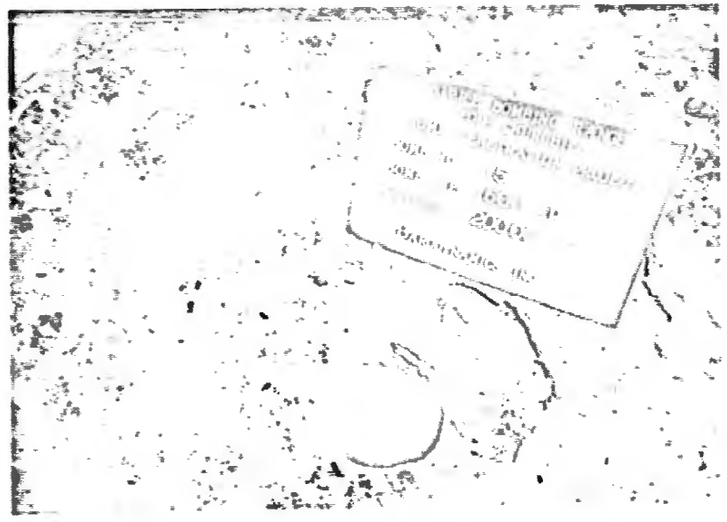

Figure 17. Tunnel in frozen glacial till by 1600 AP bomb from 20,000 ft.

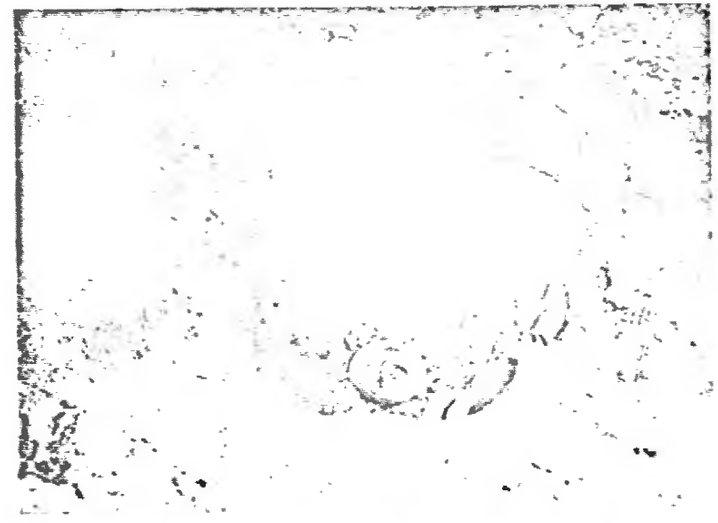

Figure 18. Plastic flow of walls of explosion cavity by blast in bomb tunnel, and recovery of bomb using well-placed drill holes.

SLSEIG

Figure 19. Craters were mapped in plan after establishing the line of flight on the ground.

Figure 20. Cross-sections of the craters were measured parallel to and at right angles to the line of flight.

A line parallel to the line of flight, or "track", of the aircraft was established on the ground at each point of impact. The crater was mapped in plan (Fig. 19) and cross-section (Fig. 20). Two cross-sections were measured--one parallel to the line-of-flight, the other at right angles to it. Several cross-sections were necessary to record the path of a bomb that penetrated deeply, and were taken at successive stages as excavation proceeded.

Bomb path and crater cross-sections: From the crater cross-sections and the final resting position of the bomb, the bomb path was reconstructed with the aid of a template so as to agree with the striking angle as obtained from bombing tables. As craters had been mapped in the field both in plan and cross-section and a bomb might deviate either to the right or to the left of the line of flight, it usually was necessary first to construct the bomb path on a warped section. The warped section then was used to determine the true length of the bomb path and to obtain the various crater measurements (Fig. 21).

The crater radius R was calculated from the crater area as measured with a planimeter, assuming the crater outline to be circular.

The volume of crater V was calculated using the true rather than the apparent crater. Cross-sections $A\overline{B}$ and CD as measured in the field were redrawn to scale on stiff paper and cut along the center line to form four templates. The centroid of each half area was determined. The volume of revolution of each half area was calculated using the equation

$$V_B = 2\pi \overline{R} A_{B2}$$

where

V_B is volume of revolution of $\frac{1}{2}$ area (area B)

$\overline{R}$ is centroid radius

A_{B2} is area of $\frac{1}{2}$ crater cross-section (area B).

The crater volume equals one-fourth of the sum of the four volumes of revolution, V_A, V_B, V_C, and V_D.

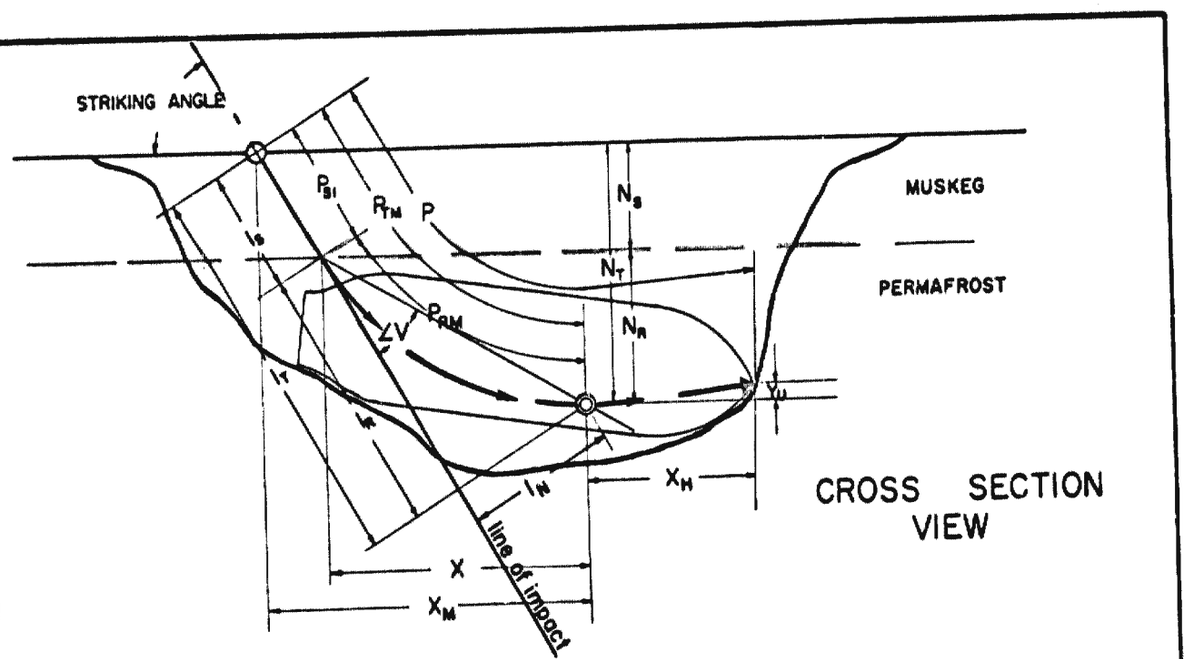

⊕ Point of impact
◎ Point of maximum penetration of nose
→ Final nose position
⟶ Path of bomb nose

N_{SN} Normal thickness of snow
N_S Normal thickness of muskeg to maximum penetration
N_R Normal thickness of permafrost to maximum penetration
N_T Normal thickness of muskeg and permafrost to maximum penetration
P_S Total path length in muskeg along arc
P_{SI} Path length in muskeg along arc on inital penetration
P_{RM} Path length in permafrost along arc to maximum penetration
P_{TM} Path length in muskeg and permafrost along arc to maximum penetration
P Total path length along arc
l_S Inclined distance in muskeg to maximum penetration along line of impact
l_R Inclined distance in permafrost to maximum penetration along line of impact
l_T Inclined distance in muskeg and permafrost to maximum penetration along line of impact
l_N Normal distance from line of impact to bomb nose at maximum penetration
X_M Total horizontal displacement in muskeg and permafrost of nose to maximum penetration
X_H Horizontal displacement of nose from maximum penetration to final position
X Horizontal displacement, in permafrost, of nose at maximum penetration
Y_U Vertical displacement of nose from maximum penetration to final position
$\angle V$ Angle of deviation, at maximum penetration, from line of impact

PLAN VIEW

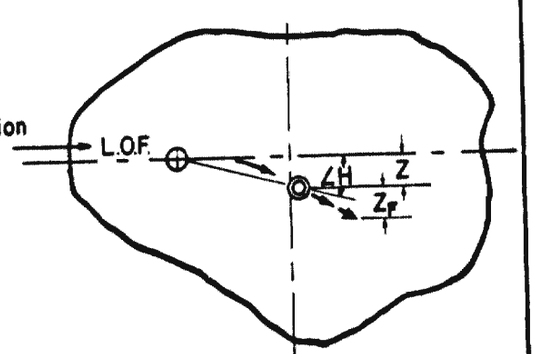

Z Horizontal deviation from line of flight to maximum penetration
Z_F Horizontal deviation, maximum penetration to final position
∠H Angle of horizontal deviation from line of flight

Figure 21. Crater measurements.

Data sheets: The data for each type of bomb are summarized in the appendix (A10-37). Ballistic data were derived from bombing tables and from charts furnished by Aberdeen Proving Ground. Bomb path and crater measurements (see Fig. 21) were compiled from various plans, cross-sections, and warped sections. The information, upon which the analysis is based, is arranged by bomb type in order of increasing weight and increasing altitude of release.

ANALYSIS OF CRATER MEASUREMENTS

Field analysis

It appeared from field observation before excavation that the crater diameter reached a maximum, then decreased with a further increase in striking velocity. The field relations suggested that ricochet was not a simple function of striking angle, but depended also upon impact energy. The field relations also indicated that, upon impact, the frozen ground behaved as if either in a brittle state or in a plastic state, and that the behavior depended both upon the type of bomb and the striking velocity. It was apparent also by comparison with features observed in previous tests (Livingston and Smith, 1951) that plastic deformation predominates in frozen ground; whereas brittle-state failure predominates in rocks such as granite and sandstone. It was evident that all of the various types of bombs were capable of penetration by plastic deformation, but that plastic deformation was exhibited to a greater degree by some types than by others.

The measurements fall into two classes, 1) those that record the shape of the path of the bomb through the frozen ground, and 2) those that record the shape of the crater. The first has an analogy in the field of ballistics. The second has an analogy in the study of craters produced by explosions.

Because striking velocity appears as a parameter in most penetration formulas, both types of crater measurements first are compared at various striking velocities. For a given type of bomb, the angle of fall increases with striking velocity.

It is not intended that the straight lines in the diagrams that follow should serve other than to aid in presenting the field data.

Crater dimensions vs striking velocity

Figures 22 and 23 show how the radius and depth of craters in frozen Churchill till vary with striking velocity. The diagrams are arranged in order of increasing bomb weight.

Lines have been placed on the figures tentatively to indicate that a linear relation may exist.

Because of the dispersion, lines have been omitted from the diagrams for the 1000 SAP and the 1000AP bomb in Figure 22.

Inspection of the other seven tentatively shows that:

1) the slope of the line differs for each type of bomb;

2) the radius of crater increases with striking velocity, but the increase is very light for the smaller bombs;

3) at a given striking velocity the radius of crater increases with the weight of the bomb;

4) for a given nominal weight of bomb (e.g., 500 GP and 500 SAP) and for a given striking velocity, the radius of crater differs for bombs of different types.

The slight increase in crater radius with increase in striking velocity for the 81-mm and 105-mm mortar shells can be explained, perhaps, by the greater resistance to penetration of the glacial till than of the overlying peat. Most of the energy at impact of the smaller shells is used in penetrating the vegetable layer. This is true also for the 100 GP bombs; an additional factor is that the casing of the 100 GP bombs deformed, which further increases the resistance to penetrations. It seemed futile to attempt drops at greater striking velocities with the 100 GP bomb.

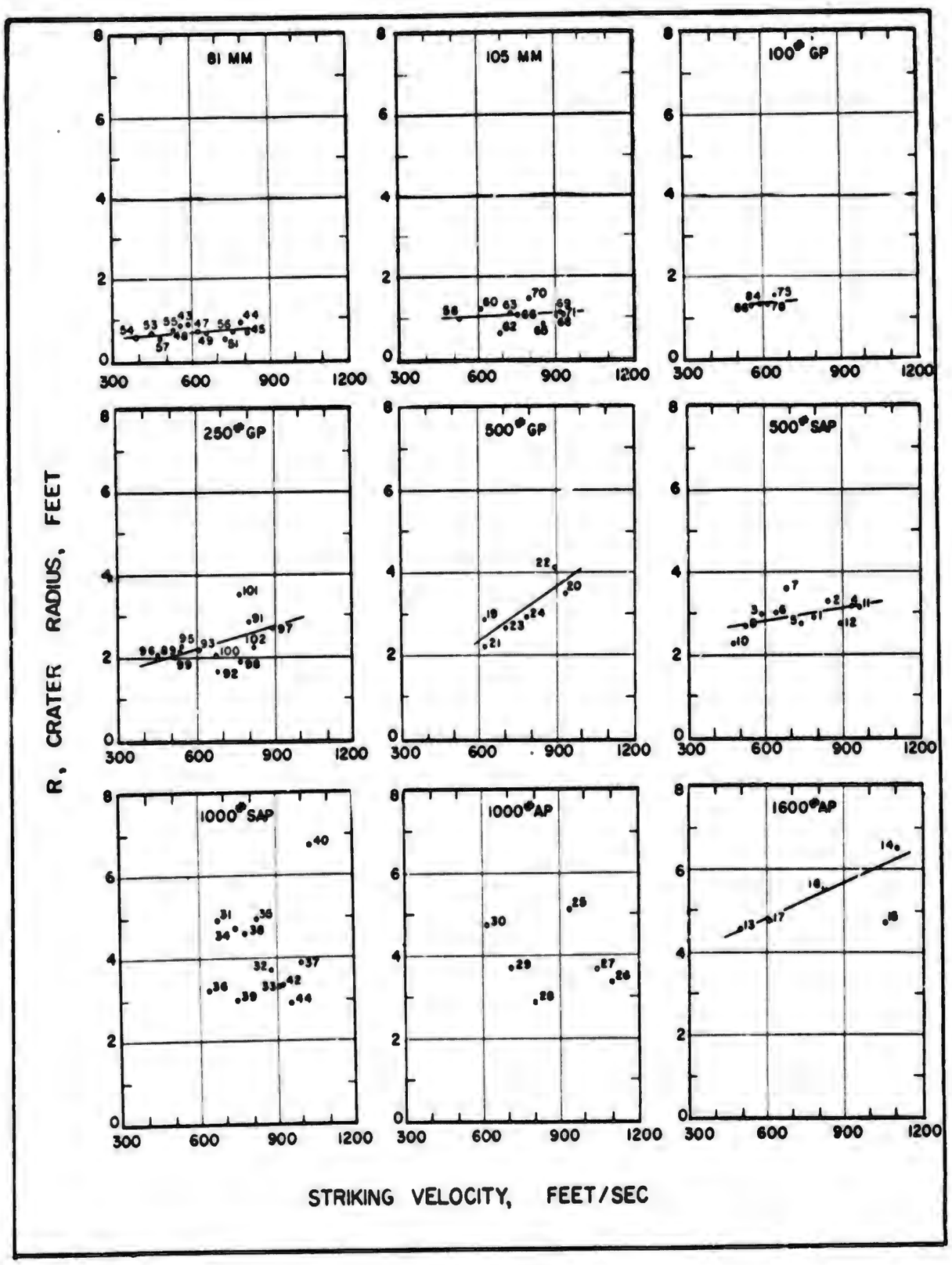

Figure 22. Crater radius vs striking velocity.

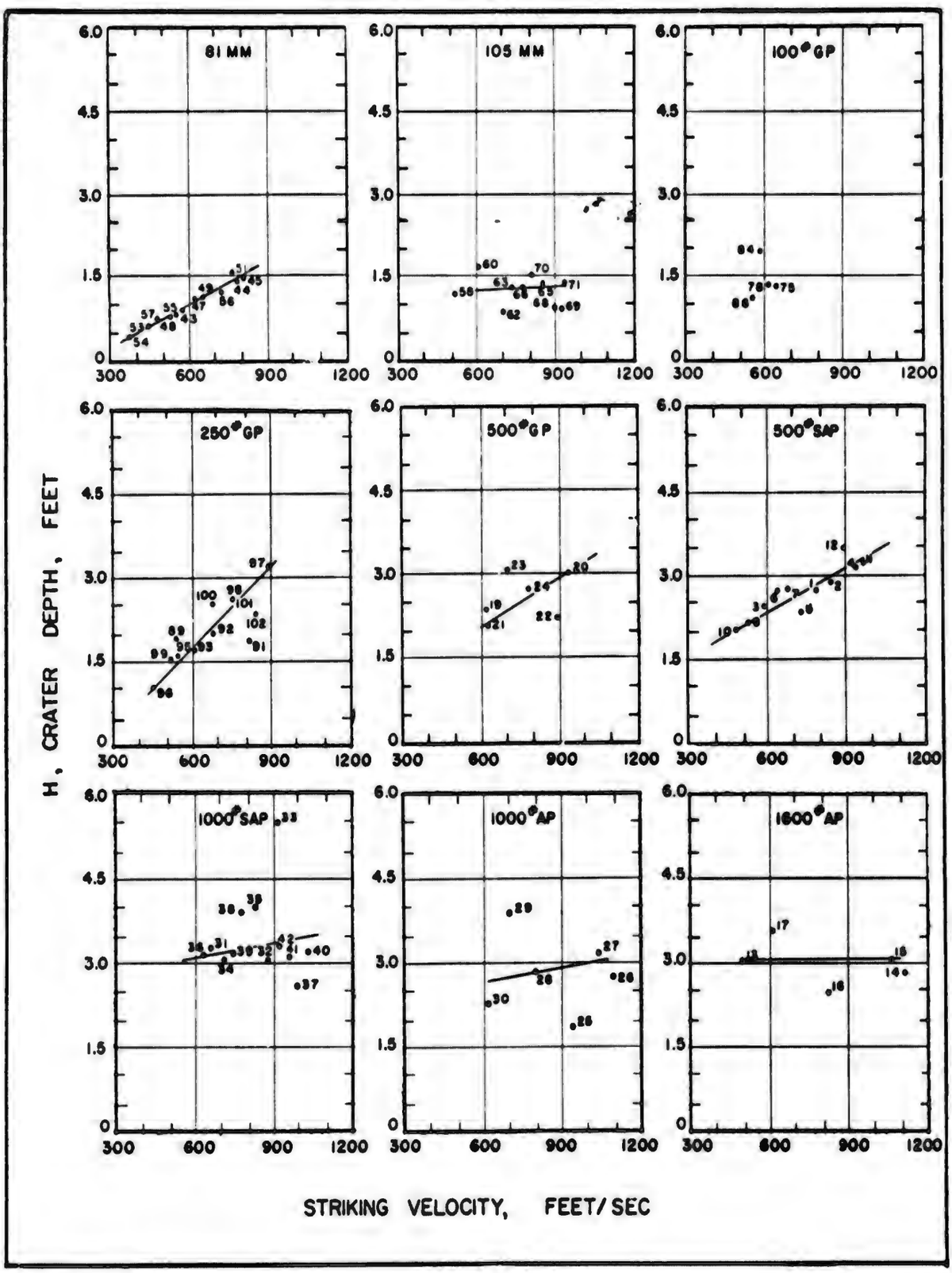

Figure 23. Crater depth vs striking velocity.

"Crater depth" (Fig. 23) was measured vertically from the surface to the bottom of the crater, but does not include the "tunnel" that the bomb forms in the frozen ground by plastic deformation. The depth of crater is the true depth as contrasted with the "apparent" depth. Both the depth measurement and the area measurement from which the crater radius is computed were obtained after all material loosened by the impact had been removed.

The four observations stated concerning the relations between crater radius and striking velocity appear to apply also to the relations between crater depth and striking velocity.

Figure 24 shows the relation between crater volume and striking velocity. As both crater depth and crater radius appear to increase with striking velocity, it would be inconsistent if crater volume did not increase also. Lines have been placed on six of the diagrams to indicate a linear trend of the data, but it should be recognized that if a linear relation between striking velocity and crater radius and crater depth holds, then a linear relation between striking velocity and crater volume is impossible. It is not intended that great significance be attached at this stage to the position of the lines. Neither is it intended to imply that the relations between radius, depth, volume, and striking velocity may not be other than linear. The relations are used as a means of presenting the data rather than, at this stage, arriving at a conclusion.

Most penetration formulas have evolved from Poncelet's attempt to derive a formula starting from Newton's second law (see Livingston and Smith, 1951, p. 207). Poncelet considered the resistance to penetration to depend both upon the strength of the material and upon the inertia of the material removed from the zone of penetration. Later formulas, such as the Petry formula, the "old" NDRC formula, the "new" NDRC formula, and the RRL formula evolved primarily from penetration studies in soils, which indicated that penetration depends not only upon striking velocity but also upon other parameters. The relations presented in preceding paragraphs also suggest that parameters other than striking velocity should be considered.

Path length and normal penetration vs striking velocity

Path length and normal penetration record the final position of a projectile in the medium. Just as the trajectory of a projectile in air is determined by the forces acting upon it, so is the trajectory of a projectile in the medium after impact. Using models of armor-piercing, semi-armor-piercing, and general-purpose bombs and a gelatin model material, it was demonstrated (Livingston and Smith, 1951, p. 155-168, 205-206) using photoelastic methods that the path of a projectile depends upon the stress distribution in the medium at various stages of penetration, and that the stress distribution is influenced by the impact energy, the shape of the nose of the bomb, the slenderness ratio of the bomb, and the angle of impact.

All measurements are referred to the nose of the projectile, on the premise that penetration occurs as a result of failure of the medium rather than that failure of the medium occurs as a result of penetration. After observing the manner of failure of frozen ground during the tests, it is evident that failure is accomplished by both brittle-state fracture and plastic deformation in varying proportions. Referring path measurements to the nose, where the energy is imparted to the medium, emphasizes the behavior of the medium rather than the force system that acts through the center of gravity of the projectile.

The term "path length" is used here primarily to designate the length of the path from impact to the point of maximum normal penetration (P_{TM} of Fig. 21), rather than the total length of the path. Thus, path length is an inclined measurement along a curved path, and normal penetration, N_T, is a measurement normal to the surface; both measurements are taken to the same point. As the surface of the Fort Churchill bombing range is level, a measurement normal to the surface is also a vertical measurement.

The distinction between this use of "path length" and the usual usage is of significance only for bombs that ricochet or, after impact, assume an upward direction

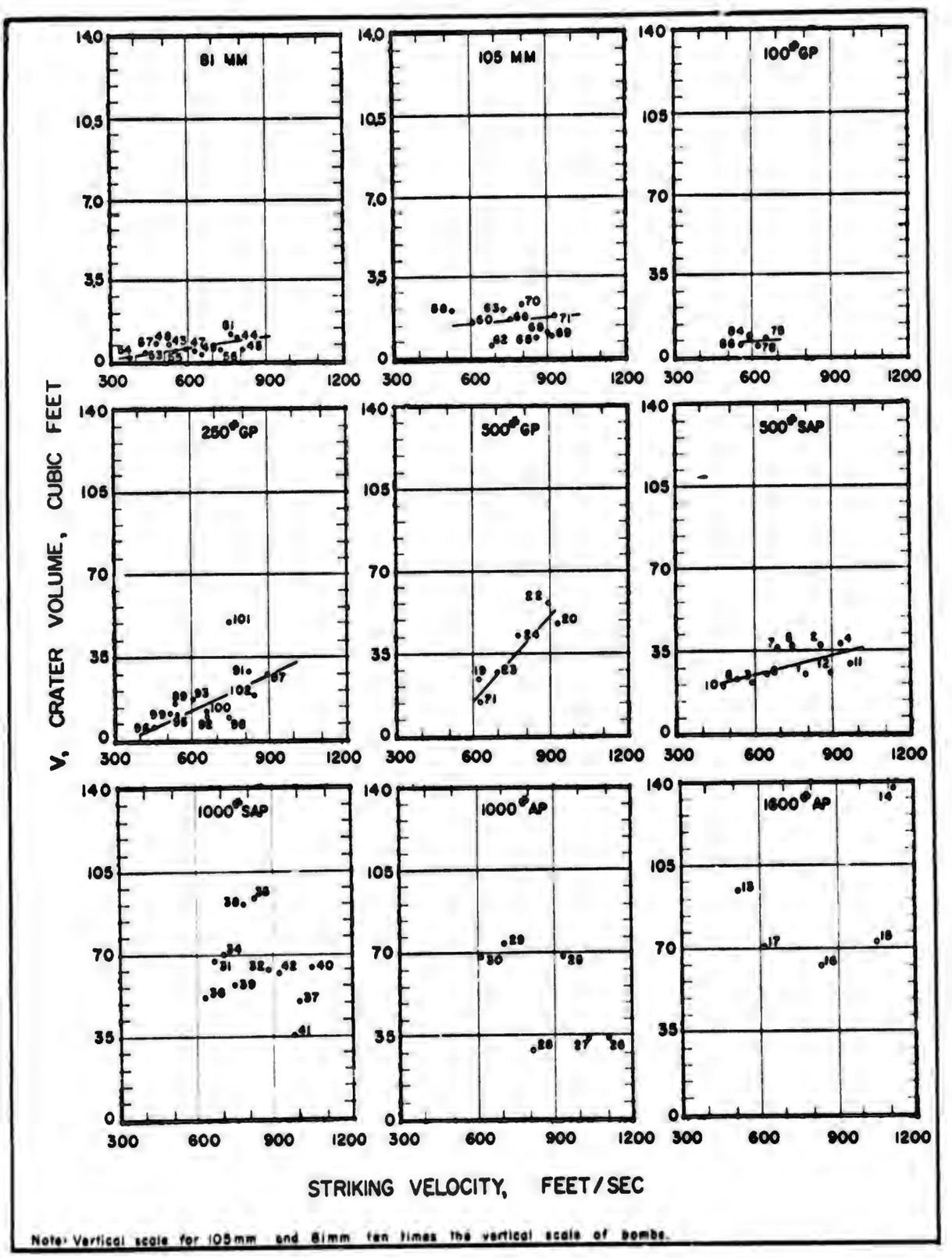

Figure 24. Crater volume vs striking velocity.

towards the surface. If the bomb ricochets, only a part of the energy of the impact is partitioned to the medium. If the bomb changes direction so as to parallel the surface or to move upward towards it, the motion of the bomb is influenced by the geometry of the pattern of failure. If motion continues, the resistance to penetration is less than if the material had not fractured previously.

Figures 25 and 26 show the relation of path length and normal penetration to striking velocity. The lines on the diagram are intended to suggest that a linear relation is not inconsistent with the field data.

Path shape, tunneling, and crater shape

The underground trajectory of bombs is generally described as J-shaped. The curvature of the path is such as to bring the bomb closer to the surface. The path of the bomb may also swerve either to the right or to the left, resulting in considerable lateral offset from the line of flight. Variables that influence the shape of the path in the medium (see Livingston and Smith, 1951, p. 91, 104, 123, 205, 206) are:

1) diameter of the bomb
2) shape of the nose
3) slenderness ratio
4) energy of impact
5) striking angle
6) type of medium
7) shape of the target
8) attitude of pre-existing planes of weakness.

The first five of these factors are dependent upon the projectile, the last three are dependent upon the medium. The number of variables that influence the shape of the underground trajectory is large, but they may be reduced to the relative magnitudes of 1) the component of stress in the medium acting upon the bomb parallel to the trajectory and 2) the component of stress at right angles to the trajectory.

Figure 27 illustrates typical variations in the shape of the underground trajectory and variations in crater shape as the altitude of release is increased. The size of the crater increases to a maximum, then decreases, and the curvature of the path decreases. As the impact energy increases, a point eventually is reached where tunneling begins. Although variation in path shape and crater shape depends also upon the type of bomb, the relations shown in the figure are typical and suggest that the size of the crater and the underground trajectory are related, and that changes in one are accompanied by changes in the other.

The effect of a bomb striking frozen ground is similar to that of a bomb striking rock. A theory of rock failure was stated and the relation between the attitude of planes of failure and the directions of principal stress in the medium were described in the report of the Bomb Penetration Project (Livingston and Smith, 1951, p. 177-194). Although tunneling is less predominant in rocks than in frozen ground, it nevertheless occurs. Inasmuch as tunneling is a phenomenon of plastic deformation it now is evident that the proportions of brittle fracture and of plastic deformation are variable. The Fort Churchill tests provide a means of observing the effects of plastic deformation to a degree beyond that possible in substances that fail predominantly by brittle-state fracture. At the same time it is possible to observe a range of failure that is due predominantly to brittle-state fracture (as illustrated by the path and crater shape of bomb 8) and to observe the transition from brittle-state fracture to plastic deformation (as illustrated by the paths and shapes of craters of bombs 7 and 11).

Path length and normal penetration vs impact energy

The linear relations between crater depth, normal penetration, path length, and striking velocity (Fig. 23-26) need not be ignored completely, but it is evident, that parameters other than striking velocity must be considered. Measurements that record the shape of the path of the bomb and the shape of the crater might be plotted against momentum, mV, or against impact energy, $\frac{1}{2}mV^2$. In either instance, striking velocity is taken into consideration.

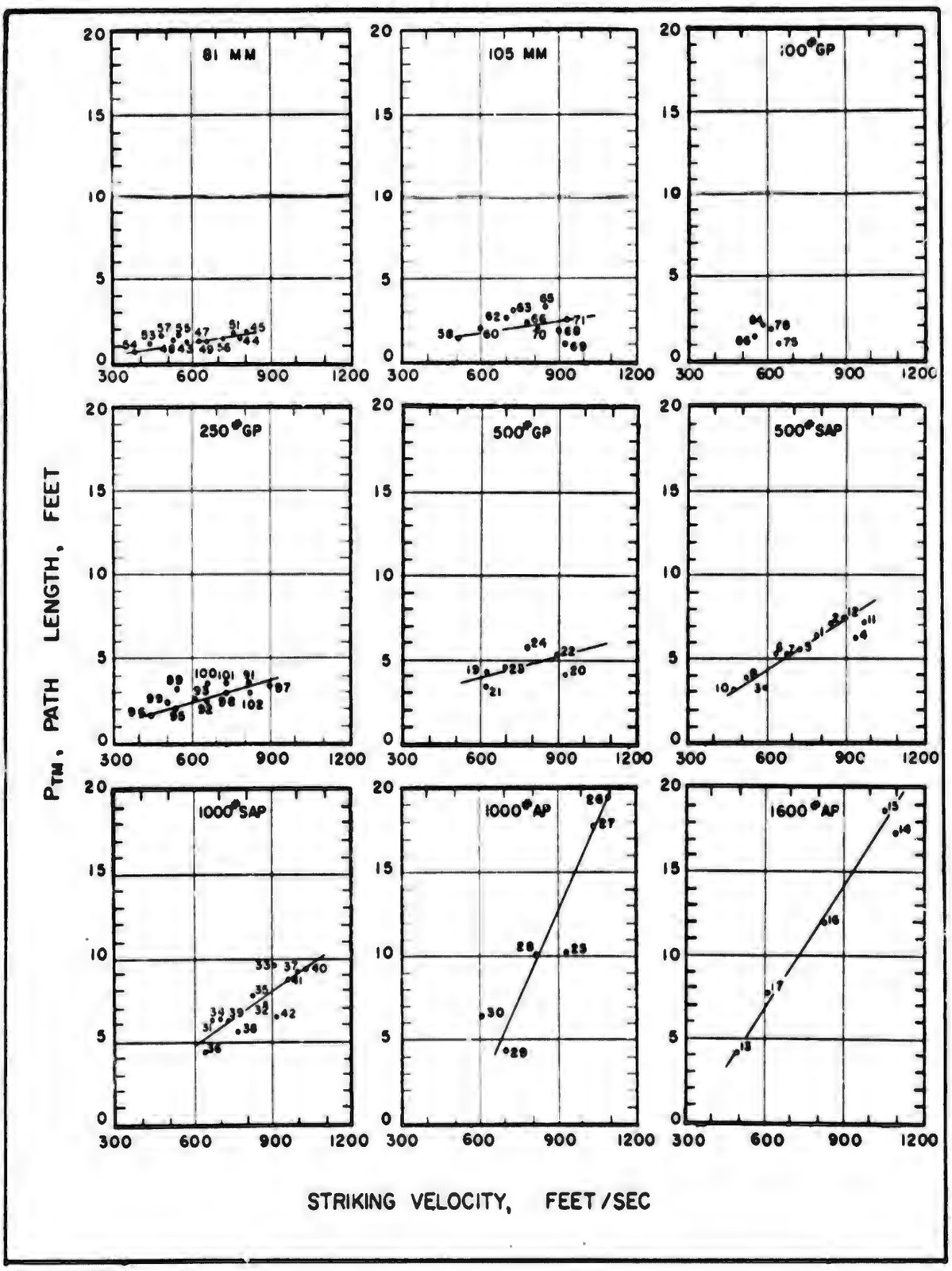

Figure 25. Path length vs striking velocity.

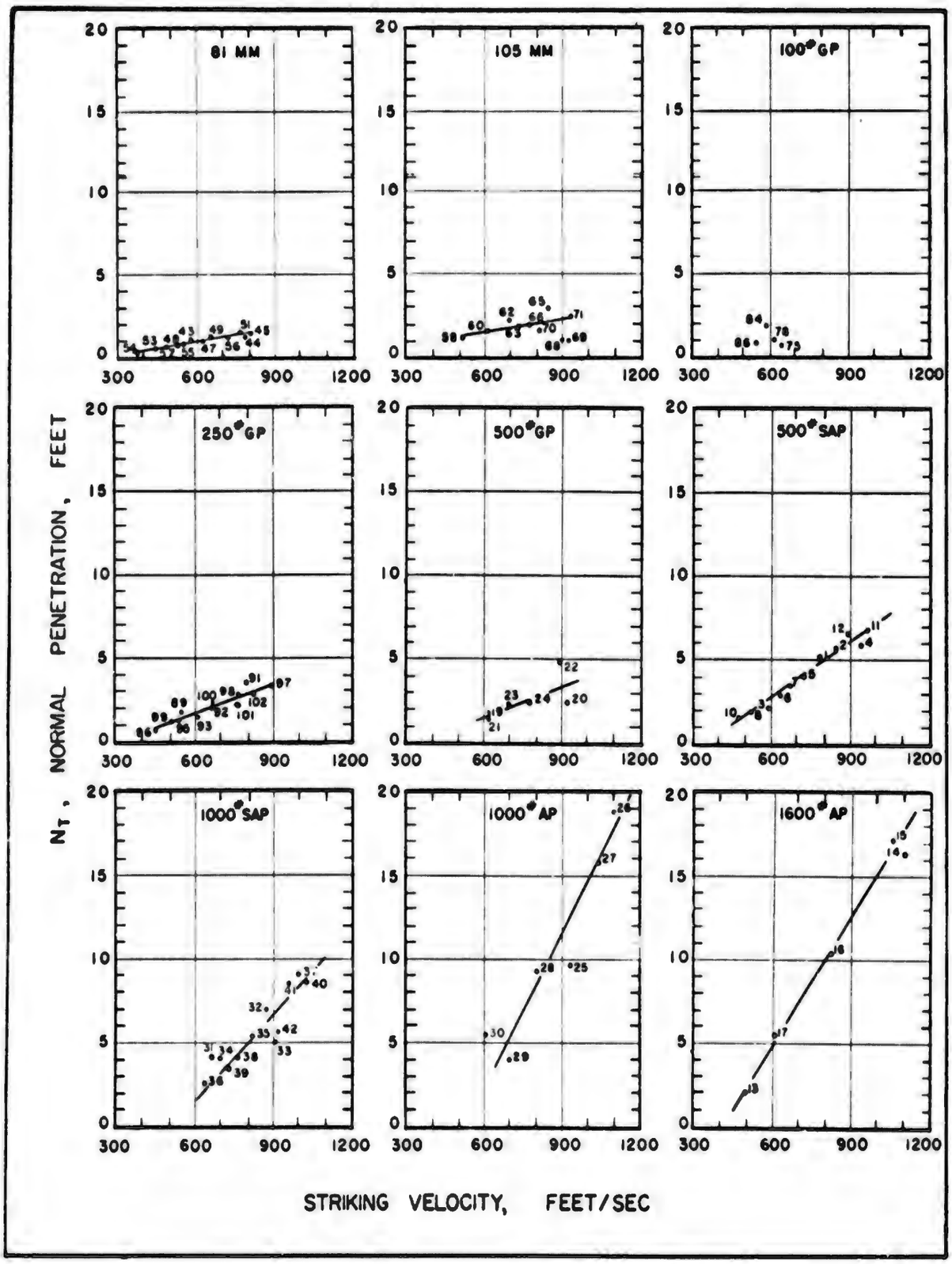

Figure 26. Normal penetration vs striking velocity.

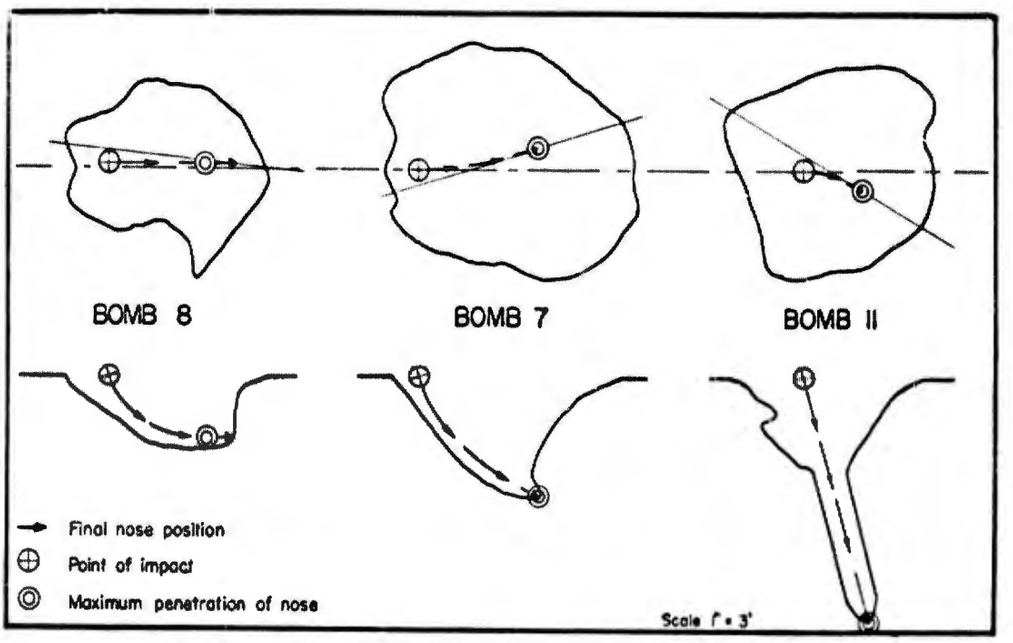

Figure 27. Comparison of craters produced with change of impact energy.

It seems desirable as a first step to consider the energy relations, as the type of failure changes and the evidence suggests that the variation in path shape and crater shape may depend upon the manner in which energy is partitioned to the medium, rather than, as assumed by Poncelet, upon Newton's second law.

The underground trajectory of a bomb is influenced by the mass of the bomb, the striking velocity, the diameter, the shape of the nose of the bomb, the slenderness ratio of the bomb, the angle of impact, and the type of material. A certain degree of geometric similarity exists among various sizes of bombs of the same type, but the variation in nose shape and slenderness ratio (Table I) of the bombs dropped at Fort Churchill is such that each size bomb will be treated as a different type at first. Although the surface of the Fort Churchill bombing range is level, the striking angle varies, depending upon the altitude of release. Variation in striking angle influences the length of the bomb path (P_{TM}) to a lesser degree than it influences normal penetration (N_T).

Figure 28 summarizes the relation between path length and impact energy. Curves have been drawn as a means of comparing the path length of each of the various types of bombs.

In Figure 29, normal penetration is compared to the impact energy times the sine of the striking angle. The relations are not straight lines on log-log paper, but curves. Comparison of the diagrams shows that the behavior of each type of bomb differs and that the curves for the various types of bombs may differ somewhat.

ANALYSIS OF PENETRATION

Correlation diagrams

The general equation (Livingston and Murphy, 1959) that expresses the model law for explosions is

$$d_c = \Delta E \sqrt[3]{w} \qquad (1)$$ Model law for explosions

where

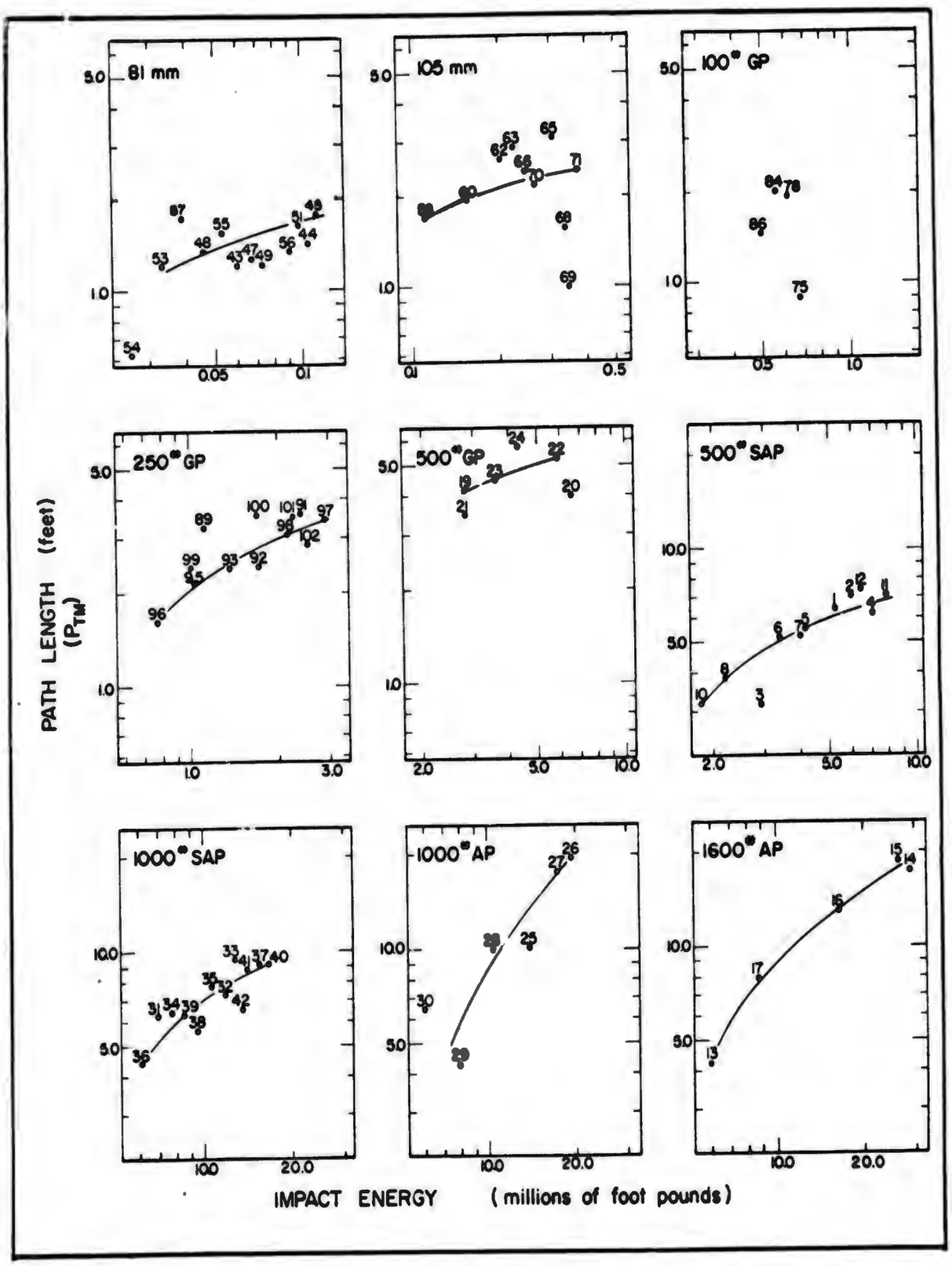

Figure 28. Path length vs impact energy.

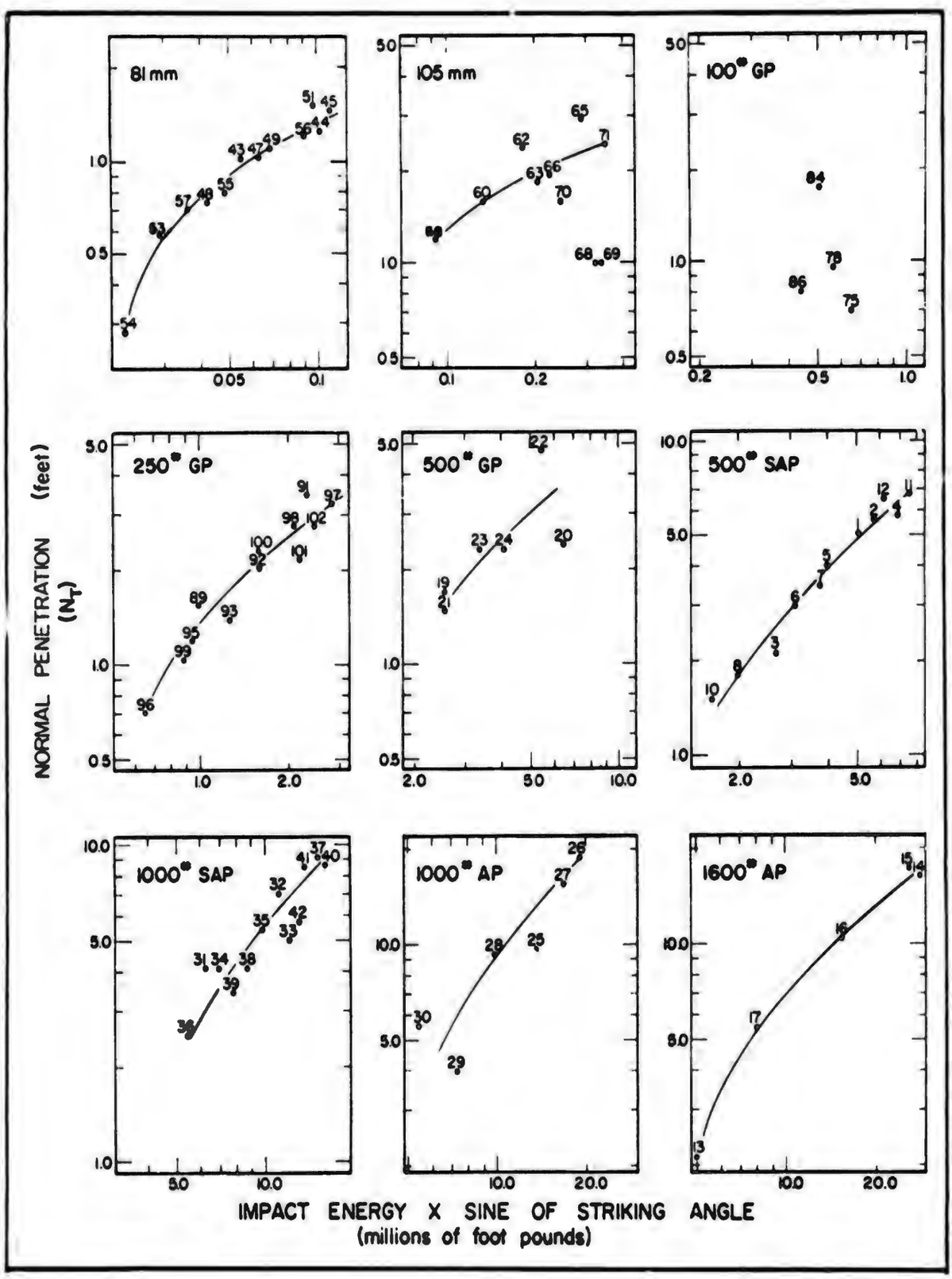

Figure 29. Normal penetration vs impact energy.

d_c is depth of center of gravity of the explosives charge (ft)

Δ is depth ratio

E is strain-energy factor

w is weight of explosives (lb).

The model law can be viewed as expressing a relation between the energy of the explosion and the mass through which the energy is propagated. This relation determines the type and severity of damage. The energy of an explosive is proportional to its weight and is determined by its chemical composition. Impact and explosion are both energy sources. The energy of impact of a projectile determines the type and severity of damage to the medium. If the behavior of the medium depends upon the relation between mass and energy, then perhaps the only fundamental difference between impact and explosion may be the manner in which the energy is partitioned to the medium.

The depth ratio Δ has been demonstrated to be a valid parameter to which energy partitioning may be referred (Livingston and Murphy, 1959). A ratio of volumes, masses, or of energy levels could be used as a parameter instead. In any event, at a given depth ratio, the medium exhibits a definite behavior which may be measured in various terms such as fracture, fragmentation, shock, gas-bubble expansion, crater dimensions, velocity, acceleration, displacement, or fly-rock travel. The standard depth, volume, mass, or energy level has been chosen arbitrarily as that at which the energy of the explosion is dissipated into the mass of earth or rock without damaging the surface above the charge by brittle-state fracture. The critical depth is the standard of reference to which the depth ratio is referred, and it can be measured in the field with little difficulty.

The strain-energy factor E is a measure of the energy absorption capacity of the medium. It depends both upon the manner in which the energy is delivered from its source and upon the ability of the medium to propagate the energy outwardly. It expresses changes in the medium with increased lateral confinement. It also expresses the relative elastic or plastic behavior of the medium at various stress ranges.

If the model law for explosions expresses a fundamental relation between energy and the mass through which the energy is propagated, it should be valid both for impact and for explosion. It is necessary, however, to define a new standard energy level for impact, because the projectile is in motion, whereas the explosive charge is at rest. It is desirable to choose a reference at which a specific event occurs with the sharpest possible transition between energy levels.

The reference chosen here is the depth at which tunneling begins. The criterion established to describe this depth is that the medium be sufficiently deformed by plastic deformation to completely encase the nose of the bomb. This depth, measured normal to the surface of the medium to the point of the nose of the bomb, is the "transition depth" and the standard depth, volume, mass, or energy level that defines the behavior of frozen ground subjected to impact is based upon this transition depth. The ratio of depths, volumes, masses, or energy levels between the situation observed and the situation at the transition depth is the "transition ratio".

Rewriting the model law for explosions using analogous terms, we may postulate a model law for impact of the form

$$y = \tau m \sqrt[3]{I} \qquad (2)$$

Model law for impact (postulated)

where

y is the vertical distance, ft, from the surface of the frozen ground to the nose of the bomb

τ is the transition ratio

m is the materials factor

I is impact energy, ft-lb .

In Figure 30, penetration N_T is plotted on log-log paper against impact energy I. As N_T (see Fig. 21) is a vertical distance at maximum penetration, it is analogous to y in eq 2. At any given value of τm, the equation $N_T = \tau m \sqrt[3]{I}$ is a straight line of slope 1 in 3 on log-log paper.

All bombs and shells dropped during the tests are plotted by bomb number on the correlation diagram, using values of N_T and I from the data sheets.

The depth at which tunneling begins was obtained from the crater cross-sections by interpolation between increments of altitude of successive bomb drops. The resulting transition depth was plotted on the correlation diagram against the interpolated numerical value of impact energy.

Livingston (1956, p. 1-11) has demonstrated that various ranges of similar behavior in cratering occur as a result of energy transfer in blasting. Penetration may be similarly classified utilizing similar principles. The offset lines of Fig. 30 that separate the tunneling range from the cratering range were drawn using successively the transition depths of the 81-mm shell, the 105-mm shell, the group of GP and SAP bombs except the 500 SAP, and the group of AP bombs plus the 500 SAP bomb. Equations of the lines were computed at τ equals 1.0 assuming m to remain constant for a limited range of impact energy.

The procedure may also be used to obtain an equation separating projectiles that have produced craters by brittle-state failure from projectiles that have ricocheted. Because of the limited number of bomb drops, the ricochet limit for the mortar shells and small bombs cannot be established with high accuracy. Moreover a difference of one-tenth foot in normal penetration produces a substantial difference in the numerical value of the product τm at low values of impact energy I. Accordingly, the limit between the cratering range and ricochet range is established here with reasonable accuracy for the large bombs, but with lesser accuracy for the mortar shells and small bombs.

It is apparent by inspection of the correlation diagram that the postulated model law upon which the diagram is based has a reasonable degree of merit. However, before further investigating model relations postulated upon the manner in which energy is partitioned to the medium in the tunneling range, the cratering range, and the ricochet range, let us review penetration formulas derived from Poncelet's original concepts.

Review of penetration formulas

The Petry formula is a modification of the Poncelet formula, which was derived using Newton's second law, assuming the resistance to penetration to be jointly proportional to the strength of the material and the inertia of the material removed from the zone of penetration. Petry assumed that the materials factor of Poncelet's formula was a constant for a given material. The Petry formula is

$$X = kP \log_{10} \left(1 + \frac{V^2}{215,000}\right) \qquad \text{Petry formula}$$

where

X is total path length, ft

k is a constant depending on the material

P is a sectional pressure (weight, lb, divided by maximum cross-sectional area, in^2)

V is striking velocity, ft/sec.

The curves of Figure 31 were calculated from the Petry formula using $k = 2.2$; k was calculated using values of X, P, and V for 500 SAP and 1000 SAP bombs obtained in Fort Churchill tests.

In general, the agreement with field data is better for the small than for the large bombs. For all practical purposes, the agreement is so close for the shells, general-purpose bombs, and the semi-armor-piercing bombs that use of the Petry formula is justified. But the formula is at variance with the field data for the armor-piercing bombs. At low velocities the result is too high, and at high velocities the result is too low.

As the same value of k gave the best agreement throughout, and the agreement for the shells is as good as for the general-purpose and semi-armor-piercing bombs, it would appear that the materials factor, k, for frozen peat is the same as for frozen glacial till. This is inconsistent with the equations presented in the correlation diagram (Fig. 30).

The modified Petry formula is written in the form,

$$X = KPS \qquad \text{Modified Petry formula}$$

where

X is total path length

P is sectional pressure

K is a constant depending upon the nature of the material

S is a constant depending upon the striking velocity V.

Laboratory tests (Livingston and Smith, 1951, p. 114-118) in which K and V were held constant demonstrate that path length in a given medium and at a given striking velocity is not directly proportional to sectional pressure. However, the formula

$$X = kP\log_{10}\left(1 + \frac{V^2}{215,000}\right)$$

may be interpreted somewhat differently than the modified Petry formula. Inasmuch as

$$P = \frac{W}{0.785d^2}$$

it may be considered that penetration varies directly as impact energy and approximately inversely as the square of the diameter of the projectile.

The "old NDRC" formula and the "new NDRC" formula were derived as a result of penetration tests on concrete.

The "old NDRC" formula is

$$y = \frac{222P \cdot d^{0.215}V^{1.5}}{Y} + 0.5d \qquad \text{Old NDRC formula}$$

where

y is normal penetration (in.)

P is sectional pressure (lb/in^2)

d is bomb diameter (in.)

V is velocity in units of 1000 ft/sec

Y is a materials factor and is equal to the square root of the compressive strength of the material.

As the sectional pressure P appears in the numerator of the formula together with $d^{0.215}$, the formula states that penetration varies inversely as $d^{1.785}$. In the Petry formula, penetration is stated to vary inversely as the square of the diameter. In the Livingston penetration formula for rocks (eq 3) penetration is stated to vary inversely as the diameter to the first power.

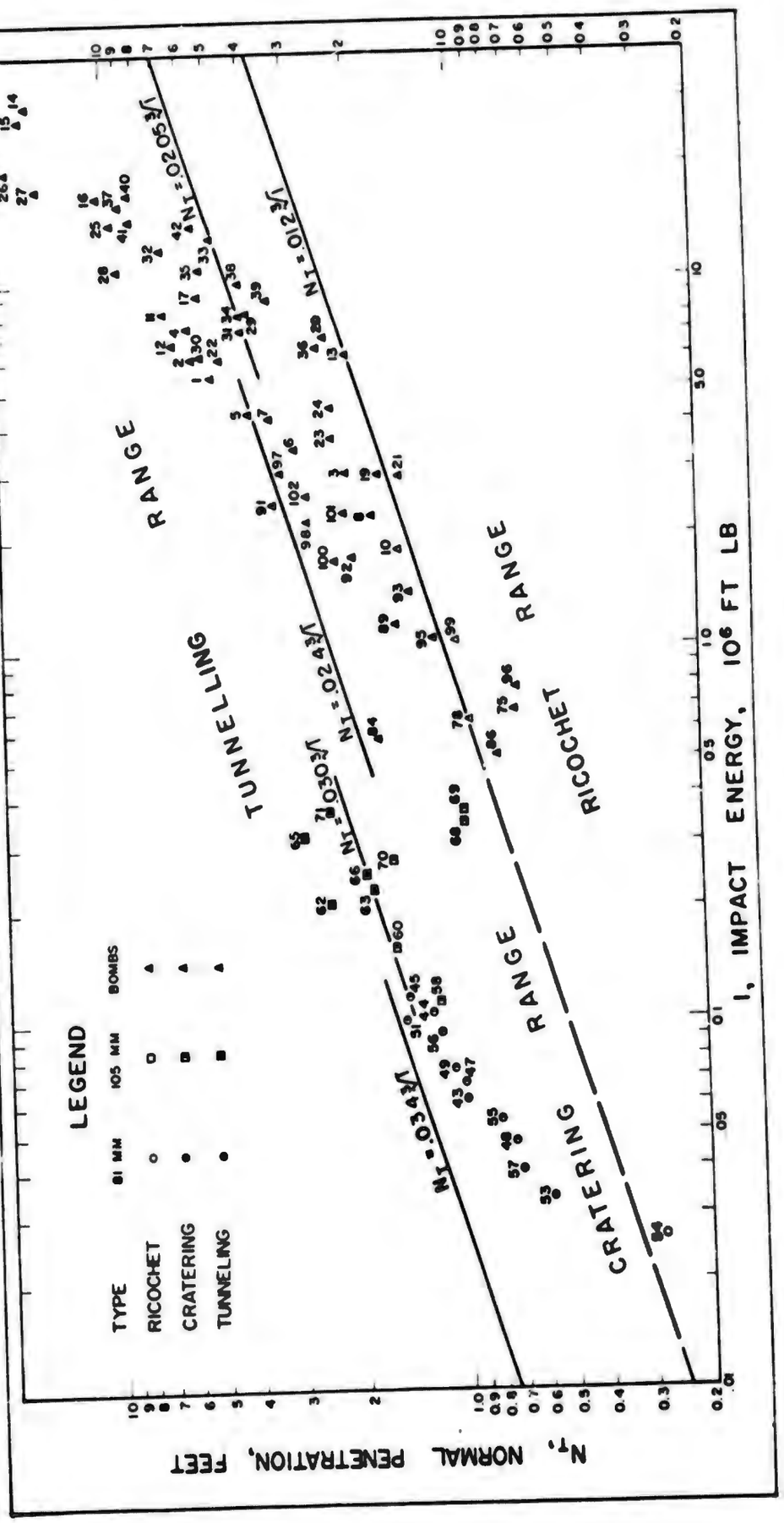

Figure 30. Correlation diagram.

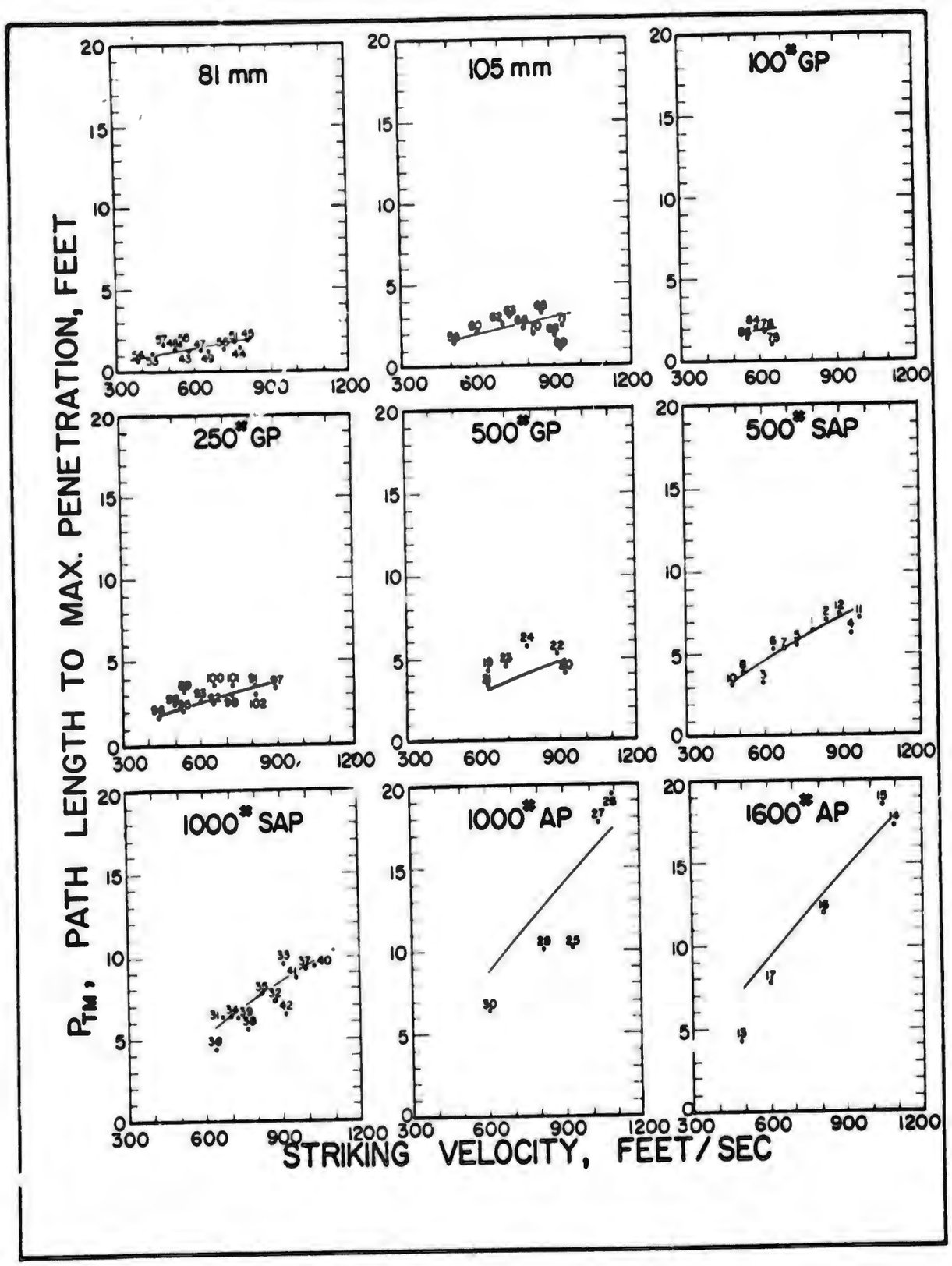

Figure 31. Observed penetration compared to penetration calculated by the Petry formula.

The "old NDRC" formula states that penetration varies inversely as the square root of the compressive strength of the material. Laboratory experiments on the relation between penetration and compressive strength and bomb penetration tests in granite and sandstone demonstrate that penetration is unrelated to the strength of the material either in simple tension or in simple compression (ibid., p. 118-119).

The "old NDRC" formula states that penetration varies as the 1.5 power of the striking velocity. The "new" NDRC formula states that penetration varies as the 1.8 power of the velocity. The Petry formula states that penetration varies as the square of the velocity.

The curves of Figure 32 show the relation between the observed penetration and penetration calculated using the "old" NDRC formula. The value of the materials factor Y was obtained using the data of Figure 6 in which the compressive strength is 1100 psi. Figure 32 shows reasonable agreement for the shells and the general-purpose bombs with the observed results, but disagreement for the semi-armor-piercing and armor-piercing bombs is greater than with the Petry formula.

The "new" NDRC formula is

$$Y = KN\,d^{0.2}\,D\,V^{1.8} + 1.0 \qquad \text{New NDRC formula}$$

where

Y is normal penetration in calibers

K is a target factor

N is a nose factor $= 0.72 + 0.25h$, where h equals caliber radius head, or the radius of the ogive divided by the bomb diameter

d is the diameter of the bomb, in.

D is sectional density of the bomb (W/d^3)

V is striking velocity in units of 1000 ft/sec.

The significant changes in the "new" NDRC formula are: 1) to introduce a nose factor that is dependent upon the caliber radius head of the bomb nose and 2) to establish the relation that penetration depends upon the sectional density (rather than upon the sectional pressure), and varies inversely as the 2.8 power of the diameter of the bomb. From field data and values of the nose factor, the numerical value of K was found to vary from 4 to 11. Because of this great variation, it was impossible to compare the "new" NDRC penetration formula with the field results.

The RRL formula is

$$y = \frac{K}{S^{.25}} \frac{W}{d^2} \left(\frac{V}{1750}\right)^n \qquad \text{RRL formula}$$

where

y is normal penetration, in.

K is a target factor

W is weight of bomb, lb

d is diameter of bomb, in.

V is striking velocity, in units of 1000 ft/sec

S is compressive strength of material, lb/in^2

n is $\frac{10.7}{S^{.25}}$.

The RRL formula states that penetration varies inversely as the square of the diameter. The target factor K includes various constants of proportionality. The

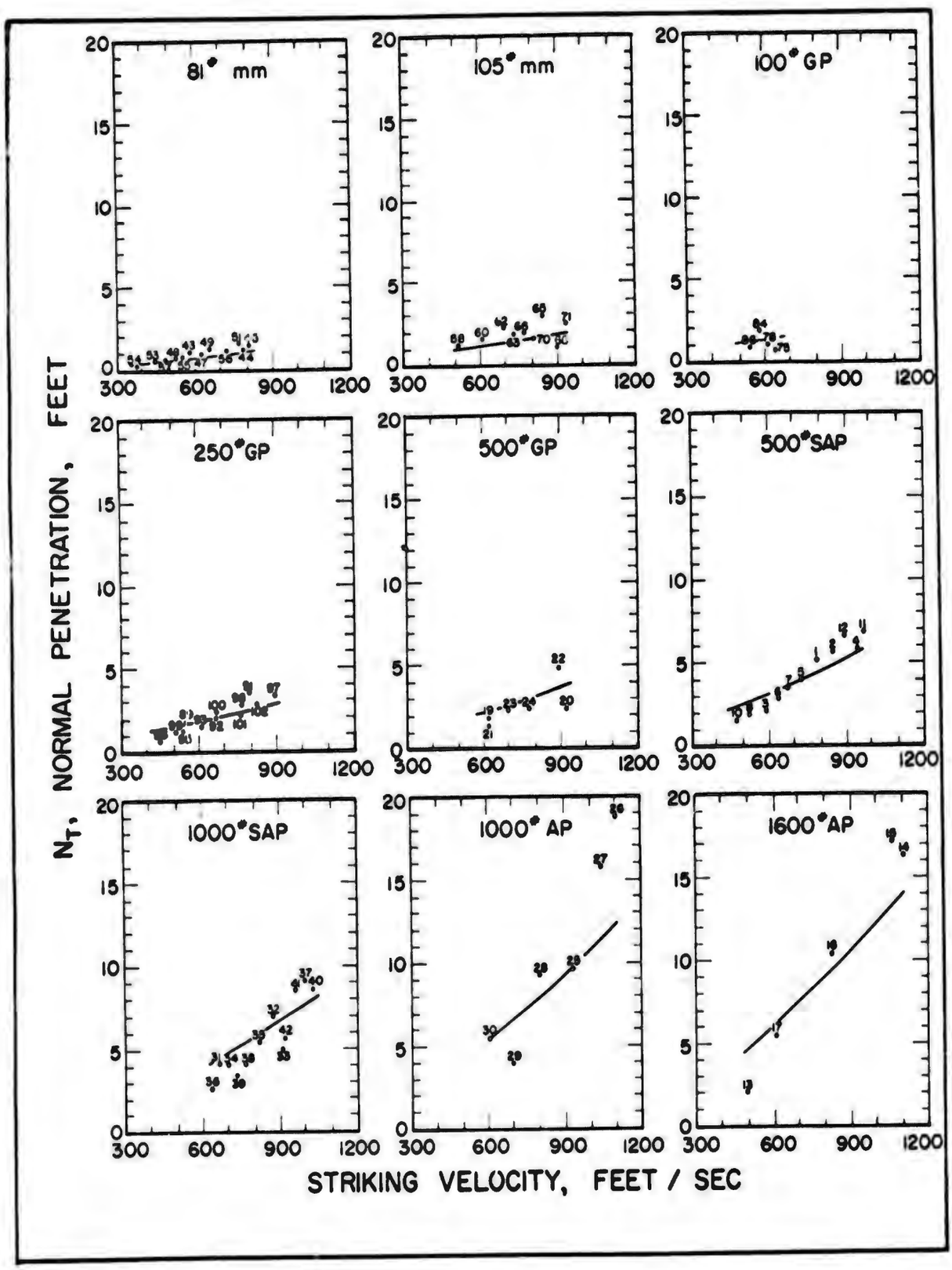

Figure 32. Observed penetration compared to penetration calculated by the old NDRC formula.

first term of the equation includes both K and the compressive strength of the material, hence may be considered to be a materials factor and to be constant at any stress range.

The compressive strength of frozen glacial till is 1100 psi; thus n of the RRL formula equals 1.858. Accordingly, normal penetration is stated to vary as the 1.858 power of the velocity.

Using the field data, the average value of the target factor K was found to be 334. This value, when substituted in the RRL formula, yields the curves of Figure 33. Results are within practical limits of accuracy for the small bombs and at low striking velocities. As the striking velocity increases, the RRL formula produces penetrations less than observed in the field. The points above the curves, particularly for the 500 SAP, 1000 SAP, and 1600 AP bombs, are all in the tunneling range (see Fig. 30).

The tentative linear relation presented in Figure 26 appears to be in better agreement with the facts than the concave upward curves obtained using the RRL formula (Fig. 33), the concave downward curves obtained using the Petry formula (Fig. 31), or the concave upward curves obtained using the "old" NDRC formula (Fig. 32).

Although the Petry formula, the NDRC formula, and RRL formula are sufficiently accurate for small projectiles and for low striking velocities, the error in estimating normal penetration or path length increases as the size of the projectile increases or as the striking velocity increases. A somewhat analogous situation was found in bomb penetration tests on granite and sandstone. Moreover, the error is greater for the armor-piercing than for other types of projectiles. Figure 30 shows that most of the armor-piercing bombs penetrated into the tunneling range. As a primary requisite for producing foxholes in frozen ground is that the projectile penetrates into the tunneling range, it is necessary to develop a penetration formula that is valid in the tunneling range.

All of the formulas include terms that express the effect of bomb diameter, materials factor, and striking velocity. Therefore a change of one variable in a given formula automatically results in a corresponding change in the other variables. For example, if penetration is represented by a general formula of the form

$$X = NR^x d^y V^z$$

where

X is path length

N is a combined nose factor and constant of proportionality

R is a materials factor

d is a projectile diameter

V is velocity,

x, y, z are exponents of R, d, and V respectively. Then, if the path length is constant, a change in y automatically results in a change in z or x, or in both z and x. It is necessary that the difference in effects of each of the three variables of the various penetration formulas be reconciled if penetration is to be placed upon a fundamental rather than an empirical basis.

Penetration of bombs in rock

Review of penetration formulas and comparison with the results of field and laboratory work done in the Bomb Penetration Project (Livingston and Smith, 1951) indicated that the formulas were inapplicable to granite and sandstone. The Livingston penetration formula was developed:

$$P = R\frac{N}{d}Q \qquad (3)$$

where

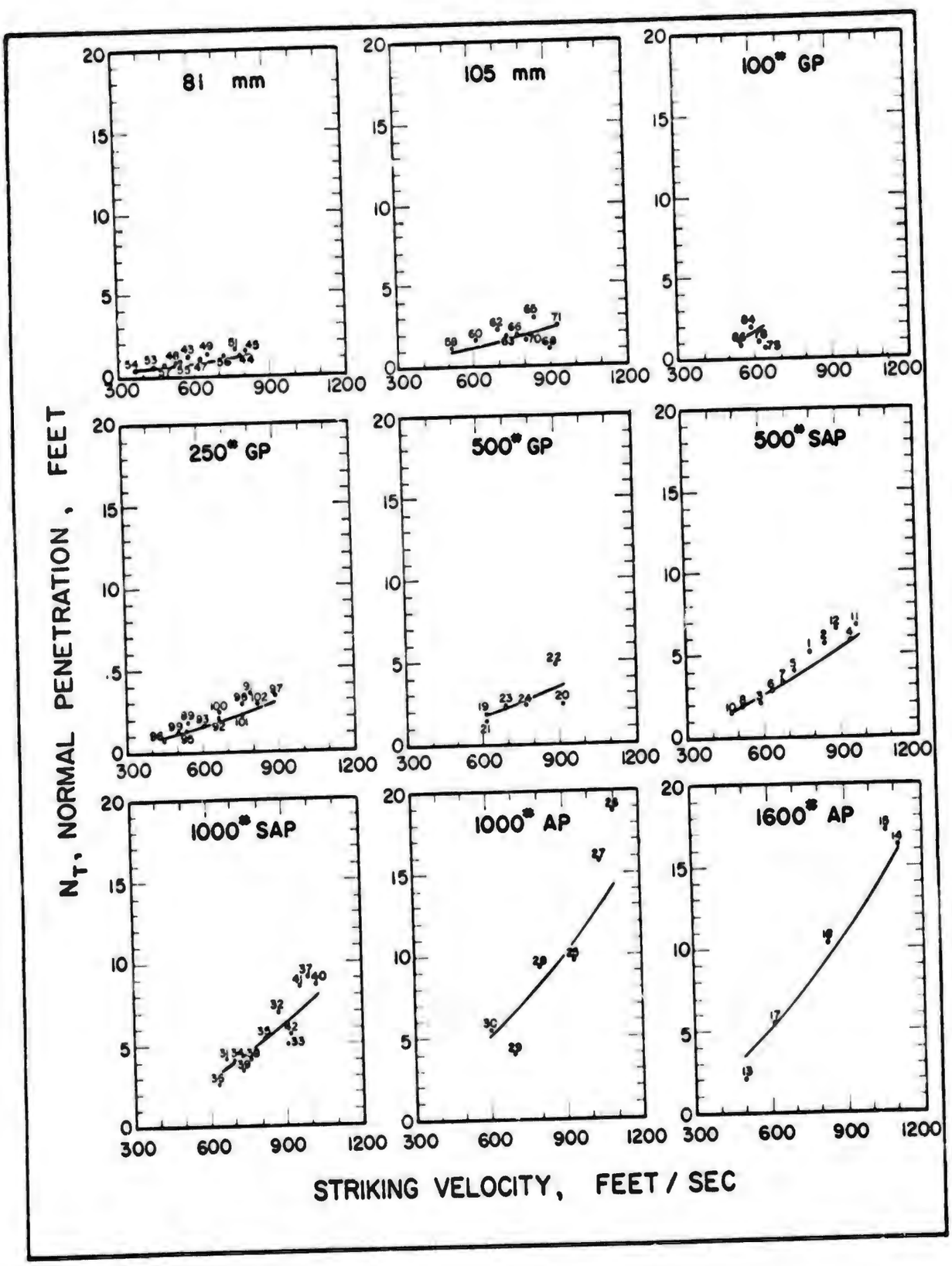

Figure 33. Observed penetration compared to penetration calculated by the RRL formula.

P is nose penetration, ft

R is a rock factor, a term which states that penetration varies inversely as the lateral component of stress induced in the medium as a result of the axially applied stress

N is a nose factor

d is the diameter of the bomb, ft

Q is a term that is determined empirically and is related both to impact energy and increased resistance to penetration at depth.

Although the Livingston penetration formula was derived from penetration tests on rocks, it is believed to be applicable also to concrete and other structural materials that exhibit predominantly brittle-state failure. The Livingston penetration formula differs from earlier formulas in that penetration is not considered to be primarily dependent upon either the sectional density or the section pressure of the projectile. Instead of assigning different constants to each of various types of materials, Livingston applies a rock factor that is a variable rather than a constant. The rock factor is referred to a prototype rock, Dakota sandstone, and is stated in terms of Poisson's ratio m_x of the material in which penetration is to be measured, rather than in terms of physical properties such as the tensile, compressive, or shear strength. Because Poisson's ratio is not a constant but varies both with stress range and with the degree of lateral confinement, the rock factor is a variable:

$$R = \frac{m_s(1-m_x)}{m_x(1-m_s)}$$

where

m_s is Poisson's ratio of Dakota sandstone at the stress range (5000 psi) at which failure occurs in simple compression

m_x is Poisson's ratio of rock $\underline{x}$ at the same stress range.

At 5000 psi, Poisson's ratio of the prototype rock, Dakota sandstone, is 0.287. Substituting this value for m_s, the rock factor reduces to

$$R = \frac{1-m_x}{2.484\,m_x}.$$

Penetration by plastic deformation

Introduction. The error in estimating normal penetration or path length in frozen glacial till, using one of the generally accepted penetration formulas, increases as the size of the projectile increases or as the striking velocity increases. A somewhat analogous situation was found in bomb penetration tests on granite and sandstone, and the desirability of accumulating additional information on the relative elastic or plastic behavior of rocks at various stress ranges was recognized.

It has been observed that a brittle substance such as Zuni granite fails in part as a brittle solid and in part by plastic deformation at high stress ranges. (Livingston and Smith, 1951). In a sense, frozen Churchill till is a "rock" type, for it exhibits both brittle-state failure and plastic deformation. However, the transition from brittle-state failure to plastic deformation with a given type of projectile occurs at a lower value of impact energy in Churchill till than in granite or sandstone.

The transformation from brittle-state failure to plastic deformation in a given material occurs at a lower value of impact energy for armor-piercing than for semi-armor-piercing bombs. Similarly, the transformation occurs at a lower value of impact energy for semi-armor-piercing than for general-purpose bombs. The effect of a change in the type of bomb that strikes a given material is analogous to the effect of a change in the type of material that is struck by a given type of projectile. It

appears, therefore, that the behavior of materials is relative and that what is observed for a given material in a given range of behavior may be applicable to another material in the same range.

Each of the generally accepted penetration formulas appears to properly reflect behavior in the range in which the various experiments were conducted, but little consideration has been given to the possibility that the behavior of a given material might not remain constant as the scale of the experiment was changed. Inasmuch as now it is known that the depth of penetration increases as the proportion of plastic deformation to brittle-state failure increases, it may be that different laws determine penetration by "pure" brittle-state failure than by "pure" plastic deformation.

It is impossible to search out these laws completely, within the scope of the present test program. However, as the proportion of plastic deformation to brittle-state failure is greater for frozen Churchill till than for either granite or sandstone, it seems desirable to utilize the available data to explore fundamentals of penetration by plastic deformation. It is impossible completely to separate the effect of brittle-state failure from the effect of plastic deformation, because frozen Churchill till exhibits both in varying proportions. The separation should be best for those drops that result in a high numerical value of the transition ratio, τ.

Let us assume that the terms "solid" and "fluid" are relative terms, and that frozen Churchill till, when subjected to stresses such as in the current test program, exhibits a range of behavior that lies somewhere in the transition from an ideal solid to an ideal fluid.

The fluid flow analogy. Let us draw an analogy between plastic deformation and fluid flow, and investigate the relation between path length and resistance to flow.

In accordance with the laws of penetration of a solid into a fluid, the resisting force, or drag, offered by the medium is

$$R_2 = C_D \rho a \frac{v^2}{2}$$

in which

R_2 is the resisting force

C_D is a coefficient of drag (dimensionless)

ρ is the density of the fluid

a is the cross-sectional area of the penetrating body projected on a plane normal to the direction of motion

v is the velocity.

When a projectile penetrates a yielding solid, it may be assumed that there is also a component of resistance proportional to the velocity (as would be the case in low velocity penetration into a fluid--viz. Stokes' Law):

$$R_1 = C_1 v.$$

Then the total resistance is

$$R = R_1 + R_2 = C_1 v + C_D \rho a \frac{v^2}{2}.$$

For convenience let $(1/2)\ C_D \rho a = C_2$

$$R = C_1 v + C_2 v^2.$$

The work done by the resisting force as the bomb moves a distance ds is

$$d(\text{Work}) = R\,ds. \qquad (4)$$

If, as the bomb moves the distance ds, its velocity changes from (v + dv) to v, the change in kinetic energy is

$$d(KE) = \frac{W}{2g}\left[(v+dv)^2 - v^2\right]$$

where

W = weight of the bomb

g = acceleration of gravity.

Neglecting $(dv)^2$, a differential of higher order,

$$d(KE) = \frac{W}{g} v\,dv. \tag{5}$$

As a first approximation, the work done on the bomb may be equated to the change in its kinetic energy, neglecting work done in deforming the bomb and the change in potential energy.

$$d(\text{work}) = d(KE)$$

$$(C_1 v + C_2 v^2)\,ds = \frac{W}{g} v\,dv$$

$$ds = \frac{W}{g}\,\frac{dv}{(C_1 + C_2 v)}. \tag{6}$$

Equation 6 may be integrated through the interval of motion.

$$\int_0^L ds = \frac{W}{g}\int_V^0 \frac{dv}{(C_1 + C_2 v)} \tag{7}$$

in which

L is the path length

V is the velocity at which the bomb enters the medium.

From eq 7

$$L = \frac{W}{C_2 g}\ln\frac{C_1}{C_1 + C_2 V}$$

$$= \frac{2W}{C_D \rho a g}\ln\frac{C_1}{C_1 + \frac{C_D \rho a V}{2}}.$$

Substituting $\frac{\pi D^2}{4} = a$ and $\delta(\text{unit weight}) = \rho g$

$$L = \frac{8W}{C_D \delta \pi D^2}\ln\frac{C_1}{C_1 + \frac{C_D \rho \pi D^2 V}{8}}.$$

Let $\frac{C_D \pi}{8} = C_3$

$$L = \frac{W}{C_3 \delta D^2}\ln\frac{C_1}{C_1 + C_3 \rho V D^2}. \tag{8}$$

Equation 8a expresses the path length of a bomb penetrating a solid in terms of the weight and diameter of the bomb; the striking velocity of the bomb, the density ρ and unit weight δ of the material penetrated, and two coefficients, C_1 and C_3, which are related to the material and its resistance to penetration by the bomb. The equation is difficult to evaluate because C_1 and C_3 are variables rather than constants, and the variation depends in a complex manner upon a series of factors. It is desirable at this state to evaluate the equation empirically using the field data. In doing so, features that are difficult to evaluate precisely are included in the numerical value of the coefficients.

Letting

$$\ln \frac{C_1}{C_1 + C_3 \rho V D^2} = Q$$

the equation becomes

$$L = \frac{Q}{C_3} \cdot \frac{W}{\delta D^2} \qquad (8a)$$

and

$$\frac{Q}{C_3} = \frac{L \delta D^2}{W}.$$

Using the path length L the unit weight of material penetrated δ, the bomb diameter D and weight W, the ratio Q/C_3 was evaluated for each projectile from the test data. Figure 34 summarizes the calculations. The unit weight was computed for each test drop using the crater cross sections which recorded the thickness of frozen peat (δ = 75 lb/ft^3) and frozen Churchill till (δ = 148.7 lb/ft^3).

The relations presented in the figure together with those of Figure 25 are interpreted to mean that, within the range of the test data, the ratio Q/C_3 is a linear function of velocity. The equation of the line that describes the variation of Q/C_3 with the velocity is of the form

$$y = mx + b.$$

To avoid confusion of symbols, the slope of the line is designated as $\Delta y/\Delta x$. The slope of the line is greater for the armor-piercing than for the semi-armor-piercing bombs, and greater for the semi-armor-piercing than for the general-purpose bombs. Also b is a negative number for all bombs. Preliminary values of the slope and of the y intercept are summarized in Table III for each type of bomb.

Table III. Preliminary values of $\frac{\Delta y}{\Delta x}$ and b of eq 9.

Bomb	$\frac{\Delta y}{\Delta x} \times 1000$	b
81-mm shell†	1.667	-0.443
81-mm shell	2.386	-0.598
105-mm shell	2.386	-0.598
250 GP bomb	2.386	-0.598
1000 SAP bomb	2.680	-0.698
500 GP bomb	2.838	-0.504
500 SAP bomb	2.846	-0.732
1600 AP bomb	3.008	-0.979
1000 AP bomb	4.475	-2.205

† Values from 81-mm drops that penetrated frozen peat only.

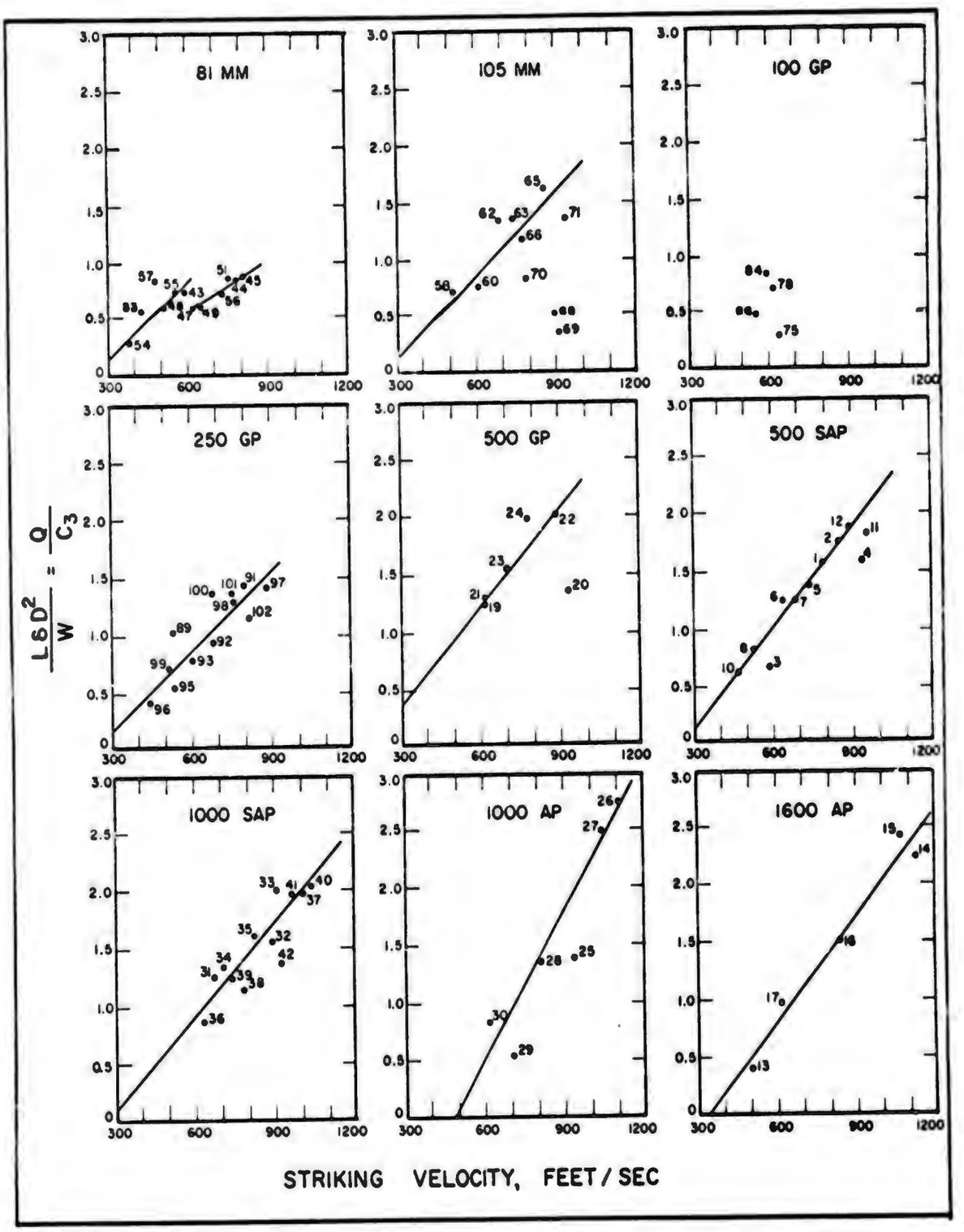

Figure 34. Variation of Q/C_3 with striking velocity.

The number of test drops with a given type of projectile in a composite of snow, peat, and till is too small to evaluate $\frac{\Delta y}{\Delta x}$ and $\underline{b}$ exactly. For this reason, the table is designated "preliminary". Equations of the lines have not been determined by the method of least squares.

Path length of each of the test projectiles can be calculated from Table III by rewriting eq 8a

$$L = \frac{W}{\delta D^2}\left(\frac{\Delta y}{\Delta x} V + b\right). \qquad (9)$$

The path length as measured in the field and the calculated path lengths are compared in Figure 35. Eq 9 produces better agreement between observed and theoretical values, including values in the range where tunneling predominates, than does the Petry formula (Fig. 31).

Curves of the path length vs energy of impact calculated from eq 9, Table III, and the average weight of projectiles of a given class dropped at Fort Churchill are shown in Figure 36.

Range of similar behavior in penetration

Figure 30 classifies the behavior of frozen Churchill till into three ranges of similar behavior in penetration, designated as the tunneling range, the cratering range, and the ricochet range. Each range is characterized by a given range of behavior of path shape, crater shape, and type of fracturing and degree of fragmentation. Regardless of the size or shape of the projectile or of the striking velocity, two projectiles with the same transition ratio τ produce craters that appear geometrically similar within normal limits of dispersion. Any discrepancies are minor and possibly indicate that the transition depth for a given type of projectile may differ slightly from the group average used in Figure 30. Because of the comparatively small number of drops with each type of bomb, it is impossible at present to determine the transition ratio more accurately.

A change in τ is accompanied by a change in the size or shape of the crater and in the shape of the underground trajectory. In the cratering range, the shape of the crater is controlled by brittle-state failure of the medium. At the upper limit of the cratering range, τ equals 1.0, and the depth, diameter, and volume approach a maximum. As the transition ratio increases beyond 1.0, the projectile tunnels below the bottom of the crater, and the length of the tunnel increases as τ increases.

Certain type of bombs are capable of penetrating further into the tunneling range than others. For example, at terminal velocity, a 1000 AP bomb is capable of penetration to $\tau = 3.5$; a 500 SAP bomb is capable of penetrating to $\tau = 1.6$; and a 500 GP bomb is capable of penetrating to $\tau = 1.1$.

A primary prerequisite of a projectile intended for making trenches and foxholes in frozen ground is that it penetrate sufficiently into the tunneling range to bury itself completely within the tunnel below the crater. Accordingly, it is essential not only to understand why a projectile penetrates to a given depth, but also to understand why certain projectiles are capable of achieving greater values of τ than others.

The underground trajectory

The underground trajectory of a projectile depends both upon the projectile and upon the medium, and it seems impossible to separate the two effects. An analogous situation exists with respect to underground explosions, and it has been found impossible to treat the explosive and the medium as separate and independent variables.

Figure 27 demonstrates that deviation of the path of a projectile from the line of action at impact decreases as the transition ratio, τ, increases. Study of underground trajectories of projectiles of the Fort Churchill tests reveals that the underground trajectory of projectiles that achieve a sufficiently high value of τ is a straight line that coincides with the line of action at impact. The view is held here that the shape of the underground trajectory is determined by the degree to which failure occurs in the brittle state or in the plastic state, and that the proportions of the two types of failure change as the striking velocity increases. Deviation of the trajectory from the line of action at impact increases as the proportion of brittle-state failure increases.

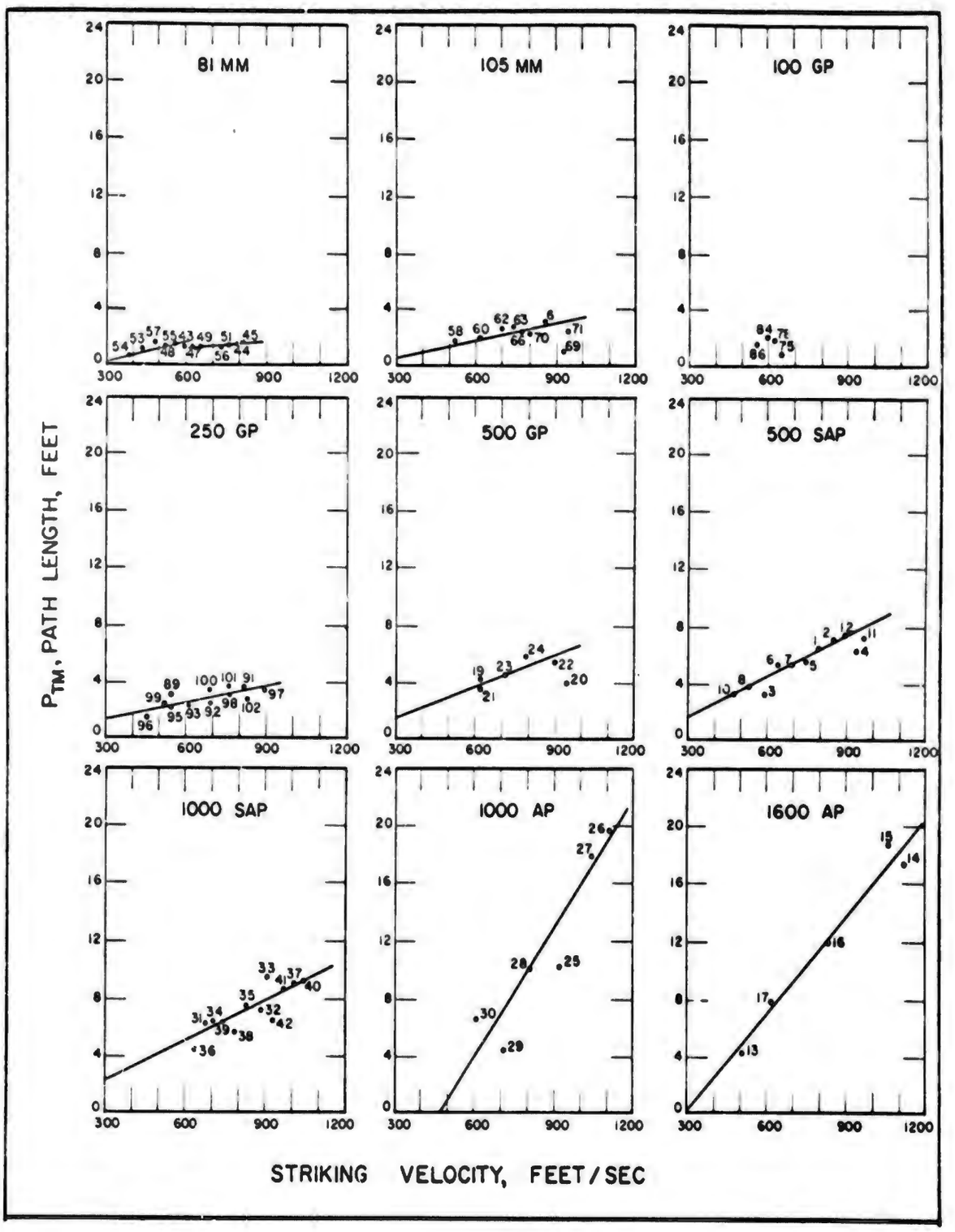

Figure 35. Observed and calculated path length vs striking velocity.

Normal penetration in relation to path length and striking velocity

If the underground trajectory of a projectile is a measure of the resistance offered by the medium at right angles to or parallel to the direction of motion of the projectile, and is dependent upon the degree to which the medium fails in the brittle state or in the plastic state, it would not be surprising to find that the ratio between normal penetration and path length is a function of τ. If a projectile does not deviate from the line of

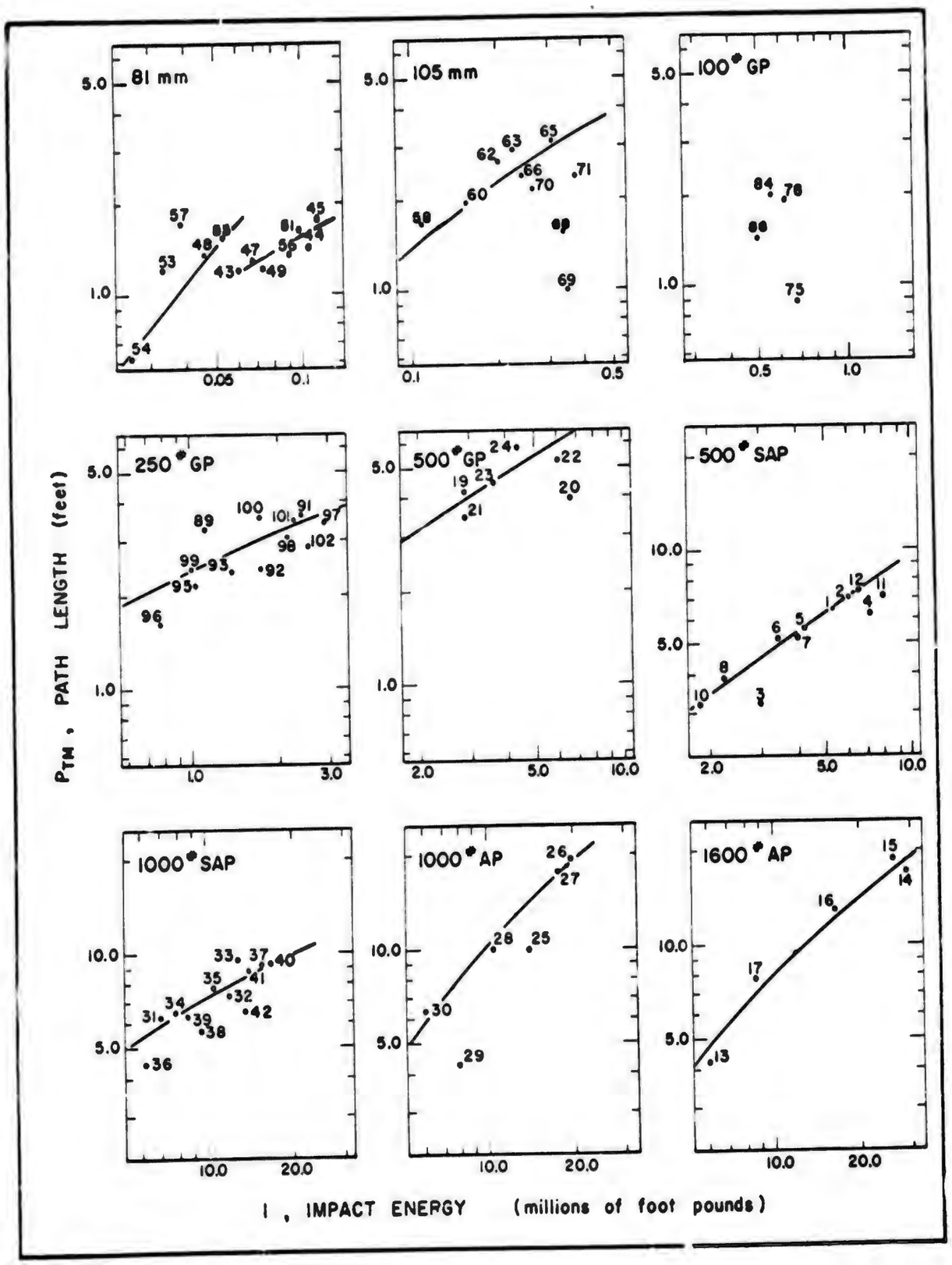

Figure 36. Observed and calculated path length vs impact energy.

action at impact and penetrates in a straight line, the normal penetration equals the path length times the sine of the striking angle, and the effect of brittle-state failure is negligible. As deviation from the line of action increases, the trajectory curves upward under the influence of brittle-state failure at the surface of the medium, and the ratio of normal penetration to path length decreases from the theoretical ratio for straight line penetration.

The upper, dashed-line curves of Figure 37 represent the theoretical ratio of N_T to P_{TM} for straight-line penetration at various striking velocities. The curves were constructed for each type of projectile, using the bombing tables to obtain the angle of fall and the striking velocity at impact, assuming the ground speed at release to be 250 mph. Most projectiles of the Fort Churchill tests were released at ground speed near 250 mph. Ratios N_T to P_{TM} for each bomb-drop were obtained from the crater measurements and plotted against the striking velocity of the projectile. The few points which fall above the dashed-line curve demonstrate the experimental error of Figure 37, 1) because the striking angle was greater than predicted, 2) the altitude of the aircraft was reported slightly in error, or 3) the ground speed of the aircraft was less than 250 mph. Most of the points fall below the theoretical limit.

The solid-line curves of Figure 37 are a means of averaging the field data. The vertical distance between the solid and dashed lines decreases as the striking velocity increases, and is proportional to the deviation of the underground trajectory from a straight line. The velocity corresponding to the intersection of the two curves is a first approximation of the transition velocity at which brittle-state failure ceases to influence the shape of the underground trajectory. Inspection shows that the transition velocity is different for each different type of projectile. It is greater than the terminal velocity of the 500 GP bomb.

The field data demonstrate that the 1000 AP bomb does not deviate from straight-line penetration over the range of striking velocities tested. It appears, therefore, that brittle-state failure has little effect upon the underground trajectory of the 1000 AP bomb. The 1600 AP bomb is similar in shape to a 1000 AP bomb, but it does not achieve straight-line penetration at striking velocities less than 1200 ft/sec.

Normal penetration and path shape are influenced by the angle of impact (Livingston and Smith, 1951, p. 204-206; Fig. 193, 194). The surface of the Fort Churchill bombing range is horizontal and therefore the angle of impact equals the angle of fall at impact. It now is evident that a variation in the slope of the target surface so as to change the striking angle has the same effect upon the shape of the underground trajectory as does a change in striking angle upon a horizontal surface. At a given striking velocity, deviation of the projectile from the line of action at impact decreases as the striking angle increases.

The Livingston penetration equations

Eq 8 may be used to express normal penetration, N_T, by multiplying both sides by θ (the ratio N_T to P_{TM} at a given striking velocity for a given projectile striking a given material).

$$N_T = L\theta = \frac{W\theta}{C_3 \delta D^2} \ln \frac{C_1}{C_1 + C_3 \rho V D^2}. \qquad (8b)$$

Until C_1 and C_3 can be evaluated separately, it seems desirable to calculate N_T using the equation

$$N_T = \frac{W\theta}{\delta D^2} \left(\frac{\Delta y}{\Delta x} V + b\right). \qquad (9a)$$

Because of the many factors involved in determining θ, the relation between path length and normal penetration must be defined for specific test conditions and target

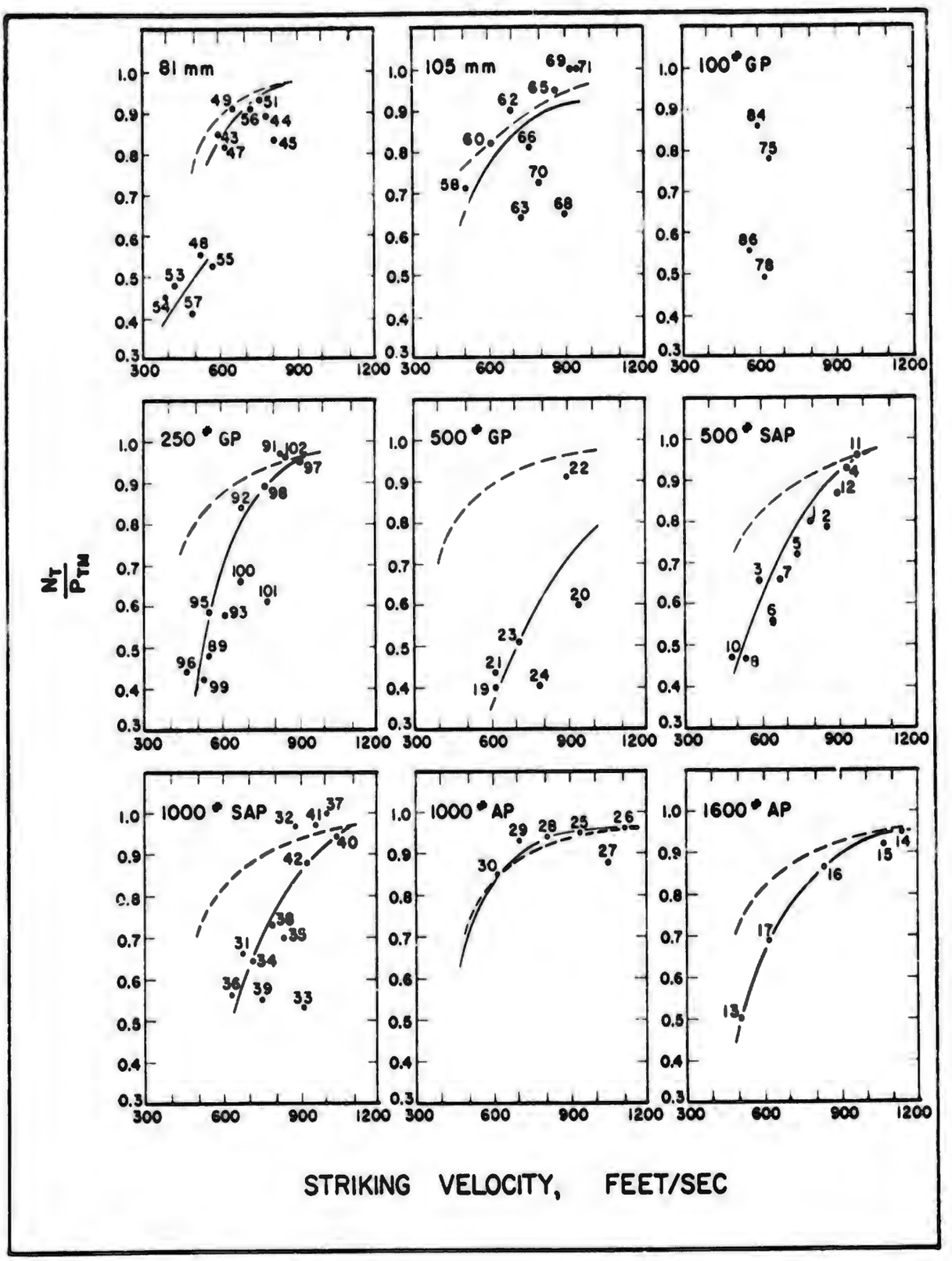

Figure 37. Observed and theoretical ratio N_T/P_{TM}.

material. Normal penetration was calculated from eq 9, using $\theta = N_T/P_{TM}$ from the solid curves in Figure 37, and various assumed striking velocities. The summary curves (Fig. 38) show excellent agreement with the observed data. To achieve such agreement, it is essential not only that the ratio Q/C_3 be reasonably correct, but also that path length vary directly as the weight of the bomb and the first power of the striking velocity and inversely as the unit weight of the material and the square of the diameter of the bomb.

Limits of the ricochet range, the cratering range, and the tunneling range evaluated from eq 2 for various groups of bombs (Fig. 30) are superimposed upon the curves of eq 9a in Fig. 39. The figure serves as a means of evaluating the performance of each of the types of bombs tested.

The Livingston penetration equations are obtained by equating N_T of the plastic deformation analogy to $\underline{y}$ of the explosions analogy. From equations 2 and 9a

$$\tau m \sqrt[3]{I} = \frac{W\theta}{\delta D^2} \left(\frac{\Delta y}{\Delta x} V + b\right).$$

The equations express the transition ratio in the form

$$\tau = \frac{W\theta}{\delta D^2 m \sqrt[3]{I}} \left(\frac{\Delta y}{\Delta x} V + b\right) \tag{10}$$

the plastic deformation index in the form

$$m = \frac{W\theta}{\delta D^2 \tau \sqrt[3]{I}} \left(\frac{\Delta y}{\Delta x} V + b\right) \tag{11}$$

and the ratio Q/C_3 in the form

$$\frac{Q}{C_3} = \frac{\delta D^2 \tau m \sqrt[3]{I}}{W\theta}. \tag{12}$$

Eq 10 makes it possible to predict the type of fracturing, the degree of fragmentation, and the shape of the underground trajectory or to classify the impact of a body upon a solid into one of three ranges of behavior – the ricochet range, the cratering range, or the tunneling range.

Eq 11 makes it possible to determine the value of $\underline{m}$ for drops at energy levels other than τ equals 1.0.

Eq 12 may prove helpful in evaluating the coefficients C_1 and C_3 and in extrapolating the data to materials other than frozen ground.

DESIGN OF A BOMB FOR PRODUCING FOXHOLES IN FROZEN GROUND

Requirements

A bomb designed to make trenches and foxholes in frozen ground must meet a series of ballistic, operational, and target requirements. It may be necessary to drop the bomb in close proximity to friendly troops who must not be placed in jeopardy from ricochet, impact, airblast, flyrock, or shrapnel. If large numbers of troops are to be entrenched at one time, each plane must carry and release a large number of bombs. Therefore, the weight of the bomb should be as little as is practical.

None of the presently available general-purpose, semi-armor-piercing, or armor-piercing bombs meets the requirements for producing foxholes in frozen ground. It is possible, however, to design such a bomb.

The 81-mm shell, the 250 GP bomb, and the 500 GP bomb have characteristics such that penetration is confined largely to the cratering range. The underground trajectory of a bomb in the cratering range is J-shaped. If the bomb is fused for delay

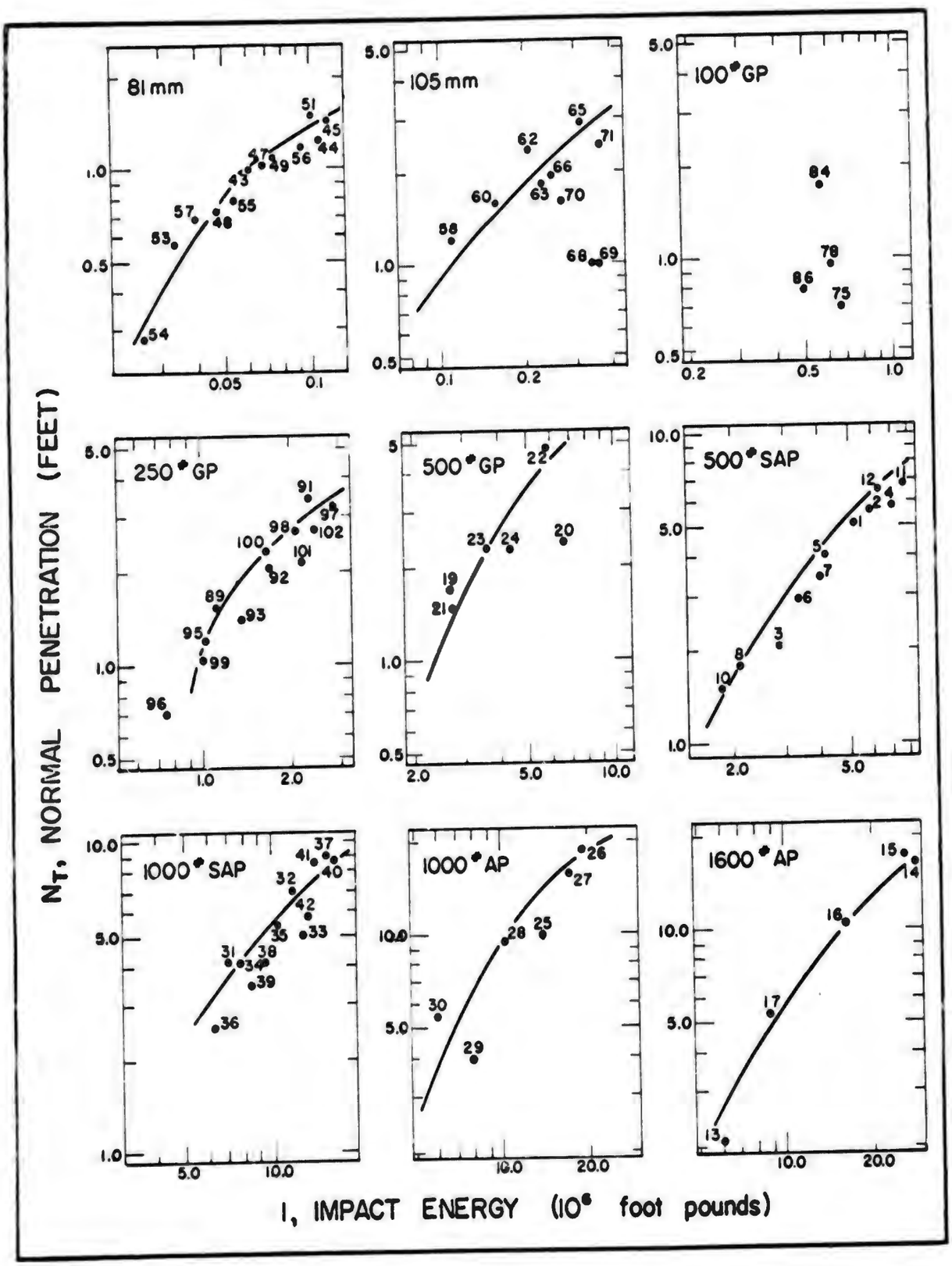

Figure 38. Comparison: observed and calculated N_T vs I.

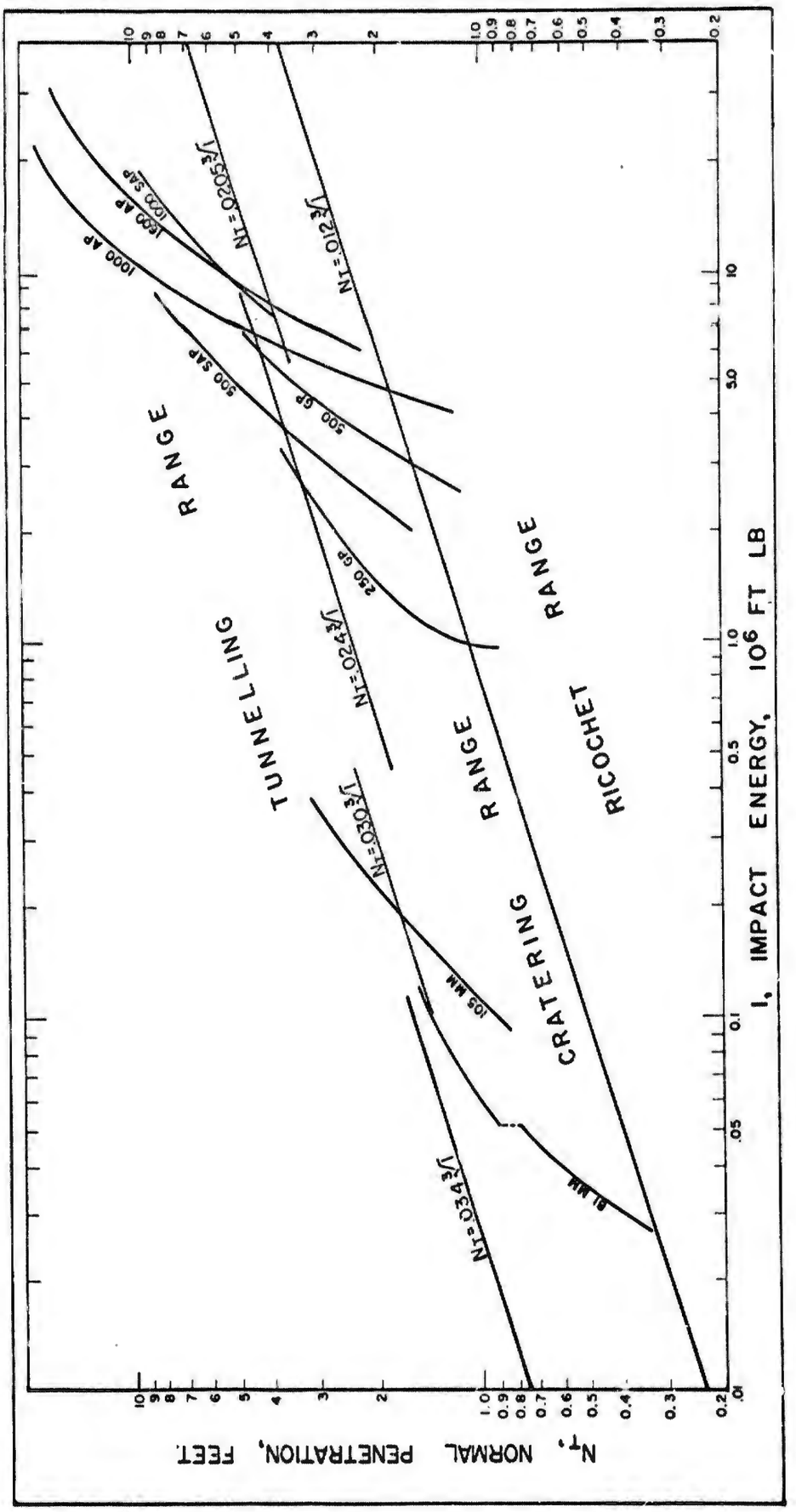

Figure 39. Normal penetration and behavior.

detonation after impact, considerable shrapnel will be thrown into the air, and the noise and airblast effect will be substantial.

The 500 SAP, 1000 SAP, 1000 AP, and 1600 AP bombs are capable of penetrating into the tunneling range, but too few could be carried on a bombing mission and the weight of their bursting charge is too great relative to their respective depths of penetration.

FH series bombs

Figures 40-42 are outline drawings of the bodies of three bombs intended for producing foxholes in frozen ground. The type is here designated FH (for foxhole). Three different weights have been designed – 30-lb (FH 30), 40-lb (FH 40), and 65-lb (FH 65). Comparison of characteristics of foxhole, general-purpose, semi-armor-piercing, and armor-piercing bombs will show:

1) The ratio of the weight of the bursting charge to the total weight of the armed bomb is less for FH series than for armor-piercing bombs. The order of decrease of charge/weight ratio is GP, SAP, AP, and FH. The order of decrease of charge/weight ratio within the FH series is FH 30, FH 65, and FH 40.

2) The slenderness ratio is greater for FH series than for armor-piercing bombs, which has a greater slenderness ratio than other conventional bombs. The order of increase of slenderness ratio within the FH series is FH 65, FH 40, and FH 30.

3) The nose of an FH bomb is sharper than that of an armor-piercing bomb, which is the sharpest of the conventional bombs. Within the FH series, the order of increase in caliber radius head, which measures nose sharpness, is FH 65, FH 40, and FH 30.

4) The center of gravity of an FH bomb is closer to the nose than that of a conventional bomb. Thus, the tendency of the FH bomb to yaw in flight is reduced and the strength of nose is increased.

5) The ratio W/D^2 is greater for FH series bombs than that of GP, SAP, or AP bombs reduced by dimensional analysis to the same diameter. Accordingly, the sectional density and the ballistic coefficient of an FH bomb equipped with a fin of optimum design should be greater than those of a conventional bomb of the same diameter. Ratios W/D^2 for the FH bombs are as follows:

FH 30 – 2.595
FH 40 – 3.086
FH 65 – 3.210

Underground explosion with FH bombs

The type and severity of damage resulting from an underground explosion depend upon the relation between the energy of the explosion and the mass of the medium to which the energy is partitioned. The depth of an explosive charge below the surface determines the mass to which the energy is partitioned. The chemical composition and the weight of an explosive determine the energy of the explosion. If the energy of the explosion exceeds a limiting amount with respect to the mass of the medium to which it is delivered, energy is partitioned both to the medium and to the atmosphere, and the efficiency of the explosion with respect to the medium is less than optimum. If the energy of the explosion is too small with respect to the mass of the medium, the energy is propagated through the medium without failure of the surface above the charge. To achieve optimum damage to the medium, the depth of the charge must bear the same relation to the weight of explosive as specified at Livingston's (1956) lower limit of the shock range.

If a bomb is designed so that, when it is delivered to achieve the proper striking velocity, the depth of penetration into the earth's surface (measured vertically to the center of gravity of the bursting charge) has the same relation to the weight of the bursting charge as at the lower limit of the shock range, then the bomb is the most efficient possible for attacking massive targets. Not only is the largest volume of material broken per pound of explosive, but noise, airblast pressure, and flyrock

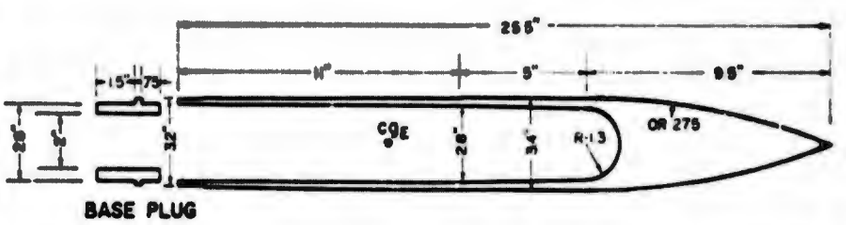

Weight	= 30 lb	Caliber Radius Head	= 8.09
Weight T.N.T.	= 6 lb	Slenderness Ratio	= 7.5
Sectional Pressure	= 3.30	Charge/Weight Ratio	= 20 %
Sectional Density	= 0.763	Nose to cg explosive	= 17.5"

Figure 40. 30-lb FH bomb.

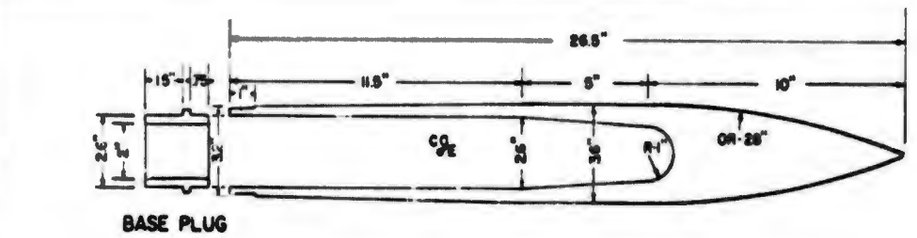

Weight	= 40 lb	Caliber Radius Head	= 7.78
Weight T.N.T.	= 5 lb	Slenderness Ratio	= 7.361
Sectional Pressure	= 3.93	Charge/Weight Ratio	= 12.5 %
Sectional Density	= 0.857	Nose to cg explosive	= 18"

Figure 41. 40-lb FH bomb.

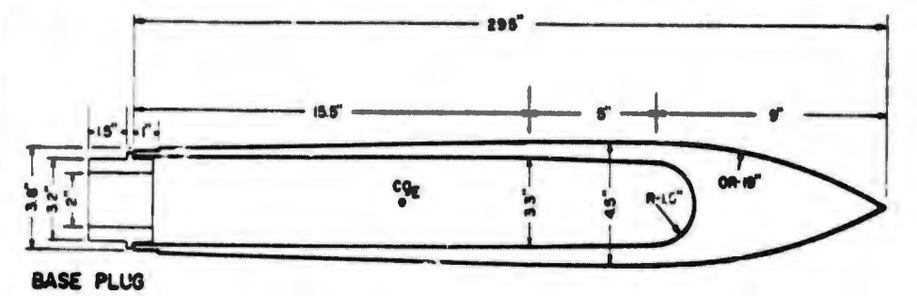

Weight	= 65 lb	Caliber Radius Head	= 4.22
Weight T.N.T.	= 10 lb	Slenderness Ratio	= 6.56
Sectional Pressure	= 4.09	Charge/Weight Ratio	= 15.38 %
Sectional Density	= 0.713	Nose to cg explosive	= 19"

Figure 42. 65-lb FH bomb.

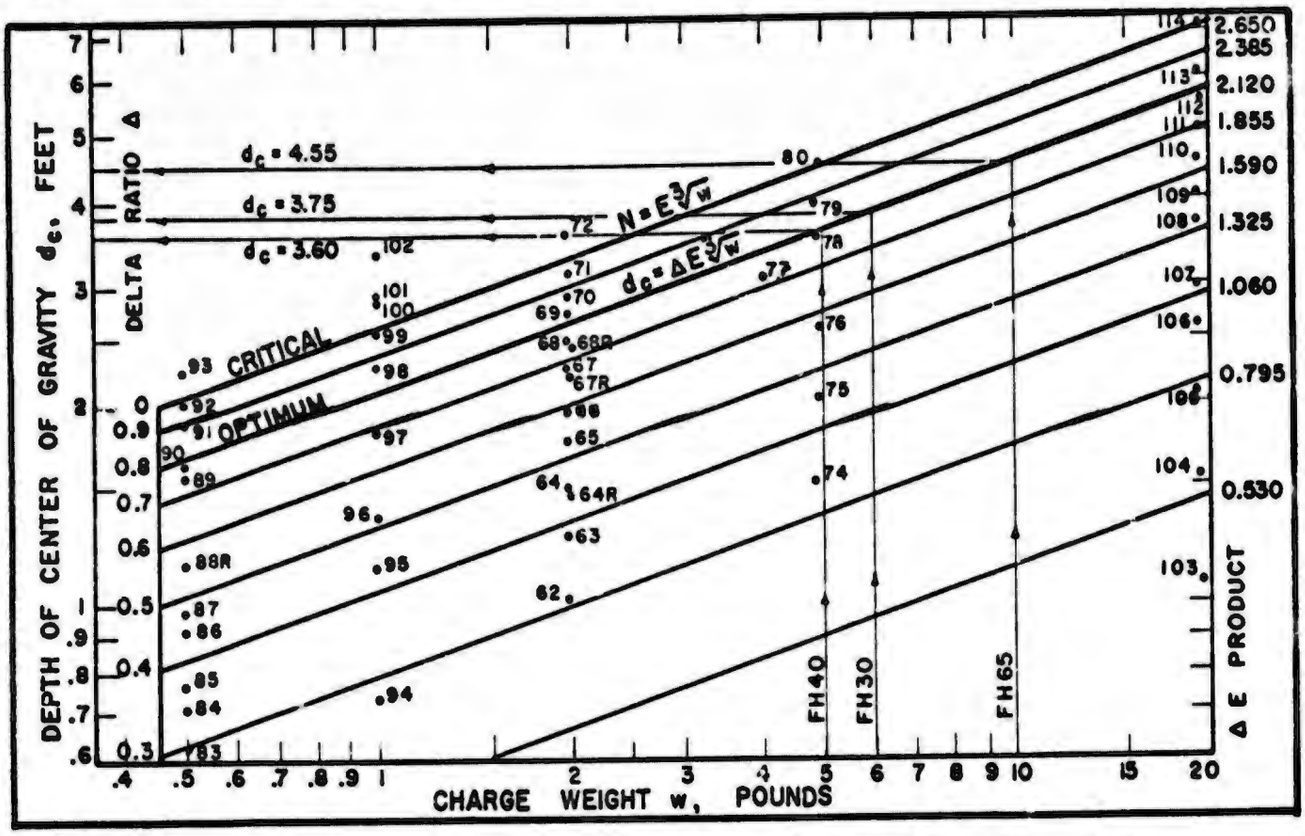

Figure 43. Correlation diagram for blasts of Military C3 in Churchill till.

travel are minimized. Furthermore, the material is broken in large chunks, which can be thrown from a foxhole by hand if necessary.

The relation between the depth of an explosives charge in frozen Churchill till and the weight of three different types of explosives was defined for various types of damage resulting from blasts of explosives placed in the bottom of a borehole The equivalent weight of explosive confined within the casing of a bomb is unknown; but as a first approximation it is assumed that, at optimum weight, the effect of confinement does not differ greatly from the effect of substituting a low-velocity, low-energy explosive such as Coalite 7S for a high-velocity, high-energy explosive such as C3.

Figure 43 from the results of the Fort Churchill blast tests (Livingston and Murphy, 1959) shows the manner of determining the weights of the bursting charges of the proposed FH bomb. The line designated "optimum" coincides with the lower limit of the shock range for blasts of C3 in frozen Churchill till. The limits of the shock range for explosives such as are used for bursting charges in bombs and the effect of the strength of the casing upon the "secondary" pressure associated with an expanding explosion cavity are not accurately known. However, Figure 43 provides a first approximation of the relation of the depth of penetration to the weight of the bursting charge for optimum ground shock and minimum air blast in frozen Churchill till. It will be necessary to investigate the effect of strength of the bomb casing in field tests using live bombs before equivalent weights can be determined accurately.

The bomb must penetrate by tunneling so that the frozen ground is not disturbed in such a way as to cause it to behave as a fractured mass when the bursting charge detonates. The depth of the tunnel below the bottom of the impact-produced crater determines the size of the foxhole and depends upon the transition ratio τ. (See Fig. 27, 39). Tunneling begins at $\tau = 1.0$, which is the lower limit of the tunneling range. The three FH bombs have been designed to produce foxholes between 4 and 5 ft deep in frozen Churchill till.

Preliminary evaluation of the proposed FH bombs

It seems unwise at this stage of development to carry the evaluation beyond an empirical solution. Determination of the ballistic characteristics of the proposed FH bombs and basic research necessary to determine numerical values of C_1 and C_3 are beyond the scope of this report.

The FH 30 bomb contains a bursting charge of 6 lb of TNT. Let us assume that the bomb is released so as to achieve a striking velocity less than or equal to its terminal velocity and that it tunnels below the impact-produced crater to the depth at which the bursting charge produces fracturing at the lower limit of the shock range. The optimum depth of a 6-lb charge of C3 in frozen Churchill till is 3.75 ft (Fig. 43). The depth is measured to the center of gravity of the charge.

Next, let us assume that the FH 30 bomb penetrates by straight-line penetration and that the striking angle is 75°. The distance from the nose to the center of gravity of the explosive charge is 17.5 in. (Fig. 40). The depth of penetration measured vertically from the surface to the tip of the nose of the bomb at optimum depth is

$$N_T = 3.75 + \left(\frac{17.5}{12.0} \times 0.966\right) = 5.15 \text{ ft.}$$

Similarly, it can be shown that N_T must be 5.05 ft for the FH 40 bomb at optimum depth and 6.07 ft for the FH 65 bomb.

The terminal velocities of the proposed FH series bombs must be determined in the field, but it is assumed here that they approach the velocity of sound. The assumption is based upon the known terminal velocities of Gavre-type projectiles (Hayes, 1953, p. 431) and upon the fact that the sectional pressures of the proposed FH bombs are greater than those of conventional bombs reduced to the same diameter by dimensional analysis. The assumption of straight-line penetration is consistent with the improved nose shape and greater slenderness ratio of the FH bomb compared to the 1000 AP bomb, which penetrates frozen Churchill till by straight-line penetration at velocities less than the velocity of sound. The assumption that tunneling occurs may be tested by calculating the transition ratio from the postulated model law for impact:

$$y = \tau m \sqrt[3]{I} . \qquad (2)$$

Given:

$W = 30$ lb

$m = 0.027$ (interpolation from Fig. 39)

$y = 5.15$ ft ($y = N_T$)

$V = 1080$ ft/sec

$$I = \frac{W}{g} \times \frac{V^2}{2} = \frac{30}{32.2} \times \frac{(1080)^2}{2} = 0.543 \times 10^6 \text{ ft-lb}$$

and

$$\tau = \frac{y}{m \sqrt[3]{I}} = \frac{5.15}{0.027 \times 81.7} = 2.33.$$

As tunneling begins at $\tau = 1.0$, the assumption of tunneling is correct.

Similarly, it can be shown that at terminal velocity impact energy for the FH 40 bomb is 0.724×10^6 ft-lb. At terminal velocity, τ is 2.12 for both the FH 40 and the FH 65 bombs.

Figure 44 shows the relationship of the FH bombs (as predicted from the theory using the Livingston penetration equations) to the 105-mm shells and the 250 GP bombs. The relations to other bombs tested may be obtained by plotting values of

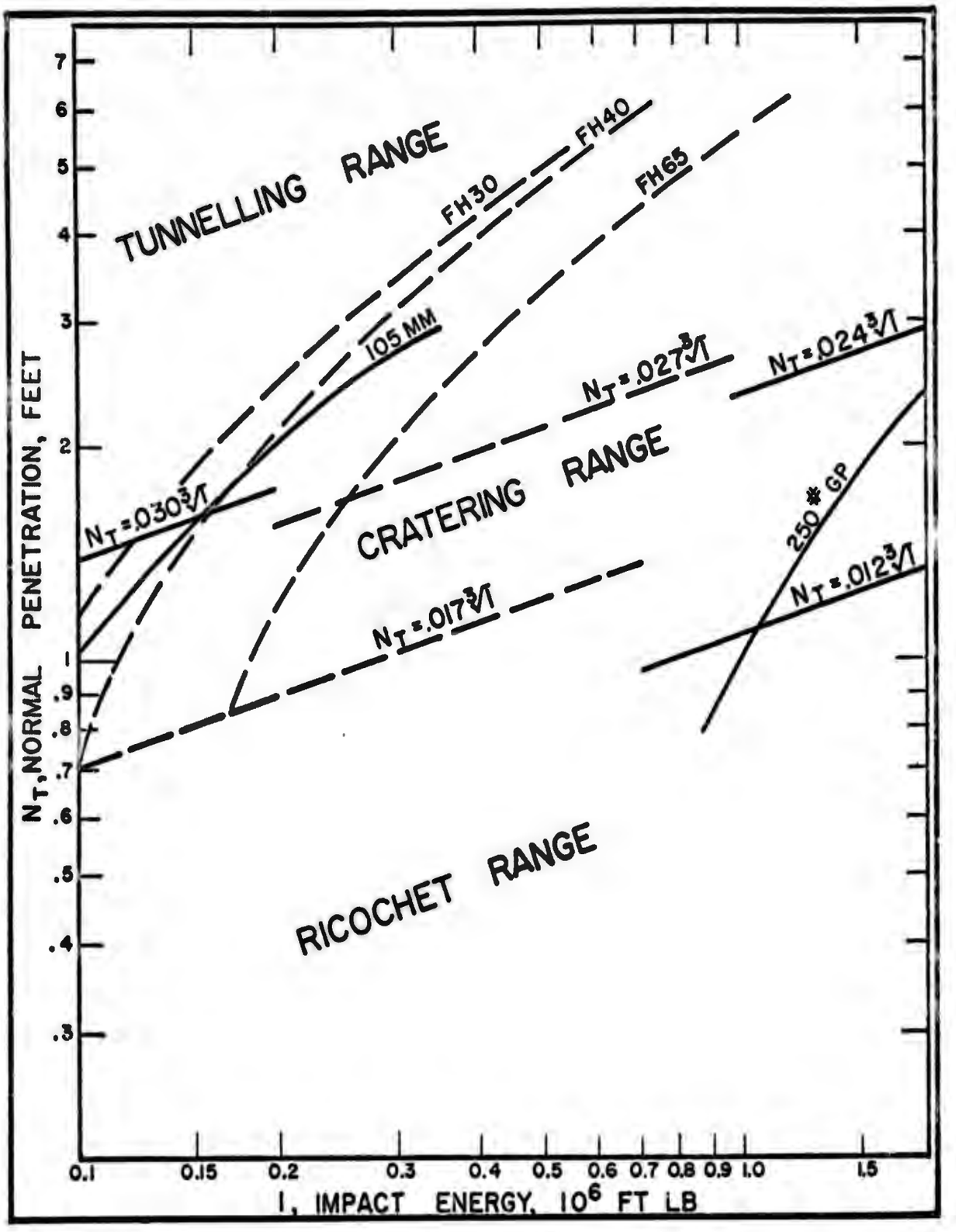

Figure 44. Preliminary evaluation, FH bomb.

$\underline{y}$ or $\underline{I}$, as calculated above in Figures 30 and 39. These values in Figure 44 are the coordinates of the upper ends of the curves of the three proposed FH bombs.

Table III shows that for bombs in the range of weight of the 105-mm shell and 250 GP bomb $1000\ \Delta y/\Delta x = 2.386$ and $\underline{b} = -0.589$. These values may be substituted in equation (9a), using values of $\underline{W}$ and $\underline{D}$ for each of the test bombs from the drawings (Fig. 40-42).

In a composite material such as peat-covered frozen Churchill till, the unit weight changes from 75 lb/ft^3 for frozen peat to 148.7 lb/ft^3 for frozen Churchill till. It is necessary therefore to obtain an approximate value of δ based upon an assumed depth of penetration. If N_T, as computed using eq 9a and the approximate value of δ, does not agree with the assumed depth, the calculation must be repeated.

The assumption in following calculations that the terminal velocity of an FH bomb equals 1080 ft/sec is a first approximation based upon the ballistic coefficient, C_g, for Gavre-type projectile and upon the known relation between the ballistic coefficient and the limiting velocity (Hayes, 1953, p. 434). The value of θ used in following calculations is based upon the assumption that the FH 30 bomb will penetrate by straight-line penetration at $\tau = 2.33$ and that the striking angle at an altitude of release sufficient to achieve terminal velocity will be approximately 75° (see data sheets). For the FH 30 bomb

$W = 30$ lb

$\theta = 0.966$

$\delta = 136.5$ lb/ft^3

$D = 3.4$ in. $= 0.283$ ft.

Substituting in eq 9a and solving for N_T

$$N_T = \frac{30 \times 0.966}{136.5 \times (0.283)^2} (0.002386 \times 1080 - 0.598) = 5.2 \text{ ft.}$$

The performance of the FH 30 bomb at altitudes of release less than that at which terminal velocity is achieved, or the performance of FH 40 or FH 65 bombs at various altitudes of release are calculated in a similar way.

In designing the FH 30 bomb, the relations between normal penetration and energy of impact were chosen using Figure 39. The weight of the bursting charge corresponding to the design depth of the center of gravity of the charge was then determined using Figure 43. The design of the bomb, aside from nose shape and stress distribution, was fixed by the requirement of producing a foxhole of a given size without throwing shrapnel. The above calculation demonstrates that the dimensions were properly chosen if the analogies upon which the Livingston penetration equations are based are valid.

A comparison of properties of the FH bombs and of the 105-mm shell (Table IV) suggests a greater maximum depth of penetration for the FH bombs than for the 105-mm shell.

Table IV. Comparison of properties of the 105-mm shell and FH bombs.

	105-mm	FH 30	FH 40	FH 65
Sectional pressure	2.00	3.30	3.93	4.09
Terminal velocity, ft/sec	1010	1080†	1080†	1080†
Nose shape (CRH)	2.83	8.09	7.78	4.22
Slenderness ratio	5.30	7.50	7.36	6.56

† Assumed

CONCLUSIONS

Penetration of bombs into materials of the earth's crust

Penetration tests have been made in a wide variety of materials under a wide range of conditions. It now appears that the behavior of various materials subjected to impact and penetration of bombs is relative and that phenomena observed in substances that behave in part plastically can be reproduced in brittle substances at higher energy levels. The hypothesis is advanced here that failure is dependent upon energy transfer and that fundamentals of energy transfer do not differ greatly for solids, liquids, and

gases. Inasmuch as the penetration of a projectile depends upon the energy of impact, it follows that a correlation must exist between energy partitioned to a substance as a result of the impact and penetration of a projectile and that partitioned to the substance as a result of an underground explosion.

Just as it is impossible in explosions research to correctly treat the explosive and the medium as separate and independent variables, it is impossible in bomb penetration research to treat the projectile and the medium as separate and independent variables. It has been observed as a result of the Fort Churchill and the New Mexico bomb penetration tests that analogous changes in 1) the type of failure, 2) the degree of fragmentation, 3) the shape of the underground trajectory or 4) the shape of the bomb crater are produced as a result of:

a) a change in bomb type at a given energy of impact in a given medium,

b) a change in the type of medium at a given energy of impact with a given type of bomb,

c) a change in the energy of impact with a given type of bomb in a given medium.

As in explosions research, it is possible to define various energy levels at which a transition in type of penetration occurs. As the energy level is increased, a transition from ricochet to penetration by brittle-state failure occurs. A further increase in energy level results in a transition to penetration by plastic deformation.

Postulated model law for penetration

Although the evidence suggests that the laws for penetration by pure brittle-state failure differ from the laws for penetration by pure plastic deformation, it seems possible to correlate the behavior of a wide range of materials by means of the equation

$$y = \tau m \sqrt[3]{I} \qquad (2)$$

where

y is the vertical distance, ft, from the surface of the frozen ground to the nose of the bomb at the end of its underground trajectory,

m, the plastic deformation index, expresses the tendency of materials to deform plastically

I is the energy of impact in foot-pounds.

The transition ratio τ is the ratio of the depth of penetration (measured vertically from a horizontal target surface to the nose of projectile) to the depth at which tunneling begins for the same type and weight of projectile in the same medium. It is a dimensionless quantity analogous to the depth ratio, Δ, in explosions research. The transition ratio may be thought of as a ratio of lengths, a ratio of volumes, a ratio of masses, or a ratio of "energy levels." The terms "energy level" is used here to describe a given ratio between the mass to which energy is delivered and the quantity of energy delivered. If the proportion of plastic deformation to brittle-state failure is constant in model and prototype, the plastic deformation index m is a constant, and geometric similarity exists at a given numerical value of τ. If the proportion is not constant at a given energy level, m is a variable rather than a constant, and geometric similarity does not exist. Values of m as determined for test drops striking frozen Churchill till are a measure of a composite of three materials – snow, frozen peat, and frozen Churchill till. The resistance of snow to penetration is low, and the effect of the snow cover was ignored in the analysis. The peat layer ranged from 6 to 15 in. thick and the depth of penetration varied, so that various proportions of peat and till were penetrated. The transition depth and the corresponding value of m are summarized for each of the test projectiles in Table V.

The table shows that the plastic deformation index decreases as the depth of penetration increases and also that the value of m depends upon the bomb. Accordingly, in future tests it seems desirable to refer the plastic deformation index to a standard bomb.

Table V. Plastic deformation index, m, composite material.

Bomb	Transition depth, ft	Plastic deformation index, m	Group
81-mm shell	1.37	.0345	1
105-mm shell	1.62	.0304	2
500 SAP	3.15	.0204	4
250 GP	3.50	.0247	3
1000 AP	3.70	.0208	4
1600 AP	4.10	.0204	4
500 GP	4.40	.0242	3
1000 SAP	5.35	.0241	3

We may liken a general-purpose bomb to a low-velocity explosive and an FH bomb to a high-velocity explosive and predict that different values of m for different types of bombs will be found in a given substance at the same energy of impact. We may predict also that the variation of m with bomb type and nose shape is not so great as the variation observable in different materials with the same bomb. Further, we may predict that m is larger in plastic-acting substances than in brittle-acting substances.

The limit between the cratering range and the tunneling range is shown (Fig. 39) as a series of lines rather than a single line because of the different physical properties of the peat and Churchill till. Equations of the various line segments have been computed at $\pi = 1.0$ assuming that the composite of frozen peat and glacial till acts as a single substance and that m for the composite substance is constant over a finite range of impact energy. The numbers .034, .030, .024, and .0205 are values of m determined for various groups of projectiles, as explained in the text. When dealing with a particular projectile the value of m of Table V should be used.

It would be unwise to assume that the penetration characteristics of all glacial deposits of the sub-arctic and arctic are similar to those of frozen Fort Churchill till. The ground might or might not be frozen to a depth substantially greater than the depth of projectile penetration, depending upon the time of year, the amount of vegetation, the thickness of snow cover, the thickness of the mantle of soil or of glacial debris that overlies bedrock, and the physical properties of the frozen ground.

Because of difference between the environment that favors the growth of timber and the environment of the open, untimbered arctic plain, it is probable that the depth of penetration of a bomb will prove greater in the timbered areas than in the open. The timbered areas are at somewhat higher elevation than the open muskeg areas. The drainage is better and the soils are more porous. The thickness of perennially frozen ground is less in the timbered areas because of better insulation by more vegetation and deeper snow and because of better protection against the cold winter wind.

The line that marks the limit between the ricochet range and the cratering range is shown in Figure 39 as unbroken. Probably it too should be a broken line, but the number of test drops was too few to pin-point accurately the transition at impact energies lower than 4 million foot-pounds. If it is assumed that experimental accuracy is greatest for the heavy bombs and that the composite of peat-covered glacial till is the equivalent of a single substance (m is constant), the numerical value of π that defines the transition from ricochet to cratering is 0.58.

The Fort Churchill bomb penetration tests provide sufficient evidence to demonstrate that the numerical value of π is a first approximation of geometric similarity. To be consistent, we must therefore postulate that the equation of the line separating the ricochet range from the cratering range in the stress range of Figure 44 for the 105-mm shell and for the proposed FH series projectiles will prove closer to

$$N = 0.58 \times 0.030 \sqrt[3]{\Gamma} = 0.017 \sqrt[3]{\Gamma}$$

than it is to

$$N_T = 0.012 \sqrt[3]{T}.$$

However, the effect of the peat cover has not been isolated completely from that of the underlying glacial till. Until this is done, it is impossible to determine whether known minor discrepancies between the shapes of the underground trajectories of various test projectiles are due to: limits of accuracy in calculating τ, variation in $\underline{m}$, or a "scale effect" not apparent in the postulated model law for penetration.

Penetration by brittle-state failure

The crater in frozen ground is the result of failure along three mutually perpendicular sets of fracture which have been observed previously in craters in rock. The mechanics of fracturing has been described and analyzed in connection with studies of the penetration of bombs into granite and sandstone (Livingston and Smith, 1951).

The behavior of granite and sandstone greatly resembles the behavior of frozen Churchill till in the cratering range. The similarity is greatest for the 81-mm shell, the 250 GP bomb, and the 500 GP bomb, which, unlike other types of bombs tested at Fort Churchill, exhibit behavior (see Fig. 39) that lies almost exclusively within the cratering range.

The penetration formulas developed as a result of tests in rocks – where behavior is almost exclusively in the cratering range and where brittle-state failure predominates over plastic deformation – are at variance with formulas developed here using the plastic deformation analogy. Although numerical values of the ratio Q/C_3 have been determined empirically and applied to the cratering range, little justification may exist for doing so. In fact, the evidence suggests that the laws for penetration by pure brittle-state failure differ from the laws for penetration by pure plastic deformation. Moreover, it appears that penetration is accomplished by a combination of both types of failure.

The view is held here that penetration in brittle-acting substances and at values of τ less than 1.0 may be more accurately expressed by the formula (Livingston and Smith, 1951, p. 209-219),

$$N_R = \frac{1 - m_x}{2.484 m_x} \cdot \frac{N}{D} \cdot Q^* . \qquad (3)$$

In frozen ground, in substances that behave in part elastically and in part plastically, and at values of τ greater than 1.0 normal penetration equals

$$N_T = \frac{W\theta}{C_3 \delta D^2} \ln \frac{C_1}{C_1 + C_3 \rho V D^2} . \qquad (8b)$$

Feasibility of using bombs released from aircraft to make trenches and foxholes rapidly in deeply frozen ground

None of the presently available general-purpose, semi-armor-piercing, or armor-piercing bombs meet the requirements of a bomb for producing foxholes in frozen ground.

Figures 40-42 are outline drawings of a bomb. It is believed that the proposed FH bomb (Fig. 40-42) will meet ballistic, operational, and target requirements. The new design is based upon the penetration equations derived and also upon a correlation of effects of impact and explosion to avoid hazards of shrapnel and airblast.

Recommendations

The Fort Churchill bomb penetration tests have been directed not only towards determining the feasibility of making trenches and foxholes in frozen ground by means of bombs released from aircraft, but also towards a study of behavior of materials of

* Q may be stated in terms of V, δ, and P.

the earth's crust subject to impact. This approach has resulted in a statement of the model laws for impact and a correlation of the effects of impact and explosion. It has also led to the concept of similar ranges of behavior in penetration and to a better understanding of the transition successively from ricochet to brittle-state failure to plastic deformation.

Accordingly, it is recommended that:

1) The proposed FH bombs be developed and tested both at Fort Churchill and on the Greenland Ice Cap.

2) A basic research project be directed towards investigating the relations among the coefficients C_1, C_3, the drag coefficient C_D, and the plastic deformation index m.

REFERENCES

Daugherty, R. L. (1937) Hydraulics, 4th ed. New York: McGraw Hill Book Company.

Hayes, T. J. (1953) Elements of ordnance. New York: John Wiley and Sons, 715 p.

King, H. W., and Wistler, C. O. (1941) Hydraulics, 4th ed. New York: John Wiley and Sons.

Livingston, C. W. (1956) Excavations in frozen ground, Part I. Explosion tests in Keweenaw silt, U. S. Army Snow Ice and Permafrost Research Establishment, Corps of Engineers, Report 30, Pt. 2.

_____ (1956) Fundamental concepts of rock failure, Symposium on rock mechanics, Quarterly of the Colorado School of Mines, vol 51, no. 3.

_____ and Murphy, G. (1950) Excavations in frozen ground, Part II, Explosion tests in frozen glacial till, Fort Churchill, U. S. Army Snow Ice and Permafrost Research Establishment, Corps of Engineers, Report 30, Pt. 2.

_____ and Smith, F. L. (1951) Bomb penetration project, Colorado School of Mines Research Foundation, 245 p. CONFIDENTIAL

Murphy, G. (1952) Mechanics of fluids. Scranton, Pennsylvania: International Textbook Company.

APPENDIX

BOMB CROSS-SECTIONS AND DATA SHEETS

CONTENTS

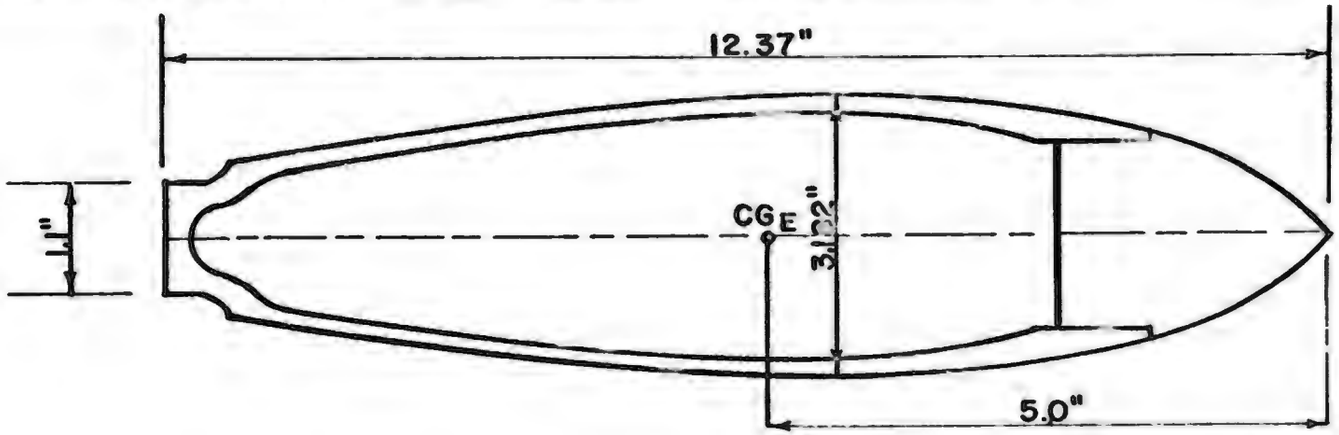

SHELL HE. 81 M M, T28E7

BARODYNAMICS, INC.
5810 W. 38TH AVE.
DENVER 14, COLO.

FORT CHURCHILL BOMBING TESTS
S.I.P.R.E. CONTRACT
CORPS OF ENGINEERS U.S. ARMY

FIG.
A-1

APRIL 1957

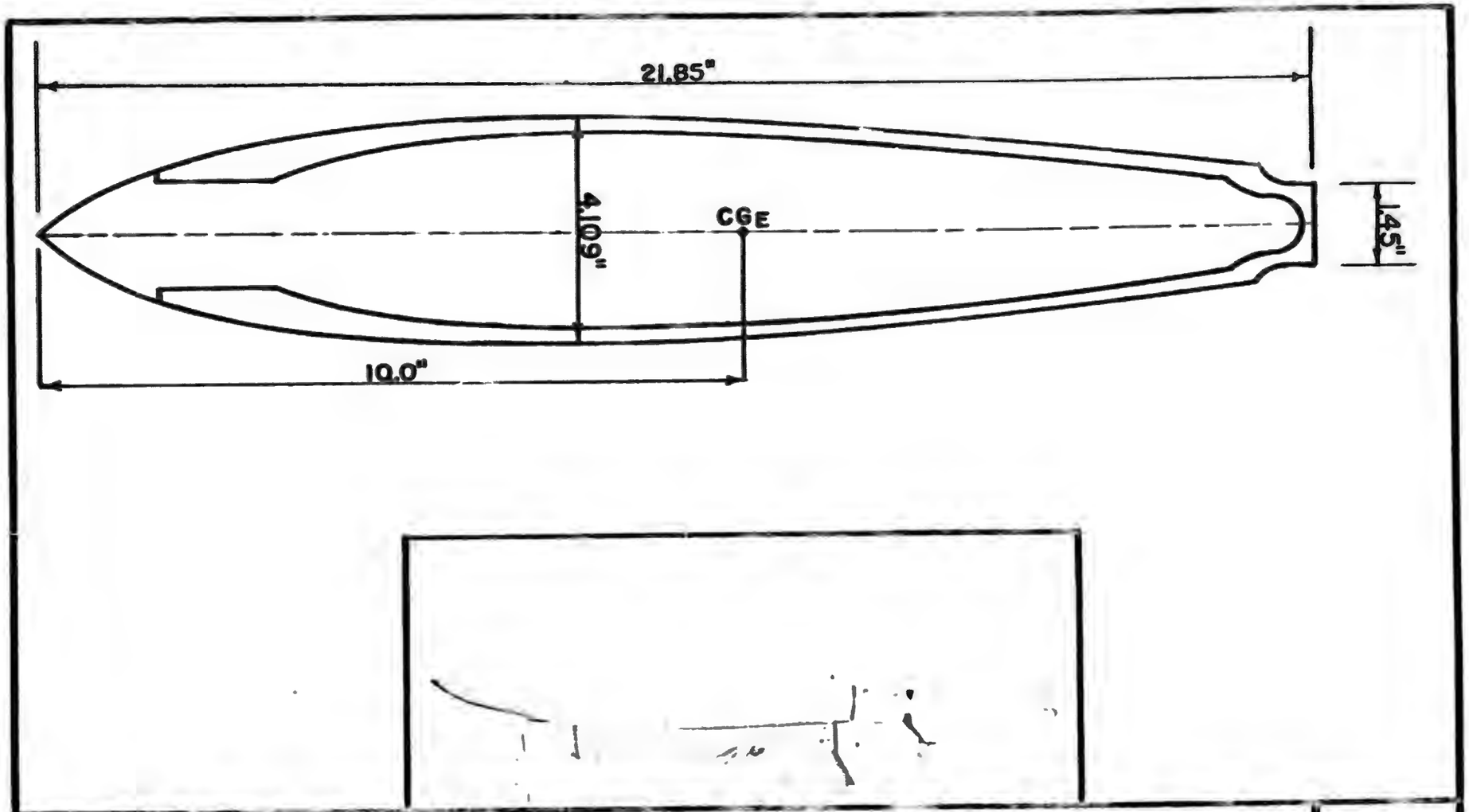

SHELL HE. 105 MM. T53E2

BARODYNAMICS, INC.
5810 W. 38TH AVE.
DENVER 14, COLO.

FORT CHURCHILL BOMBING TESTS
S.I.P.R.E. CONTRACT
CORPS OF ENGINEERS U.S. ARMY

FIG. A-2

APRIL 1957

GPO 808611-8

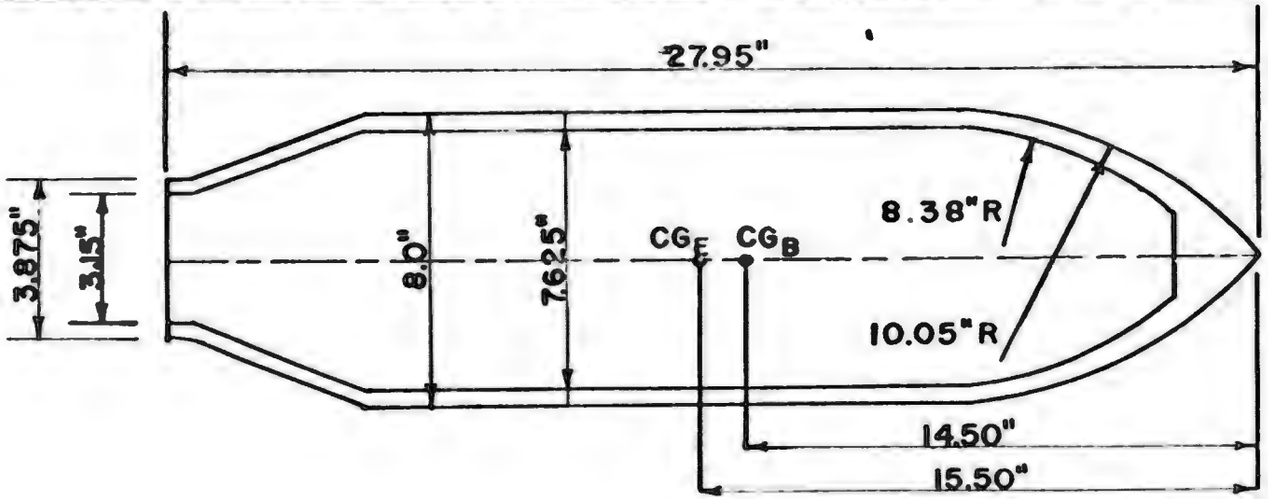

100 lb. G.P. AN-M30A1

BARODYNAMICS, INC.
5810 W. 38TH AVE.
DENVER 14, COLO.

FORT CHURCHILL BOMBING TESTS
S.I.P.R.E. CONTRACT
CORPS OF ENGINEERS U.S. ARMY

FIG. A-3

APRIL 1957

SL8219

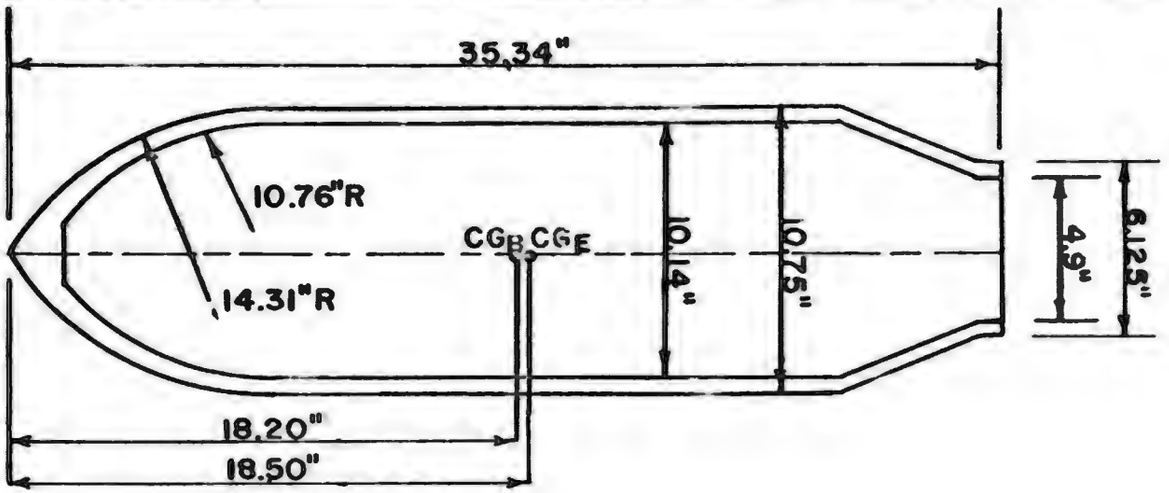

250 lb. G.P. AN-M57A1

BARODYNAMICS, INC.
5810 W. 38TH AVE.
DENVER 14, COLO.

FORT CHURCHILL BOMBING TESTS
S.I.P.R.E. CONTRACT
CORPS OF ENGINEERS U.S. ARMY

FIG. A-4

APRIL 1957

SL8219

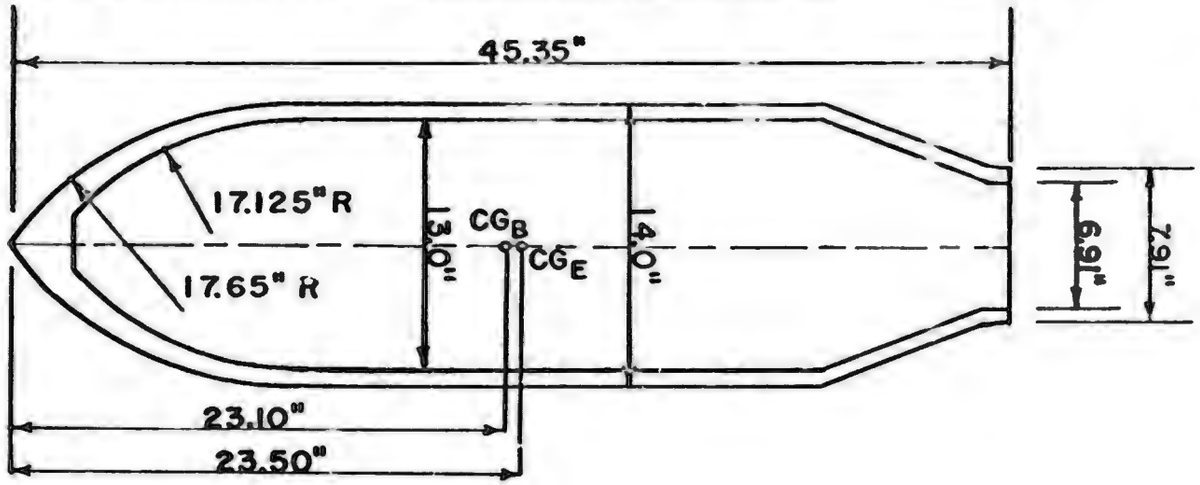

500 lb. G.P. AN-M64 A1

BARODYNAMICS, INC.
5810 W. 38TH AVE.
DENVER 14, COLO.

FORT CHURCHILL BOMBING TESTS
S.I.P.R.E. CONTRACT
CORPS OF ENGINEERS U.S. ARMY

FIG. A-5

APRIL 1957

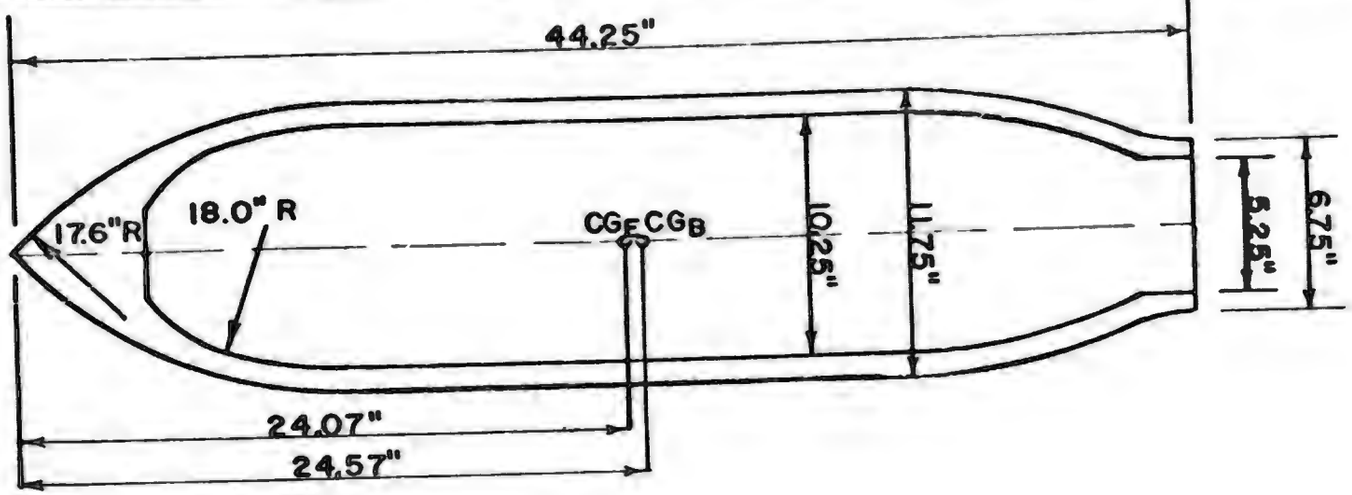

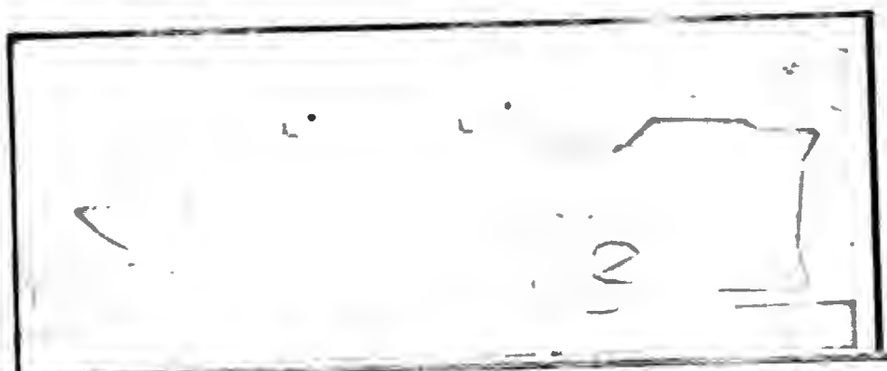

500 lb. SAP AN-M58A2

BARODYNAMICS, INC.
5810 W. 38TH AVE.
DENVER 14, COLO.

FORT CHURCHILL BOMBING TESTS
S.I.P.R.E. CONTRACT
CORPS OF ENGINEERS U.S. ARMY

FIG. A-6

APRIL 1957

608875

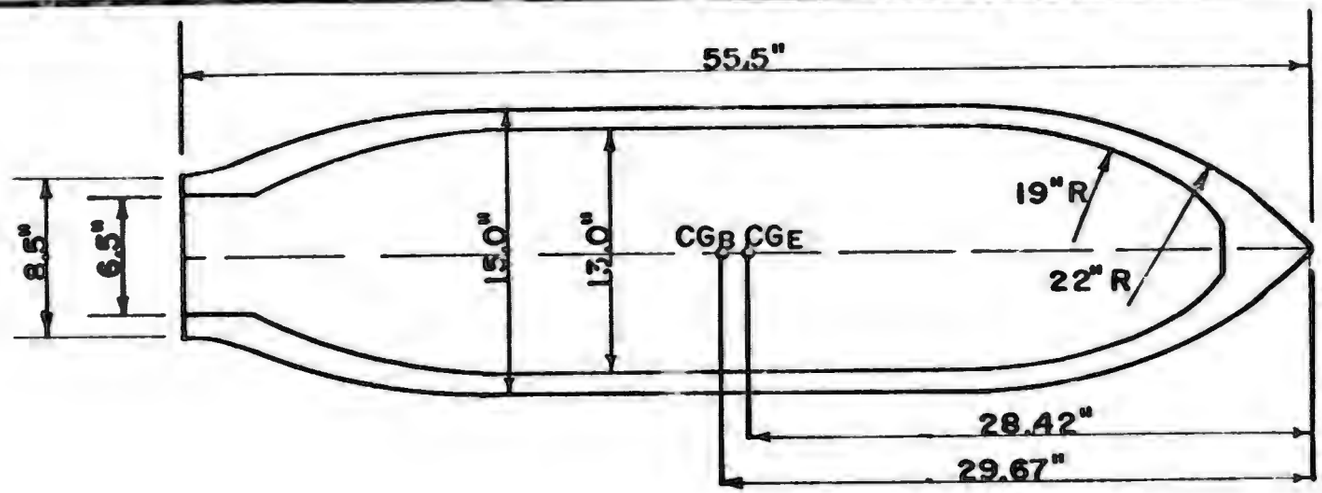

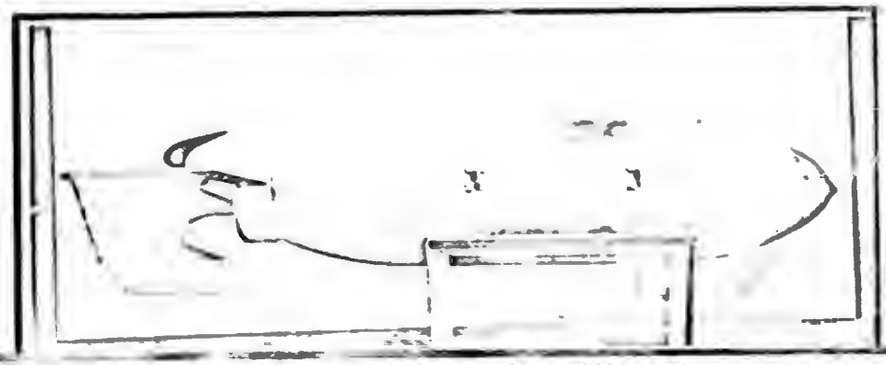

1000 lb. SAP AN-M59A1

BARODYNAMICS, INC.
5810 W. 38TH AVE.
DENVER 14, COLO.

FORT CHURCHILL BOMBING TESTS
S.I.P.R.E. CONTRACT
CORPS OF ENGINEERS U.S. ARMY

FIG. A-7

APRIL 1957

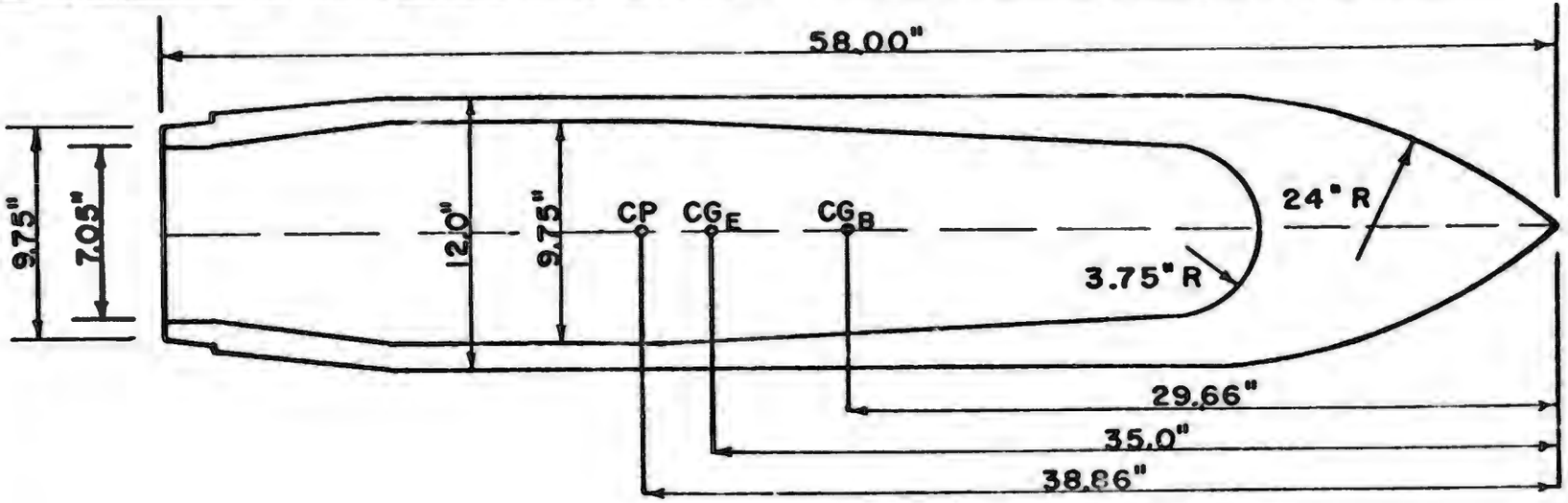

1000 lb. AP AN-MK1

BARODYNAMICS, INC.
5810 W. 38TH AVE.
DENVER 14, COLO.

FORT CHURCHILL BOMBING TESTS
S.I.P.R.E. CONTRACT
CORPS OF ENGINEERS U.S. ARMY

FIG. A-8

APRIL 1957

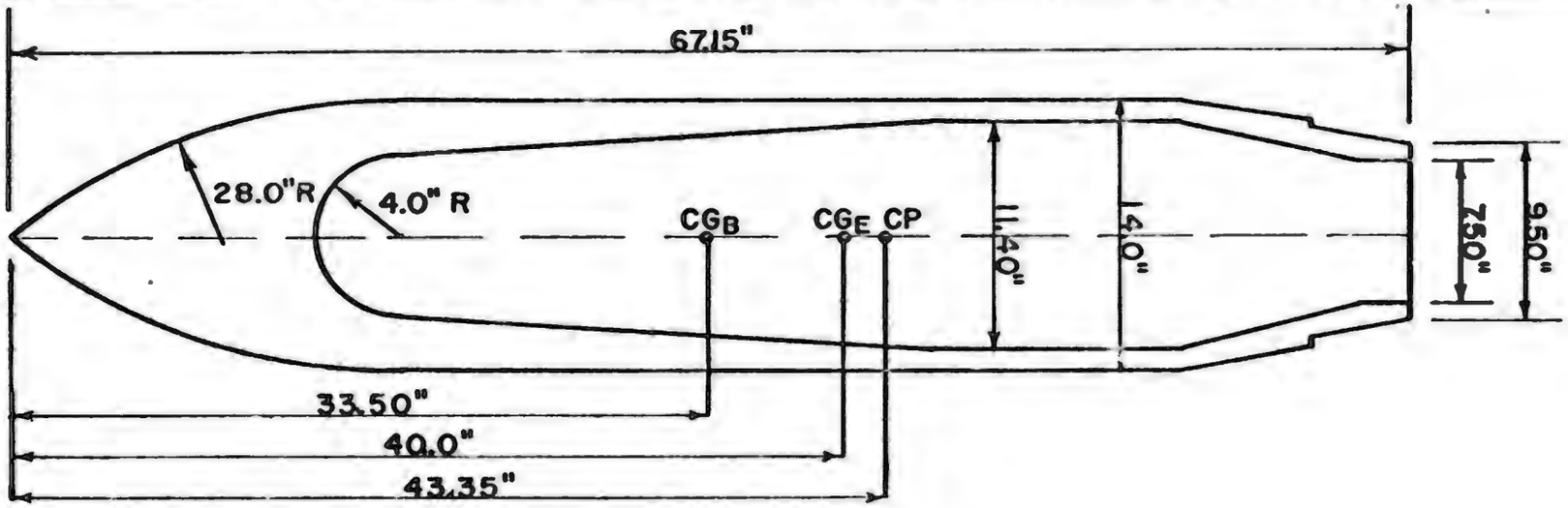

1600 lb. AP AN-MK I

BARODYNAMICS, INC.
5810 W. 38TH AVE.
DENVER 14, COLO.

FORT CHURCHILL BOMBING TESTS
S.I.P.R.E. CONTRACT
CORPS OF ENGINEERS U.S. ARMY

FIG. A-9

APRIL 1957

Bomb Type	Bomb Number	BALLISTIC MEASUREMENTS														
		Altitude of Release Above Target (feet)	Speed of Release Ground Speed (MPH)	Weight of Bomb (lbs)	Striking Velocity (fps)	Impact Energy (10^6 ft lbs)	Striking Angle (degrees)	Impact Energy x Sine Striking Angle (10^6 ft lbs)	True Air Speed (MPH)	Azimuth/Wind Velocity in MPH at Release Altitude	Heading Azimuth (degrees)	Air Temperature (°F)	Altimeter Setting	Range Error (feet)	Drift Error (feet)
81 mm MORTAR	54	2000	175	11	388	0.026	59	0.022	195	320/21	338	-22	2981	420 N	0
	53	2750	180	11	436	0.033	62	0.029	197	315/22	338	-22	2981	1255 N	265 E
	57	3600	182	11	479	0.039	65	0.036	202	310/23	337	-22	2981	1370 N	200 E
	48	4300	198	11	521	0.046	65	0.042	203	280/10	337	-21	2978	1080 N	30 E
	55	5100	200	11	555	0.053	67	0.048	206	290/10	338	-22	2978	1020 N	180 E
	43	6000	203	11	591	0.060	68	0.055	210	300/09	338	-23	2978	570 N	70 W
	47	7000	207	11	625	0.067	70	0.063	213	300/07	339	-24	2978	290 N	130 E
	49	8100	213	11	654	0.073	71	0.069	218	300/07	339	-25	2978	450 N	260 E
	56	11750	182	11	731	0.091	76	0.089	221	340/39	340	-31	2976	300 N	850 E
	51	13250	189	11	758	0.098	77	0.096	223	330/36	338	-33	2976	80 S	520 E
	44	15000	184	11	782	0.105	78	0.102	223	330/40	338	-34	2976	175 S	1220 E
	45	17500	175	11	808	0.112	80	0.110	228	330/53	337	-36	2976	1030 N	1010 E

DATA SHEET A

GPO 806611-7

Bomb Type	Bomb Number	BOMB PATH MEASUREMENTS																
		N_{SN}	N_S	N_R	$N_T = N_S + N_R$	P_S	P_{SI}	P_{RM}	P_{TM}	P	I_S	I_R	I_T	I_N	X_M	X_H	X	Y_U
81 mm Mortar	54	1.80	0.28	0	0.28	1.28	0.62	0	0.62	1.28	0.55	0	0.55	0.32	0.58	ric.	0	0.43
	53	1.40	0.58	0	0.58	1.20	1.20	0	1.20	1.20	1.00	0	1.00	0.60	1.00	0	0	0
	57	1.00	0.70	0	0.70	1.70	1.70	0	1.70	1.70	1.30	0	1.30	1.00	1.30	0.20	0	0
	48	1.00	0.74	0	0.74	1.35	1.35	0	1.35	1.35	1.10	0	1.10	0.60	1.08	0	0	0
	55	1.30	0.80	0	0.80	1.52	1.52	0	1.52	1.52	1.25	0	1.25	0.80	1.22	0	0	0
	43	1.30	0.70	0.32	1.02	0.80	0.80	0.40	1.20	1.20	0.75	0.41	1.16	0.18	0.63	0	0.25	0
	47	1.30	1.03	0	1.03	1.25	1.25	0	1.25	1.25	1.20	0	1.20	0.25	0.67	0	0	0
	49	1.40	0.90	0.20	1.10	1.00	1.00	0.21	1.21	1.21	0.95	0.25	1.20	0.08	0.50	0	0.10	0
	56	2.00	1.00	0.20	1.20	1.10	1.10	0.22	1.32	1.32	1.05	0.25	1.30	0.18	0.50	0	0.13	0
	51	0.80	1.30	0.20	1.50	1.40	1.40	0.21	1.61	1.61	1.35	0.22	1.57	0.18	0.58	0	0.10	0
	44	1.30	0.90	0.35	1.25	1.00	1.00	0.40	1.40	1.40	0.92	0.43	1.35	0.32	0.62	0	0.20	0
	45	1.60	1.35	0.10	1.45	1.65	1.65	0.10	1.75	1.75	1.40	0.18	1.58	0.52	0.90	0	0.08	0

DATA SHEET B

Bomb Type	Bomb Number	BOMB PATH MEASUREMENTS							CRATER MEASUREMENTS							
		Angle V (degrees)	Z	Z_F	Angle H (degrees)	Prototype Normal Penetration	Prototype Path Length	Prototype Inclined Penetration	Crater Volume (cubic feet)	Crater Depth (feet)	Plan Area of Crater (square feet)	Crater Radius (feet)	$K_2 = \frac{V}{\pi r^2 h}$	Prototype Crater Volume	Prototype Crater Depth	Prototype Crater Radius
81 mm Mortar	54	31	0.05	-	2.5 L	1.00	4.57	1.96	0.29	0.43	0.87	0.53	.78	13.18	1.53	1.89
	53	29	0.05	0.03	3.5 L	1.90	3.92	3.27	0.35	0.64	1.34	0.66	.41	12.07	2.09	2.16
	57	35.5	0.3	0.1	13.0 L	2.13	5.17	3.95	0.76	0.75	1.05	0.57	.96	21.11	2.28	1.73
	48	28.5	0.1	0.05	6.5 L	2.13	3.88	3.16	0.71	0.80	1.66	0.73	.53	16.90	2.30	2.10
	55	32	0.1	0	4.0 R	2.19	4.16	3.42	0.41	0.81	2.03	0.81	.25	8.54	2.22	2.22
	43	21	0	0	0	2.68	3.15	3.04	0.60	0.90	2.17	0.83	.31	10.91	2.36	2.18
	47	11	0	0	0	2.59	3.15	3.02	0.46	1.08	1.45	0.68	.29	7.30	2.72	1.71
	49	14	0	0	0	2.68	2.95	2.93	0.33	1.12	1.37	0.66	.22	4.78	2.73	1.61
	56	35	0	0	0	2.70	2.97	2.92	0.47	1.23	1.01	0.57	.38	5.28	2.76	1.28
	51	35	0	0	0	3.28	3.52	3.43	1.29	1.56	1.33	0.65	.62	13.44	3.41	1.42
	44	38	0	0	2.0 L	2.67	2.99	2.88	1.13	1.40	2.74	0.93	.30	11.08	2.99	1.99
	45	18	0.09	0	6.0 R	3.03	3.65	3.30	0.48	1.45	1.34	0.66	.25	4.36	3.03	1.38

DATA SHEET C

Bomb Type	NORMAL PENETRATION AND PATH LENGTH DATA												
	Bomb Number	$\sqrt[3]{I}$	Transition Ratio τ	Ratio N_T/P_{TN}	Average Density, δ	$\frac{W \ln V}{L\delta D^2}$	$\frac{L\delta D^2}{W}$						
81mm	54	0.138	0.29	0.45	75.0	19.85	0.30						
"	53	0.149	0.57	0.48	75.0	10.64	0.57						
"	57	0.158	0.63	0.41	75.0	7.59	0.81						
"	48	0.166	0.63	0.55	75.0	9.80	0.64						
"	55	0.174	0.67	0.53	75.0	8.66	0.73						
"	43	0.182	0.79	0.85	98.1	8.49	0.75						
"	47	0.189	0.77	0.82	75.0	110.75	0.60						
"	49	0.194	0.80	0.91	81.0	10.45	0.62						
"	56	0.209	0.80	0.91	87.3	9.04	0.73						
"	51	0.214	0.96	0.93	84.8	7.62	0.87						
"	44	0.219	0.79	0.89	95.6	7.86	0.85						
"	45	0.222	0.88	0.83	80.0	7.50	0.89						

DATA SHEET D

Bomb Type	Bomb Number	BALLISTIC MEASUREMENTS														
		Altitude of Release Above Target (feet)	Speed of Release Ground Speed (MPH)	Weight of Bomb (lbs.)	Striking Velocity (fps)	Impact Energy (10^6 ft. lbs.)	Striking Angle (degrees)	Impact Energy x Sine Striking Angle (10^6 ft. lbs.)	True Air Speed (MPH)	Azimuth/Wind Velocity in MPH at Release Altitude	Heading Azimuth (degrees)	Air Temperature (^{0}F)	Altimeter Setting	Range Error (feet)	Drift Error (feet)
105 mm Howitzer	58	3500	193	26.6	515	0.110	57	0.092	203	265/31	332	-17	3035	590 S	185 E
	60	5200	205	26.6	609	0.154	61	0.134	210	260/23	334	-17	3035	90 S	830 E
	62	7300	203	26.6	696	0.201	64.5	0.181	218	280/25	334	-17	3035	245 S	580 E
	63	8500	207	26.6	734	0.223	66	0.204	222	290/23	336	-18	3035	90 N	420 E
	66	9750	208	26.6	768	0.244	67	0.225	226	300/23	336	-20	3035	310 S	1105 E
	70	11000	214	26.6	798	0.264	68.5	0.245	231	300/23	336	-22	3035	3090 S	1100 E
	65	14000	234	26.6	858	0.305	71	0.288	230	240/25	334	-26	3029	700 S	400 E
	68	17000	226	26.6	900	0.335	73	0.321	231	250/35	331	-33	3029	3400 S	700 E
	69	18500	233	26.6	915	0.347	74	0.333	246	250/40	331	-34	3029	820 S	1350 W
	71	20000	207	26.6	930	0.358	75.5	0.347	245	250/46	332	-39	3029	3900 S	400 E
100 Lb. GP	86	4750	206	104	554	0.496	63	0.442	207	250/31	332	-15	3021	300 S	60 E
	84	5600	214	102.5	592	0.559	66	0.510	210	240/33	332	-17	3021	650 S	150 W
	78	6300	230	103	618	0.611	68	0.567	226	240/33	332	-19	3021	350 S	280 E
	75	7200	237	102.5	645	0.663	70	0.623	227	230/37	332	-21	3021	240 S	180 E

DATA SHEET A

Bomb Type	Bomb Number	BOMB PATH MEASUREMENTS																
		N_{SN}	N_S	N_R	$N_T = N_S + N_R$	P_S	P_{SI}	P_{RM}	P_{TM}	P	I_S	I_R	I_T	I_N	X_M	X_H	X	Y_U
105 mm Howitzer	58	1.00	0.83	0.37	1.20	1.20	1.20	0.50	1.70	1.70	1.00	0.60	1.60	0.30	1.15	0	0.38	0
	60	1.30	1.25	0.35	1.60	1.55	1.55	0.40	1.95	1.95	1.45	0.45	1.90	0.20	1.15	0	0.25	0
	62	1.10	1.00	1.38	2.38	1.10	1.10	1.55	2.65	2.65	1.10	1.60	2.70	0	1.20	0	0.70	0
	63	1.20	1.00	0.85	1.85	1.22	1.22	1.66	2.88	2.88	1.10	1.45	2.55	1.06	1.86	0.20	1.20	0
	66	1.30	1.00	0.95	1.95	1.12	1.12	1.29	2.41	2.41	1.10	1.28	2.38	0.45	1.40	0	0.85	0
	70	2.00	1.35	0.25	1.60	1.80	1.80	0.40	2.20	2.20	1.45	0.55	2.00	0.65	1.35	0	0.28	0
	65	1.70	1.00	1.93	2.93	1.05	1.05	2.05	3.10	3.10	1.08	2.08	3.16	0	1.06	0	0.69	0
	68	1.40	0.95	0.05	1.00	1.50	1.50	0.05	1.55	1.55	1.00	0.25	1.25	0.80	1.10	0	0	0
	69	1.40	1.00	0	1.00	1.00	1.00	0	1.00	1.00	1.00	.0	1.00	0.08	0.58	0	0	0
	71	1.40	0.70	1.75	2.45	0.70	0.70	1.75	2.45	2.45	0.70	1.80	2.50	0	0.32	0	0.23	0
100 Lb. GP	86	2.30	0.80	0	0.80	3.06	1.45	0	1.45	3.06	1.15	0	1.15	0.50	1.00	ric.	0	1.10
	84	0.80	1.05	0.70	1.75	1.28	1.28	0.75	2.03	2.03	1.18	0.80	1.98	0.30	1.04	-0.30	0.40	0
	78	1.00	0.90	0.05	0.95	2.70	1.50	0.45	1.95	4.18	1.00	0.50	1.50	0.95	1.50	1.50	0.41	1.50
	75	1.00	0.70	0	0.70	2.30	0.90	0	0.90	3.10	0.80	0	0.80	0.20	0.48	1.70	0	1.25

DATA SHEET B

Bomb Type	Bomb Number	BOMB PATH MEASUREMENTS							CRATER MEASUREMENTS							
		Angle V (degrees)	Z	Z_F	Angle H (degrees)	Prototype Normal Penetration	Prototype Path Length	Prototype Inclined Penetration	Crater Volume (cubic feet)	Crater Depth (feet)	Plan Area of Crater (square feet)	Crater Radius (feet)	$K_2 = \frac{V}{\pi r_h^2}$	Prototype Crater Volume	Prototype Crater Depth	Prototype Crater Radius
105 mm Howitzer	58	24	0.65	0	29.5 L	2.63	3.76	3.54	2.03	1.17	3.01	0.98	.59	22.07	2.59	2.17
	60	19	0.12	0	7 L	3.13	3.81	3.71	1.48	1.64	4.52	1.20	.20	11.04	3.20	2.34
	62	0	0.20	0	12.5 L	4.20	4.68	4.77	0.46	0.85	1.22	0.62	.44	2.54	1.50	1.10
	63	35	0	0	0	3.15	4.90	4.34	2.04	1.29	3.87	1.11	.41	10.00	2.19	1.89
	66	20	0.52	0	24 R	3.21	3.96	3.91	1.63	1.30	3.58	1.07	.35	7.24	2.14	1.76
	70	31.5	1.96	0	56 L	2.56	3.51	3.19	2.31	1.50	6.52	1.44	.25	9.43	2.40	2.30
	65	0	0	0	0	4.44	4.70	4.79	0.90	1.35	2.40	0.87	.28	3.13	2.05	1.32
	68	32	0.20	0	10 L	1.46	2.27	1.83	0.99	0.92	3.22	1.01	.33	3.08	1.35	1.48
	69	3	0	0	0	1.44	1.44	1.44	0.80	0.90	3.76	1.10	.24	2.40	1.30	1.59
	71	0	0	0	0	3.49	3.49	3.56	1.81	1.40	3.75	1.09	.34	5.22	1.99	1.55
100 Lb. GP	86	23	0.39	1.50	22 L	1.05	4.02	1.51	4.04	1.10	5.47	1.32	.67	9.14	1.44	1.73
	84	20	0.80	0.15	31.5 L	2.19	2.54	2.48	8.56	2.00	5.62	1.34	.76	16.78	2.50	1.68
	78	33	0.15	0.50	6.5 L	1.15	5.05	1.81	3.83	1.30	5.73	1.35	.51	6.75	1.57	1.63
	75	15	0.75	1.32	42.5 R	0.82	3.63	.94	7.24	1.28	7.89	1.58	.72	11.62	1.50	1.85

DATA SHEET C

Bomb Type	NORMAL PENETRATION AND PATH LENGTH DATA												
	Bomb Number	$3\sqrt{I}$	Transition Ratio τ	Ratio N_T/P_{TM}	Average Density, δ	$\frac{W \ln V}{2CD^2}$	$\frac{2Cn^2}{W}$						
105 MH	58	0.222	0.86	0.71	97.7	8.56	0.73						
"	60	0.249	1.00	0.82	93.0	8.01	0.80						
"	62	0.272	1.38	0.90	117.7	4.78	1.37						
"	63	0.281	1.01	0.64	108.9	4.75	1.38						
"	66	0.290	1.03	0.81	110.9	5.64	1.18						
"	70	0.298	0.85	0.73	86.5	7.95	0.84						
"	65	0.313	1.48	0.95	123.5	4.06	1.68						
"	68	0.322	0.49	0.65	78.7	12.58	0.54						
"	69	0.326	0.48	1.00	75.0	20.66	0.33						
"	71	0.329	1.16	1.00	127.6	4.92	1.38						
100 GP	86	0.793	0.43	0.55	75.0	13.46	0.47						
"	84	0.825	0.92	0.86	104.5	7.78	0.82						
"	78	0.848	0.47	0.49	78.9	9.77	0.66						
"	75	0.872	0.34	0.78	75.0	22.32	0.29						

DATA SHEET D

Bomb Type	Bomb Number	BALLISTIC MEASUREMENTS														
		Altitude of Release Above Target (feet)	Speed of Release Ground Speed MPH	Weight of Bomb (lbs.)	Striking Velocity (fps)	Impact Energy (10^6 ft. lbs.)	Striking Angle (degrees)	Impact Energy x Sine Striking Angle (10^6 ft. lbs.)	True Air Speed (MPH)	Azimuth/Wind Velocity in MPH at Release Altitude	Heading Azimuth(degrees)	Air Temperature(^{0}F)	Altimeter Setting	Range Error (feet)	Drift Error (feet)
250 Lb. GP	96	2500	202	243	451	0.768	57	0.644	219	340/17	335	-13	2999	30 S	570 E
	99	3800	192	240	521	1.013	60	0.877	196	250/25	333	-10	2962	170 N	150 E
	95	4200	202	229	541	1.042	63	0.928	219	340/17	335	-15	2999	120 N	120 E
	89	4200	192	249	539	1.125	62	0.993	196	250/25	333	-15	2962	150 S	250 E
	93	5800	196	240	607	1.375	66	1.256	213	340/17	335	-20	2999	250 S	270 W
	100	8250	197	235	681	1.695	69	1.582	196	240/18	335	-10	2962	960 S	350 E
	92	8250	197	239	681	1.723	69	1.609	196	240/18	335	-10	2962	330 S	80 E
	98	11750	196	237	766	2.162	74	2.078	225	331/29	339	-25	3013	1500 S	40 E
	101	11750	196	249	766	2.271	74	2.183	225	331/29	339	-25	3013	400 S	100 E
	91	14500	198	231	818	2.403	75	2.321	236	360/40	341	-30	3013	120 S	600 W
	102	15000	196	239	826	2.535	76	2.460	234	360/40	341	-30	3013	500 N	910 E
	97	20000	196	237	890	2.911	77	2.836	259	330/63	331	-40	3013	740 N	1170 W

DATA SHEET A

GPO 808611-6

Bomb Type	Bomb Number	BOMB PATH MEASUREMENTS																
		N_{SN}	N_S	N_R	$N_T = N_S + N_R$	P_S	P_{SI}	P_{RM}	P_{TM}	P	I_S	I_R	I_T	I_N	X_M	X_H	X	Y_U
250 Lb. GP	96	2.20	0.70	0	0.70	3.50	1.60	0	1.60	3.50	1.20	0	1.20	0.75	1.30	ric.	0	0.90
	99	1.40	0.88	0.15	1.03	3.10	1.40	1.00	2.40	4.80	1.00	0.95	1.95	1.35	2.15	ric.	1.04	1.55
	95	0.90	1.20	0	1.20	4.36	2.15	0	2.15	4.36	1.35	0.45	1.80	0.95	1.70	2.02	0	0.80
	89	1.30	1.15	0.40	1.55	1.92	1.92	1.30	3.22	3.22	1.30	1.30	2.60	1.70	2.70	0	1.25	0
	93	1.00	1.00	0.40	1.40	2.70	1.20	1.20	2.40	5.40	1.55	0.90	2.45	1.05	1.80	2.36	1.20	1.50
	100	1.00	1.05	1.25	2.30	1.20	1.24	2.26	3.50	3.50	1.10	1.85	2.95	1.40	2.38	0	1.80	0
	92	2.30	1.05	1.00	2.05	1.12	1.12	1.30	2.43	2.43	1.10	1.25	2.35	0.65	1.38	0	0.81	0
	98	1.30	1.00	1.75	2.75	1.08	1.08	2.02	3.10	3.10	1.05	1.95	3.00	0.65	1.42	0	1.10	0
	101	1.10	1.10	1.05	2.15	1.16	1.16	2.35	3.51	5.28	1.15	1.48	2.63	1.25	2.00	2.15	1.60	0.18
	91	1.20	1.40	2.06	3.46	1.45	1.45	2.10	3.55	3.55	1.45	2.10	3.55	0	0.73	0	0.43	0
	102	1.30	1.15	1.60	2.75	1.20	1.20	1.65	2.85	2.85	1.15	1.65	2.80	0	0.65	0	0.35	0
	97	1.30	1.20	2.05	3.25	1.30	1.30	2.10	3.40	3.40	1.25	2.10	3.35	0	0.70	1.30	0.45	0.37

DATA SHEET B

Bomb Type	Bomb Number	BOMB PATH MEASUREMENTS							CRATER MEASUREMENTS							
		Angle V (degrees)	Z	Z_F	Angle H (degrees)	N_P	P_P	I_P	Crater Volume (cubic feet)	Crater Depth (feet)	Plan Area of Crater (square feet)	Crater Radius (feet)	$K_2 = \frac{V}{\pi r^2 h}$	V_P	H_P	R_P
250 Lb. GP	96	32	0.25	-	10 L	0.81	4.05	1.39	5.75	1.00	13.05	2.04	.44	8.91	1.16	2.36
	99	44.5	0.15	-	5 R	1.08	5.02	2.04	11.51	1.56	12.55	2.00	.59	13.12	1.63	2.09
	95	28	0	0.35	0 R	1.23	4.47	1.84	10.41	1.62	15.29	2.21	.42	11.22	1.66	2.26
	89	54	0.10	0	2.5R	1.55	3.23	2.61	14.13	1.94	14.81	2.17	.49	14.23	1.94	2.17
	93	50	0	0.50	0 R	1.30	5.00	2.27	15.70	1.72	14.98	2.18	.61	12.50	1.59	2.02
	100	37	0.42	0.20	12 L	1.98	3.02	2.54	12.66	2.52	12.96	2.03	.39	8.00	2.17	1.75
	92	27	0.10	0	3.5R	1.75	2.08	2.01	10.25	2.14	8.18	1.62	.59	6.37	1.83	1.38
	98	18.5	0.21	0	9 R	2.17	2.44	2.36	9.88	2.70	10.58	1.84	.35	4.75	2.13	1.45
	101	40	0.15	0.75	5 R	1.65	4.06	2.02	49.06	2.70	38.82	3.52	.47	22.47	2.08	2.71
	91	0	0.03	0	3.5R	2.60	2.67	2.67	29.14	1.91	25.58	2.85	.60	12.55	1.44	2.14
	102	0	0.09	0	9 R	2.04	2.11	2.07	17.92	2.37	16.26	2.28	.46	7.28	1.76	1.69
	97	0	0	0	0	2.29	2.39	2.36	27.43	3.22	22.13	2.66	.38	9.67	2.27	1.87

DATA SHEET C

Bomb Type	NORMAL PENETRATION AND PATH LENGTH DATA												
	Bomb Number	$3\sqrt{\tau}$	Transition Ratio τ	Ratio N_T/R_{TM}	Average Density, δ	$\frac{W \ln V}{L\delta D^2}$	$\frac{L\delta D^2}{W}$						
250 GP	96	0.91	0.32	0.44	75.0	15.28	0.40						
"	99	1.00	0.43	0.42	85.7	9.08	0.69						
"	95	1.01	0.49	0.59	75.0	11.64	0.54						
"	89	1.03	0.62	0.48	94.0	6.16	1.02						
"	93	1.11	0.52	0.58	96.1	8.33	0.77						
"	100	1.19	0.79	0.66	115.1	4.82	1.35						
"	92	1.20	0.70	0.84	111.0	7.17	0.91						
"	98	1.29	0.85	0.89	121.9	5.25	1.27						
"	101	1.32	0.68	0.61	111.0	5.05	1.31						
"	91	1.34	1.08	0.97	118.9	4.70	1.42						
"	102	1.36	0.85	0.96	117.9	5.91	1.13						
"	97	1.43	0.97	0.96	121.5	4.89	1.39						

DATA SHEET D

Bomb Type	Bomb Number	BALLISTIC MEASUREMENTS														
		Altitude of Release Above Target (feet)	Speed of Release Ground Speed (MPH)	Weight of Bomb (lbs.)	Striking Velocity (fps)	Impact Energy (10^6 ft. lbs.)	Striking Angle (degrees)	Impact Energy x Sine Striking Angle (10^6 ft. lbs.)	True Air Speed (MPH)	Azimuth/Wind Velocity in PMH at Release Altitude	Heading Azimuth (degrees)	Air Temperature (^oF)	Altimeter Setting	Range Error (feet)	Drift Error (feet)
500n Lb. GP	19	5700	195	468	620	2.797	66	2.555	212	020/23	347	-16	3076	1137 N	293 E
	21	5700	195	470	620	2.809	66	2.566	212	020/23	347	-16	3076	1243 N	293 E
	23	7750	213	464	706	3.596	69	3.357	220	350/08	340	-21	3076	665 S	350 E
	24	10100	223	454	782	4.316	70	4.056	228	310/06	339	-24	3076	1490 S	10 E
	22	15540	226	472	894	5.865	75	5.435	245	040/36	347	-33	3073	500 S	470 E
	20	20000	225	484	940	6.649	76	6.452	237	040/23	344	-43	3073	3140 S	830 E

Bomb Type	Bomb Number	BOMB PATH MEASUREMENTS																
		N_{SN}	N_S	N_R	$N_T = N_S + N_R$	P_S	P_{SI}	P_{RM}	P_{TM}	P	I_S	I_R	I_T	I_N	X_M	X_H	X	Y_U
500 Lb. GP	19	1.70	1.15	0.55	1.70	3.99	2.32	1.90	4.22	9.63	1.25	1.68	2.93	3.00	3.75	3.95	1.82	3.50
	21	1.60	1.40	0.08	1.48	3.02	3.02	0.45	3.47	3.47	1.50	1.00	2.50	2.15	3.00	0	0.45	0
	23	1.00	1.00	1.30	2.30	1.20	1.20	3.33	4.53	4.53	1.08	2.40	3.48	2.42	3.53	0	3.00	0
	24	1.30	1.00	1.30	2.30	2.72	2.72	3.10	5.82	6.95	1.10	2.10	3.20	1.65	2.73	2.45	2.35	1.25
	22	0.90	1.10	3.70	4.80	1.14	1.14	4.14	5.28	5.28	1.12	4.10	5.22	0.82	2.20	0	1.82	0
	20	1.30	1.10	1.30	2.40	2.40	1.20	2.80	4.00	7.42	1.15	1.90	3.05	2.10	2.82	-	2.40	-

DATA SHEET B

Bomb Type	Bomb Number	BOMB PATH MEASUREMENTS							CRATER MEASUREMENTS							
		Angle V (degrees)	Z	Z_F	Angle H (degrees)	Prototype Normal Penetration	Prototype Path Length	Prototype Inclined Penetration	Crater Volume (cubic feet)	Crater Depth (feet)	Plan Area of Crater (square feet)	Crater Radius (feet)	$K_2 = \frac{V}{\pi r^2 h}$	Prototype Crater Volume	Prototype Crater Depth	Prototype Crater Radius
500 Lb. GP	19	60	0.4	0.55	7 R	1.24	7.03	2.14	24.04	2.35	25.20	2.83	.41	9.41	1.72	2.06
	21	40	0	0.05	0	1.08	2.53	1.82	15.55	2.09	15.19	2.20	.49	6.06	1.53	1.61
	23	45	0	0.5	0	1.53	3.02	2.32	27.51	3.06	21.35	2.61	.42	8.19	2.04	1.74
	24	38	0.16	0.45	3 R	1.44	4.34	2.00	43.38	2.75	26.17	2.89	.60	10.70	1.72	1.81
	22	12	1.89	0	94 L	2.73	3.00	2.97	56.68	2.20	52.44	4.09	.49	10.43	1.25	2.32
	20	47	0.20	-	5 R	1.29	3.99	1.64	47.27	3.00	37.08	3.44	.42	7.33	1.61	1.85

DATA SHEET C

Bomb Type	NORMAL PENETRATION AND PATH LENGTH DATA												
	Bomb Number	$\sqrt[3]{I}$	Transition Ratio τ	Ratio N_T/P_{TM}	Average Density, δ	$\frac{W \ln V}{L\delta D^2}$	$\frac{L\delta D^2}{W}$						
500 GP	19	1.41	0.49	0.40	98.8	5.34	1.21						
"	21	1.41	0.43	0.43	126.2	5.08	1.33						
"	23	1.54	0.61	0.51	116.7	4.26	1.53						
"	24	1.63	0.58	0.40	116.7	3.40	1.97						
"	22	1.80	1.10	0.91	131.8	3.40	2.02						
"	20	1.88	0.51	0.60	114.9	5.14	1.33						

DATA SHEET D

8-11808 040

Bomb Type	Bomb Number	BALLISTIC MEASUREMENTS													
		Altitude of Release Above Target (feet)	Speed of Release Ground Speed (MPH)	Weight of Bomb (lbs.)	Striking Velocity (fps)	Impact Energy (10^6 ft. lbs.)	Striking Angle (degrees)	Impact Energy x Sine Striking Angle (10^6 ft. lbs.)	True Air Speed (MPH)	Azimuth/Wind Velocity in MPH at Release Altitude	Heading Azimuth (degrees)	Air Temperature (^oF)	Altimeter Setting	Range Error (feet)	Drift Error (feet)
500 Lb. SAP	10	3000	169	522	474	1.823	62	1.610	200	310/35	335	-17	2981	50 N	30 W
	8	4000	176	505	528	2.189	64	1.967	204	300/35	334	-18	2981	380 N	430 E
	3	5000	187	538	592	2.931	65	2.657	207	300/26	335	-18	2981	300 N	30 E
	6	6000	195	523	643	3.362	67	3.095	212	300/22	336	-19	2981	0	125 W
	7	7250	187	545	688	4.011	69	3.744	196	300/24	336	-21	2961	490 S	130 E
	5	8750	198	483	743	4.145	70	3.895	219	310/24	337	-22	2961	1790 S	480 E
	1	10250	192	546	788	5.271	72	5.013	214	320/25	338	-23	2961	70 N	500 E
	2	12500	218	530	850	5.953	73	5.693	225	280/15	337	-22	2981	20 N	430 E
	12	14400	227	517	896	6.453	73	6.171	242	040/35	347	-30	3073	2820 S	1490 E
	4	16500	234	529	932	7.144	74	6.867	229	240/25	335	-32	2981	140 S	1165 W
	11	18500	242	543	966	7.887	74	7.582	237	240/25	335	-34	2981	80 N	25 W

GPO 830611-3

DATA SHEET A

Bomb Type	Bomb Number	BOMB PATH MEASUREMENTS																
		N_{SN}	N_S	N_R	$N_T = N_S + N_R$	P_S	P_{SI}	P_{RM}	P_{TM}	P	I_S	I_R	I_T	I_N	X_M	X_H	X	Y_U
500 Lb. SAP	10	1.30	0.90	3.60	1.50	2.45	1.30	1.90	3.20	6.31	1.00	1.55	2.55	1.65	2.70	ric.	1.79	1.98
	8	1.00	0.85	0.95	1.80	1.03	1.03	2.82	3.85	4.60	0.95	2.32	3.27	2.70	3.10	0.75	2.55	0.05
	3	1.80	0.90	1.20	2.10	1.00	1.00	2.15	3.16	5.05	1.00	1.80	2.80	1.00	2.15	1.76	1.71	0.69
	6	1.20	0.80	2.15	2.95	0.88	0.88	4.35	5.23	5.23	0.85	3.50	4.35	2.45	3.98	0	3.62	0
	7	1.60	1.00	2.45	3.45	1.10	1.10	4.15	5.25	5.25	1.10	3.55	4.65	2.20	3.72	0	3.29	0
	5	1.30	0.80	3.20	4.00	0.90	0.90	4.65	5.55	5.55	0.85	4.15	5.00	2.20	3.78	0	3.39	0
	1	1.20	1.05	4.05	5.10	1.11	1.11	5.30	6.41	6.41	1.10	5.00	6.10	1.80	3.73	0	3.38	0
	2	0.80	1.00	4.60	5.60	1.05	1.05	6.00	7.05	7.05	1.08	5.55	6.63	1.90	4.00	0	3.64	0
	12	1.50	0.98	5.52	6.50	1.03	1.03	6.42	7.45	7.45	1.05	6.30	7.33	1.05	3.55	0	3.19	0
	4	1.30	1.00	4.80	5.80	1.26	1.26	4.95	6.21	6.21	1.30	4.95	6.25	0.40	1.47	0	1.15	0
	11	1.20	0.90	5.96	6.86	0.93	0.93	6.21	7.14	7.14	0.95	6.20	7.15	0	1.95	0	1.70	0

DATA SHEET B

Bomb Type	Bomb Number	BOMB PATH MEASUREMENTS							CRATER MEASUREMENTS							
		Angle V (degrees)	Z	Z_F	Angle H (degrees)	Prototype Normal Penetration	Prototype Path Length	Prototype Inclined Penetration	Crater Volume (cubic feet)	Crater Depth (feet)	Plan Area of Crater (square feet)	Crater Radius (feet)	$X_2 = \frac{V}{\pi r^2 h}$	Prototype Crater Volume	Prototype Crater Depth	Prototype Crater Radius
500 Lb. SAP	10	46	0.15	-	4 L	1.28	5.39	2.18	19.30	2.00	16.76	2.31	.58	11.99	1.71	1.97
	8	49	0	0.05	0	1.44	3.60	2.62	23.36	2.17	21.52	2.62	.50	11.88	1.74	2.10
	3	29	0.05	0.05	1.5 L	1.52	3.66	2.03	22.78	2.43	26.60	2.91	.35	8.57	1.76	2.11
	6	35	0.35	0	5.5 L	2.02	3.58	2.98	24.56	2.70	28.19	3.00	.32	7.94	1.85	2.05
	7	32	0.63	0	10	2.23	3.39	3.00	36.39	2.75	40.53	3.59	.33	9.72	1.77	2.32
	5	28	1.10	0	19.5 R	2.55	3.54	3.18	36.84	2.34	23.32	2.73	.67	9.46	1.49	1.74
	1	19	0.52	0	11 L	2.98	3.75	3.57	26.61	2.72	25.86	2.87	.38	5.31	1.59	1.68
	2	19	0.20	0	13 L	3.15	3.96	2.68	36.94	2.87	32.90	3.23	.39	6.49	1.61	1.81
	12	10	0.30	0	5 R	3.55	4.07	4.01	26.02	3.50	23.85	2.76	.31	4.22	1.91	1.51
	4	4	0.50	0	18 L	3.05	3.27	3.29	37.79	3.10	30.49	3.12	.40	5.50	1.63	1.64
	11	0	0.52	0	16 R	3.50	3.64	3.65	29.40	3.20	30.27	3.10	.30	3.88	1.63	1.58

DATA SHEET C

Bomb Type	NORMAL PENETRATION AND PATH LENGTH DATA												
	Bomb Number	$\sqrt[3]{I}$	Transition Ratio τ	Ratio N_T/P_{TM}	Average Density, δ	$\frac{W \ln V}{L\delta D^2}$	$\frac{L\delta D^2}{W}$						
500 SAP	10	1.22	0.51	0.47	104.5	10.10	0.61						
"	8	1.30	0.57	0.47	113.9	7.84	0.80						
"	3	1.43	0.61	0.66	117.1	9.51	0.67						
"	6	1.50	0.80	0.56	128.7	5.31	1.22						
"	7	1.59	0.92	0.66	127.3	5.42	1.21						
"	5	1.61	1.02	0.72	134.0	4.89	1.35						
"	1	1.74	1.19	0.80	133.5	4.13	1.56						
"	2	1.81	1.25	0.79	135.5	3.85	1.74						
"	12	1.86	1.41	0.87	137.6	3.67	1.86						
"	4	1.93	1.20	0.93	136.0	4.51	1.54						
"	11	1.99	1.40	0.96	139.0	3.85	1.80						

DATA SHEET D

Bomb Type	Bomb Number	BALLISTIC MEASUREMENTS													
		Altitude of Release Above Target (feet)	Speed of Release Ground Speed (MPH)	Weight of Bomb (lbs.)	Striking Velocity (fps)	Impact Energy (10^6 ft. lbs.)	Striking Angle (degrees)	Impact Energy x Sine Striking Angle (10^6 ft lbs.)	True Air Speed (MPH)	Azimuth/Wind Velocity in MPH at Release Altitude	Heading Azimuth (degrees	Air Temperature(^oF)	Altimeter Setting	Range Error (feet)	Drift Error (feet)
1000 Lb. SAP	36	5000	237	990	636	6.226	61	5.445	219	210/29	335	-15	2999	490 S	365 W
	31	5750	243	990	676	7.034	62	6.210	223	200/29	335	-16	2999	430 S	40 W
	34	6800	230	990	710	7.759	64	6.973	215	220/31	334	-17	3001	190 S	290 W
	39	7800	236	990	746	8.566	65	7.763	220	210/26	335	-17	2998	460 N	100 E
	38	9100	216	990	784	9.461	68	8.772	213	240/35	331	-19	3001	150 N	300 W
	35	10200	230	990	828	10.553	69	9.852	219	220/29	335	-20	2998	1150 N	20 W
	32	11700	249	990	880	11.920	70	11.201	220	210/48	336	-22	2994	1680 S	1670 W
	33	13000	251	990	912	12.802	71	12.105	227	215/48	330	-22	2994	2040 N	820 E
	42	14500	195	1014	928	13.583	74	13.057	235	315/43	335	-30	3022	530 S	540 W
	41	16200	188	985	964	14.224	75	13.739	228	315/43	335	-35	3022	30 S	600 W
	37	18100	199	990	1006	15.577	76	15.115	240	315/43	335	-40	3022	620 N	380 E
	40	20000	192	985	1040	16.555	77	16.131	233	315/43	335	-40	3022	550 N	210 W

Bomb Type	Bomb Number	BOMB PATH MEASUREMENTS																
		N_{SN}	N_S	N_R	$N_T = N_S + N_R$	P_S	P_{SI}	P_{RM}	P_{TM}	P	I_S	I_R	I_T	I_N	X_M	X_H	X	Y_U
1000 Lb. SAP	36	1.20	1.05	1.48	2.53	1.20	1.20	3.20	4.40	6.18	1.20	2.60	3.80	1.45	3.25	1.80	2.63	0.15
	31	1.40	1.10	3.00	4.10	1.31	1.31	4.92	6.24	6.24	1.30	4.55	5.85	1.88	4.63	0	3.92	0
	34	1.20	1.00	3.08	4.08	1.12	1.12	5.30	6.42	6.42	1.10	4.55	5.65	2.40	4.60	0	4.10	0
	39	1.30	1.10	2.35	3.45	1.20	1.20	5.12	6.32	6.32	1.22	4.03	5.25	2.82	4.86	0	4.35	0
	38	2.00	1.00	3.10	4.10	1.15	1.15	4.45	5.60	5.60	1.09	4.10	5.19	1.90	3.71	0	3.15	0
	35	6.50	0.95	4.45	5.40	1.00	1.00	6.75	7.75	7.75	1.00	5.82	6.82	3.00	5.12	0	4.75	0
	32	1.30	1.00	6.00	7.00	1.03	1.03	6.20	7.23	7.23	1.05	6.20	7.25	0	1.76	0	1.50	0
	33	1.30	0.95	4.05	5.00	1.03	1.03	8.45	9.48	9.48	1.00	6.15	7.15	5.10	7.23	0	6.86	0
	42	1.30	0.90	4.80	5.70	0.95	0.95	5.55	6.50	6.50	0.95	5.32	6.27	1.60	3.06	0	2.80	0
	41	1.30	0.75	7.75	8.50	0.75	0.75	8.00	8.75	8.75	0.78	8.00	8.78	0.26	2.58	0	2.40	0
	37	1.30	1.40	7.65	9.05	1.45	1.45	7.72	9.17	9.17	1.45	7.65	9.10	0.20	1.31	0	1.10	0
	40	1.40	0.80	7.85	8.65	0.90	0.90	8.35	9.25	9.25	0.90	8.30	9.20	0.80	2.90	0	2.70	0

DATA SHEET B

Bomb Type	Bomb Number	BOMB PATH MEASUREMENTS							CRATER MEASUREMENTS							
		Angle V (degrees)	Z	Z_F	Angle H (degrees)	Prototype Normal Penetration	Prototype Path Length	Prototype Inclined Penetration	Crater Volume (cubic feet)	Crater Depth (feet)	Plan Area of Crater (square feet)	Crater Radius (feet)	$k_2 = \frac{V}{\pi r^2 h}$	Prototype Crater Volume	Prototype Crater Depth	Prototype Crater Radius
1000 Lb. SAP	36	29.5	0.26	0.65	6 L	1.44	3.51	2.16	53.05	3.15	33.78	3.28	.50	9.74	1.79	1.86
	31	22	0.25	0	4 L	2.23	3.39	3.18	66.40	3.23	76.83	4.95	.27	10.69	1.76	2.69
	34	28	1.00	0	12.5 R	2.14	3.36	2.96	70.01	3.00	70.20	4.73	.33	10.04	1.57	2.48
	39	35	1.65	0.15	19 R	1.74	3.19	2.65	57.06	3.15	28.00	2.99	.65	7.35	1.59	1.51
	38	26	2.50	0	47 R	1.99	2.72	2.52	90.69	3.60	66.72	4.61	.36	10.34	1.84	2.24
	35	27	0.80	0	9 L	2.52	3.62	3.19	95.38	3.90	76.60	4.94	.32	9.68	1.82	2.31
	32	0	0.15	0	5 R	3.13	3.23	3.24	63.16	3.05	44.27	3.75	.47	5.64	1.36	1.67
	33	39.5	0.30	0.11	3.5 R	2.17	4.12	3.11	170.16	5.50	34.50	3.32	.89	14.06	2.39	1.44
	42	17	5.35	0	84 R	2.42	2.75	2.66	62.22	3.30	35.92	3.38	.52	4.77	1.40	1.43
	41	2	2.50	0	72.5 R	3.56	3.66	3.67	35.40	3.10	26.91	2.93	.42	2.58	1.30	1.23
	37	6	0	0	0	3.66	3.71	3.68	50.63	2.70	47.43	3.89	.41	3.35	1.09	1.57
	40	6	0	0	0	3.42	3.66	3.64	65.36	3.20	140.13	6.68	.15	4.05	1.26	2.64

DATA SHEET C

Bomb Type	NORMAL PENETRATION AND PATH LENGTH DATA													
	Bomb Number	$3\sqrt{I}$	Transition Ratio τ	Ratio N_T/P_{TM}	Average Density, δ	$\frac{W \ln y}{L\delta D^2}$	$\frac{L\delta D^2}{W}$							
1000 SAP	36	1.84	0.65	0.56	118.1	7.88	0.82							
"	31	1.92	1.02	0.66	128.9	5.15	1.27							
"	34	1.98	1.00	0.64	130.6	4.99	1.32							
"	39	2.05	0.80	0.55	125.2	5.30	1.25							
"	38	2.12	0.92	0.73	130.7	5.79	1.15							
"	35	2.19	1.18	0.70	135.7	4.03	1.66							
"	32	2.28	1.48	0.97	138.2	4.34	1.57							
"	33	2.34	1.02	0.53	135.5	3.41	2.02							
"	42	2.39	1.13	0.88	137.1	4.85	1.40							
"	41	2.42	1.67	0.97	142.2	3.50	1.96							
"	37	2.50	1.72	0.99	137.3	3.52	1.98							
"	40	2.55	1.60	0.94	141.9	3.34	2.07							

DATA SHEET 3

Bomb Type	Bomb Number	BALLISTIC MEASUREMENTS													
		Altitude of Release Above Target (feet)	Speed of Release Ground Speed (MPH)	Weight of Bomb (lbs.)	Striking Velocity (fps)	Impact Energy (10^6 ft. lbs.)	Striking Angle (degrees)	Impact Energy x Sine Striking Angle 10^6 ft. lbs.)	True Air Speed (MPH)	Azimuth/Wind Velocity in MPH at Release Altitude	Heading Azimuth (degrees	Air Temperature(^{0}F)	Altimeter Setting	Range Error (feet)	Drift Error (feet)
1000 Lb. AP	30	5000	205	1017	616	6.000	64	5.393	191	215/29	333	-15	2964	240 S	470 E
	29	7500	192	1017	707	7.904	68	7.328	178	215/29	333	-15	2964	1340 S	570 E
	28	10000	199	1012	811	10.349	71	9.785	214	298/20	336	-20	2970	200 N	210 E
	25	14500	172	1017	936	13.859	77	13.504	225	340/52	338	-31	3013	1020 N	270 W
	27	20000	200	1012	1048	17.281	78	16.893	242	290/63	339	-32	2960	480 S	1370 E
	26	24500	183	1016	1106	19.322	79	18.967	210	297/75	335	-45	2950	90 N	170 W
1600 Lb. AP	13	3000	197	1515	503	5.957	57	4.996	207	310/11	337	-10	2997	50 S	150 E
	17	5000	196	1530	610	8.849	64	7.953	219	340/23	340	-20	3000	600 S	360 E
	16	10000	199	1545	830	16.543	70	15.545	214	298/20	336	-20	2970	200 N	50 W
	15	20000	181	1520	1064	26.745	77	26.059	236	290/63	326	-35	2950	600 S	1340 E
	14	23400	189	1496	1120	29.166	78	28.529	253	298/75	325	-42	2960	410 N	420 W

DATA SHEET A

Bomb Type	Bomb Number	BOMB PATH MEASUREMENTS																
		N_{SN}	N_S	N_R	$N_T = N_S + N_R$	P_S	P_{SI}	P_{RM}	P_{TM}	P	I_S	I_R	I_T	I_N	X_M	X_R	X	Y_U
1000 Lb. AP	30	1.00	1.20	4.30	5.50	1.40	1.40	5.10	6.50	6.50	1.35	5.10	6.45	0.70	3.40	0	2.69	0
	29	1.30	0.90	3.08	3.98	1.00	1.00	3.30	4.30	4.30	1.00	3.32	4.32	0	1.65	0	1.28	0
	28	1.40	1.00	8.40	9.40	1.05	1.05	9.00	10.05	10.05	1.05	9.00	10.05	0.20	3.60	0	3.20	0
	25	1.10	0.75	8.95	9.70	0.80	0.80	9.40	10.20	10.20	0.80	9.40	10.20	0	2.86	0	2.64	0
	27	1.30	0.60	15.12	15.72	0.60	0.60	17.30	17.90	17.90	0.60	16.65	17.25	4.45	8.40	0	8.23	0
	26	1.10	1.00	17.80	18.80	1.00	1.00	18.60	19.60	19.60	1.00	18.50	19.50	1.90	5.45	0	5.25	0
1600 Lb. AP	13	1.90	0.90	1.20	2.10	2.28	2.28	3.05	4.20	10.05	1.10	2.55	3.65	1.52	3.30	5.50	2.64	1.70
	17	1.30	1.10	4.35	5.45	1.22	1.22	6.64	7.86	7.86	1.25	6.15	7.40	2.45	5.55	0	5.00	0
	16	0.80	0.90	9.45	10.35	1.00	1.00	10.95	11.95	11.95	0.95	10.80	11.75	1.55	5.80	0	5.40	0
	15	1.30	0.90	16.30	17.20	0.90	0.90	17.75	18.65	18.65	0.90	17.40	18.30	2.80	7.04	0	6.80	0
	14	1.90	1.00	15.42	16.42	1.00	1.00	16.25	17.25	17.25	1.00	16.15	17.15	1.68	5.22	0	4.98	0

Bomb Type	Bomb Number	BOMB PATH MEASUREMENTS							CRATER MEASUREMENTS							
		Angle V (degrees)	Z	Z_F	Angle H (degrees)	Prototype Normal Penetration	Prototype Path Length	Prototype Inclined Penetration	Crater Volume (cubic feet)	Crater Depth (feet)	Plan Area of Crater (square feet)	Crater Radius (feet)	$K_2 = \frac{V}{\pi r^2 h}$	Prototype Crater Volume	Prototype Crater Depth	Prototype Crater Radius
1000 Lb AP	30	7.5	0	0	0	3.14	3.71	3.69	68.27	2.25	70.81	4.75	.43	12.66	1.29	2.71
	29	0	0	0.40	0	2.05	2.22	2.23	74.91	3.90	42.63	3.69	.45	10.22	2.01	1.90
	28	1	0.95	0	15 L	4.39	4.70	4.70	28.86	2.80	25.83	2.87	.40	2.95	1.31	1.34
	25	0	0	0	0	4.08	4.29	4.29	66.14	1.80	82.78	5.13	.47	5.05	0.76	2.16
	27	9	0	0	0	6.17	6.96	6.71	34.02	3.20	41.90	3.65	.22	2.01	1.25	1.42
	26	6	0.30	0	3 R	7.0[illegible]	7.34	7.30	34.49	2.70	34.95	3.34	.36	1.82	1.01	1.25
1600 Lb AP	13	31	0.15	0.2	2.5 R	1.23	5.88	2.13	93.78	3.10	65.00	4.55	.47	18.77	1.81	2.66
	17	22	0.75	0	7.5 L	2.73	3.93	3.70	70.77	3.70	71.85	4.78	.27	8.90	1.85	2.39
	16	8	1.52	0	16.5 R	4.14	4.78	4.70	63.77	2.50	96.21	5.54	.27	4.10	1.00	2.22
	15	10	1.00	0	8 L	5.81	6.30	6.18	71.58	3.10	70.50	4.74	.33	2.75	1.05	1.60
	14	6	0	0	0	5.37	5.64	5.60	137.02	2.80	132.61	6.50	.37	4.80	0.92	2.12

GPO 808611-4

DATA SHEET C

Bomb Type	NORMAL PENETRATION AND PATH LENGTH DATA												
	Bomb Number	$\sqrt[3]{T}$	Transition Ratio τ	Ratio N_T/P_{TM}	Average Density, δ	$\frac{W \ln V}{L\delta D^2}$	$\frac{L\delta D^2}{W}$						
1000 AP	30	1.82	1.44	0.85	132.6	7.58	132.6						
"	29	1.99	0.97	0.93	132.0	11.70	132.0						
"	28	2.18	2.20	0.94	140.9	4.82	140.9						
"	25	2.40	1.90	0.95	143.0	4.72	143.0						
"	27	2.58	2.85	0.88	145.9	2.71	145.9						
"	26	2.68	3.30	0.96	144.8	2.52	144.8						
1600 AP	13	1.81	0.56	0.50	117.1	14.12	0.44						
"	17	2.07	1.27	0.69	135.8	6.73	0.95						
"	16	2.55	1.95	0.87	142.3	4.44	1.51						
"	15	2.98	2.70	0.92	144.8	2.86	2.41						
"	14	3.08	2.50	0.95	144.2	3.16	2.22						

DATA SHEET D

APPENDIX B: TERMINOLOGY AND SYMBOLS

Terminology

The terminology used in this report is an outgrowth of research dealing with penetration of projectiles in soils, concrete, armor-plate, and rocks, and of research dealing with explosions in rocks, soils, and frozen ground. It incorporates terminology that is standard in the science of exterior ballistics and includes several terms that are employed in air navigation. In an effort to coordinate impact and explosion, various terms used in explosion research such as "optimum depth", "depth ratio", "critical depth", and "strain-energy factor" are included. Certain terms such as "transition ratio", "transition depth", "tunneling range", "cratering range" and "ricochet range", were coined in an effort to further the analysis of penetration of projectiles as failure progresses through the brittle state to the plastic state.

The ballistic coefficient (C) is derived from equations of motion of projectiles and is equal to

$$C = \frac{m}{id^2}$$

where,

C is the ballistic coefficient

i is a form factor

d is the diameter of the projectile

m is the weight of the projectile.

As the ballistic coefficient increases, the retardation due to air resistance decreases, and the range of the projectile increases.

Caliber radius head (CRH): a dimensionless quantity that is a measure of the sharpness of the nose of the projectile, and is equal to the radius of the ogive of the bomb nose divided by the diameter of the bomb. Some bomb penetration formulas include a factor that takes into account the shape of the nose of the bomb.

Charge/weight ratio is the ratio of the weight of the explosive charge to the total weight of the bomb, expressed as a percentage. Bombs designed for air burst, such as general-purpose bombs, have a higher charge/weight ratio than semi-armor-piercing or armor-piercing bombs.

Cratering range (Fig. 30) is the range in which a projectile penetrates by a cratering action. It lies between the region in which a projectile ricochets and the region in which it penetrates by tunneling. The cratering action is the process whereby framentation of the medium is a result of three mutually perpendicular systems of fractures considered here to be indicative of brittle-state failure.

Critical depth (N) is the minimum depth, measured from the surface to the center of gravity of a given explosive charge, at which the energy of the explosion is dissipated into the medium without visibly damaging the surface above the charge. The critical depth is related to the charge weight by the strain-energy equation

$$N = E\sqrt[3]{w}$$

where,

N is the critical depth, ft

E is the strain-energy factor

w is the weight of the explosives charge, lb.

The drift error is the bombing error measured at right angles to the line of flight, or track, of the aircraft. (See also range error.)

Depth ratio (Δ) is the ratio of the depth of an explosive charge to the critical depth of a charge of the same weight and of the same explosive. The depth ratio is a means of comparing the volumes of two spheres which represent stressed volumes in the medium as wave fronts from charges at different depths strike the surface. One sphere is of radius equal to the charge depth; the other is of radius equal to the critical depth.

The depth ratio not only is a ratio of volumes or of masses in a given material, it also is a reciprocal ratio of average energy densities within the two stressed volumes. Thus, the depth ratio is a means of comparing effects of explosions in various media.

Drag of projectile is the reaction opposing motion of a projectile due to the resistance of the medium. The term usually is applied in connection with the motion of bodies in fluids. In this report the term is applied in the same sense to projectile penetration of frozen ground by plastic deformation.

Heading, as used in connection with bombing, is the bearing of a longitudinal axis of the aircraft at the instant of release. If there is no cross wind, the heading is the direction of flight with respect to the ground and is the same as the track or line of flight of the aircraft. If there is a cross wind, the heading differs from the direction of flight by the drift angle. In the tests at Fort Churchill, the bombing run was always in the same direction, but the heading varied depending upon the direction and velocity of the wind.

Impact energy (I) of a projectile is the kinetic energy of impact.

$$I = \frac{W}{g} \cdot \frac{V^2}{2}$$

where

W is gross weight of projectile

g is the acceleration of gravity

V is striking velocity.

Line of flight (LOF) is the direction of motion of the aircraft at the instant of release with respect to the ground. The terms "line of flight" and the "track" are synonymous.

Line of impact is the tangent to the trajectory of the projectile at impact; it makes an angle with the horizontal equal to the angle of fall. The line of impact is referred to also as the "line of action" of the projectile.

Normal penetration (y, N_T) is the depth of penetration of the nose of the projectile measured normal to the target surface.

Ogive is the curved nose or head of the projectile. Usually the curve of the ogive is the arc of a circle and the radius is expressed in calibers (see caliber radius head).

Optimum depth (d_0) is the depth at which a given explosive charge produces the greatest volume of excavation per unit weight of explosive. Optimum depth may be calculated from the equation

$$d_0 = \Delta E \sqrt[3]{w}$$

where,

d_0 is optimum depth, ft

Δ is the depth ratio at which the phenomenon occurs

E is the strain-energy factor

w is weight of the explosive charge, lb.

Optimum depth depends both upon properties of the medium and characteristics of the explosive. At optimum depth only a small portion of the energy of the explosion is partioned to the atmosphere.

Path length (P, P_{TM}, L):

Path length (P) is the travel distance of the nose of a projectile along its trajectory in the medium (see Fig. 21). In the analysis, path length P_{TM} is used to designate the

distance measured along the trajectory from impact to the point of maximum normal penetration. Total length $\underline{P}$ differs from P_{TM} in the cratering range, and a distinction between the two is made because the energy required for penetrating from $\underline{P}$ to P_{TM} is much less than that required to penetrate the same distance in unbroken frozen ground.

Plastic deformation refers to the deformation of solids by "flow", at great confinement and high stress. Creep and relaxation may be thought of as plastic deformation under static or geologic loading in which the time interval is great compared to that for dynamic loading. It now is evident that materials also are capable of deforming plastically under dynamic loading. Whether this process is somewhat analogous to creep, whether intergranular crushing occurs, and the nature of the relationship between shearing stress and rate of strain are matters of conjecture at present.

Poisson's ratio is the ratio of the differential lateral strain to the differential axial strain for the specific stress range in which a specimen is tested.

The range error is the bombing error measured parallel to the line of flight, or track, of the aircraft.

Ricochet range: The range in which a projectile that strikes a massive target rebounds or ricochets to such an extent that it comes to rest outside of the crater. At the upper limit of the ricochet range ricochet ceases and the projectile remains within the crater.

Sectional density (D_s): Weight of a projectile divided by the cube of its diameter.

Sectional pressure (P): Weight of a projectile divided by its cross-sectional area.

Slenderness ratio (l/d): Ratio of the length of a projectile to its diameter.

Strain-energy factor (E): The behavior of various materials of the earth's crust may be compared by the relations between failure criteria and mass, energy and time. The relations may be observed in the field by subjecting the material to a dynamic load using an explosive and measuring its energy absorption capacity. The dynamic strain characteristics of the medium are expressed by the strain-energy factor

$$E = \frac{N}{\sqrt[3]{w - w_1}}$$

where

E is the strain-energy factor

N is the critical depth, ft

w is the total weight of explosive, lb

w_1 is the weight of explosive partitioned to inelastic behavior of the medium, lb.

Striking angle: The angle between the tangent to the trajectory of a projectile at impact and the surface of the target. At the SIPRE Fort Churchill bombing range, where the target surface is horizontal, the striking angle equals the angle of fall at impact.

Terminal velocity: The velocity at which the component of gravitational force acting along the trajectory is opposed by an equal force due to air resistance. As air resistance is a function of air density, terminal velocity usually is referred to air of standard density (59F at sea level).

Track: Direction of an aircraft with respect to the ground (see line of flight). The track differs from the heading by the drift angle.

Transition depth: The depth, measured vertically, at which the medium under impact of a projectile begins to fail by plastic deformation. The transition depends upon both the projectile and the medium.

Transition ratio (τ): The ratio of the vertical depth of penetration of a projectile to the vertical depth at which tunneling of the same type and weight of projectile in the same medium begins. The transition ratio is a dimensionless quantity. Projectiles having a transition ratio greater than 1.0 penetrate in part by plastic deformation, and the proportion of penetration by plastic deformation increases as τ increases. The transition ratio also indicates the shape of the trajectory of the projectile in the frozen ground: the trajectory approaches a straight line as the proportion of penetration by plastic deformation increases.

Tunneling range: The range in which a projectile penetrates primarily by plastic deformation. As used here, "plastic deformation" is not necessarily identical to "plastic flow". The lower limit of the tunneling range is the transition depth, and coincides with the upper limit of the cratering range. Whether a projectile is capable of entering the tunneling range depends not only upon the projectile, but also upon the medium and the energy of impact.

Symbols

In reviewing earlier penetration formulas, the symbols of the original author have been retained. These are not repeated here.

Area of crater cross sections A, B	A_A, B_B
Centroid radius of sections A, B	$\bar{R}_A$, $\bar{R}_B$
Coefficients of resistance	C_1, C_3
Depth of center of gravity of explosive charge	d_c
Depth of crater	H
Depth of normal penetration	N_T, y, N_R
Depth ratio	Δ
Diameter of bomb	D, d
Distance	s
Drag coefficient	C_D
Energy of impact (KE)	I
Nose factor	N
Path length	L, P_{TM}, P
Plastic deformation index	m
Radius of crater	R
Resistance	R, R_1, R_2
Rock factor	R
Strain-energy factor	E
Striking velocity	V
Transition ratio	τ
Unit weight	δ
Velocity	v
Volume	V
Weight of explosive	w
Weight of bomb	W

GPO 808611-3